USGS
science for a changing world

Geologic Map of Big Bend National Park, Texas

Prepared in cooperation with the National Park Service

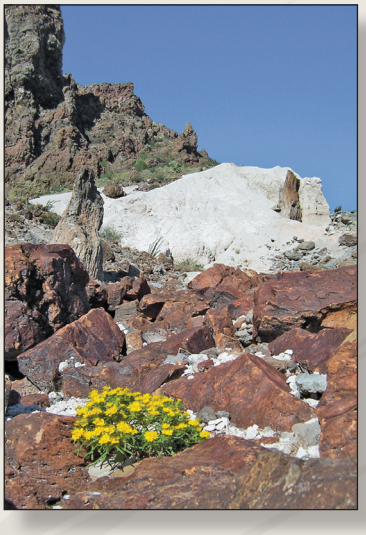

Pamphlet to accompany Scientific Investigations Map 3142

2011

U.S. Department of the Interior
U.S. Geological Survey

Front Cover Photographs (left to right):
Ocotillo bloom *(Daniel P. Miggins)*
Yucca bloom *(Daniel P. Miggins)*
Burro Mesa near pouroff *(Robert B. Scott)*
Santa Elena Canyon *(NPS Big Bend Visitor Photo Gallery)*
Volcanic landscape near Castolon *(NPS Big Bend Visitor Photo Gallery)*
Mule Ear Peaks *(NPS Big Bend Visitor Photo Gallery)*

Geologic Map of Big Bend National Park, Texas

By Kenzie J. Turner, Margaret E. Berry, William R. Page, Thomas M. Lehman, Robert G. Bohannon, Robert B. Scott, Daniel P. Miggins, James R. Budahn, Roger W. Cooper, Benjamin J. Drenth, Eric D. Anderson, and Van S. Williams

Prepared in cooperation with the National Park Service

Scientific Investigations Map 3142

U.S. Department of the Interior
U.S. Geological Survey

U.S. Department of the Interior
KEN SALAZAR, Secretary

U.S. Geological Survey
Marcia K. McNutt, Director

U.S. Geological Survey, Reston, Virginia: 2011

For more information on the USGS—the Federal source for science about the Earth, its natural and living resources, natural hazards, and the environment, visit http://www.usgs.gov or call 1–888–ASK–USGS.

For an overview of USGS information products, including maps, imagery, and publications, visit http://www.usgs.gov/pubprod

To order this and other USGS information products, visit http://store.usgs.gov

Suggested citation:
Turner, K.J., Berry, M.E., Page, W.R., Lehman, T.M., Bohannon, R.G., Scott, R.B., Miggins, D.P., Budahn, J.R., Cooper, R.W., Drenth, B.J., Anderson, E.D., and Williams, V.S., 2011, Geologic map of Big Bend National Park, Texas: U.S. Geological Survey Scientific Investigations Map 3142, scale 1:75,000, pamphlet 84 p.

Contents

Figures

Tables

Geologic Map of Big Bend National Park, Texas

By Kenzie J. Turner,[1] Margaret E. Berry,[1] William R. Page,[1]
Thomas M. Lehman,[2] Robert G. Bohannon,[1] Robert B. Scott,[3]
Daniel P. Miggins,[1] James R. Budahn,[1] Roger W. Cooper,[4]
Benjamin J. Drenth,[1] Eric D. Anderson,[1] and Van S. Williams[1]

Introduction

The purpose of this map is to provide the National Park Service and the public with an updated digital geologic map of Big Bend National Park (BBNP). The geologic map report of Maxwell and others (1967) provides a fully comprehensive account of the important volcanic, structural, geomorphological, and paleontological features that define BBNP. However, the map is on a geographically distorted planimetric base and lacks topography, which has caused difficulty in conducting GIS-based data analyses and georeferencing the many geologic features investigated and depicted on the map. In addition, the map is outdated, excluding significant data from numerous studies that have been carried out since its publication more than 40 years ago.

This report includes a modern digital geologic map that can be utilized with standard GIS applications to aid BBNP researchers in geologic data analysis, natural resource and ecosystem management, monitoring, assessment, inventory activities, and educational and recreational uses. The digital map incorporates new data, many revisions, and greater detail than the original map of Maxwell and others (1967). Locations for features discussed in the text are shown in figures 1 and 2. Although some geologic issues remain unresolved for BBNP, the updated map serves as a foundation for addressing those issues.

Funding for the Big Bend National Park geologic map was provided by the United States Geological Survey (USGS) National Cooperative Geologic Mapping Program and the National Park Service. The Big Bend mapping project was administered by staff in the USGS Geology and Environmental Change Science Center, Denver, Colo. Members of the USGS Mineral and Environmental Resources Science Center completed investigations in parallel with the geologic mapping project. Results of these investigations (Gray and Page, 2008) addressed some significant current issues in BBNP and the U.S.-Mexico border region, including contaminants and human health (Gray and others, 2008), ecosystems (Shanks and others, 2008a), and water resources (Shanks and others, 2008b). Funding for the high-resolution aeromagnetic survey in BBNP, and associated data analyses and interpretation, was from the USGS Crustal Geophysics and Geochemistry Science Center. Mapping contributed from university professors and students was mostly funded by independent sources, including academic institutions, private industry, and other agencies.

[1]U.S Geological Survey, Denver, Colorado
[2]Texas Tech University, Lubbock, Texas
[3]U.S. Geological Survey, Corvallis, Oregon
[4]Lamar University, Beaumont, Texas

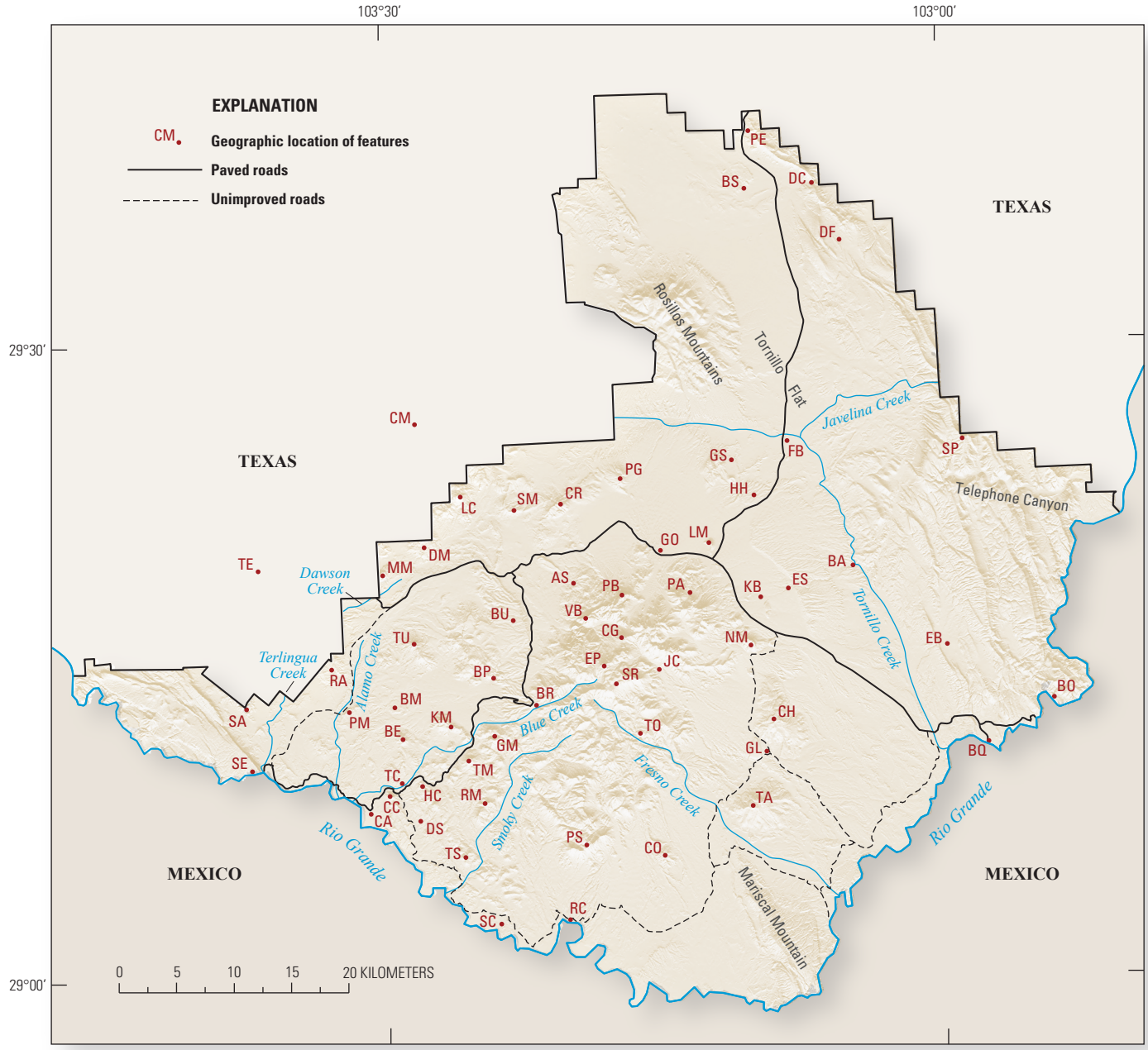

Figure 1. Index map of BBNP showing geographic location of features (keyed to red abbreviations) discussed in the text:

Ash Spring, AS
Bantu Shut-In, BA
Bee Mountain, BE
Black Mesa, BM
Blue Creek Ranch, BR
Bone Spring, BS
Boquillas Crossing, BQ
Boquillas Canyon, BO
Burro Mesa, BU
Burro Mesa Pouroff, BP
Casa Grande Peak, CG
Castolon, CA
Cerro Castellan, CC
Chilicotal Mountain, CH
Christmas Mountains, CM
Cow Heaven Mountain, CO
Croton Peak, CR
Dagger Flat, DF
De la Ho Spring, DS
Dog Canyon, DC
Dogie Mountain, DM
Emory Peak, EP
Ernst Basin, EB
Estufa Spring, ES
Fossil Bone Exhibit, FB
Glenn Spring, GL
Goat Mountain, GM
Grapevine Spring, GS
Government Spring, GO
Hannold Hill, HH
Horseshoe Canyon, HC
Juniper Canyon, JC
K-Bar Park housing, KB
Kit Mountain, KM
Little Christmas Mountain, LC
Lone Mountain, LM
Maverick Mountain, MM
Nugent Mountain, NM
Paint Gap Hills, PG
Panther Spring, PA
Pena Mountain, PM
Persimmon Gap, PE
Pulliam Bluff, PB
Punta de la Sierra, PS
Rattlesnake Mountain, RA
Round Mountain, RM
Reed Camp, RC
Santa Elena Canyon, SE
Sierra Aguja, SA
Sierra de Chino, SC
Slickrock Mountain, SM
South Rim, SR
Sue Peaks, SP
Talley Mountain, TA
Terlingua, TE
Tortuga Mountain, TO
Trap Mountain, TM
Triangulation Station Mountain, TS
Tuff Canyon, TC
Tule Mountain, TU
Vernon Bailey Peak, VB

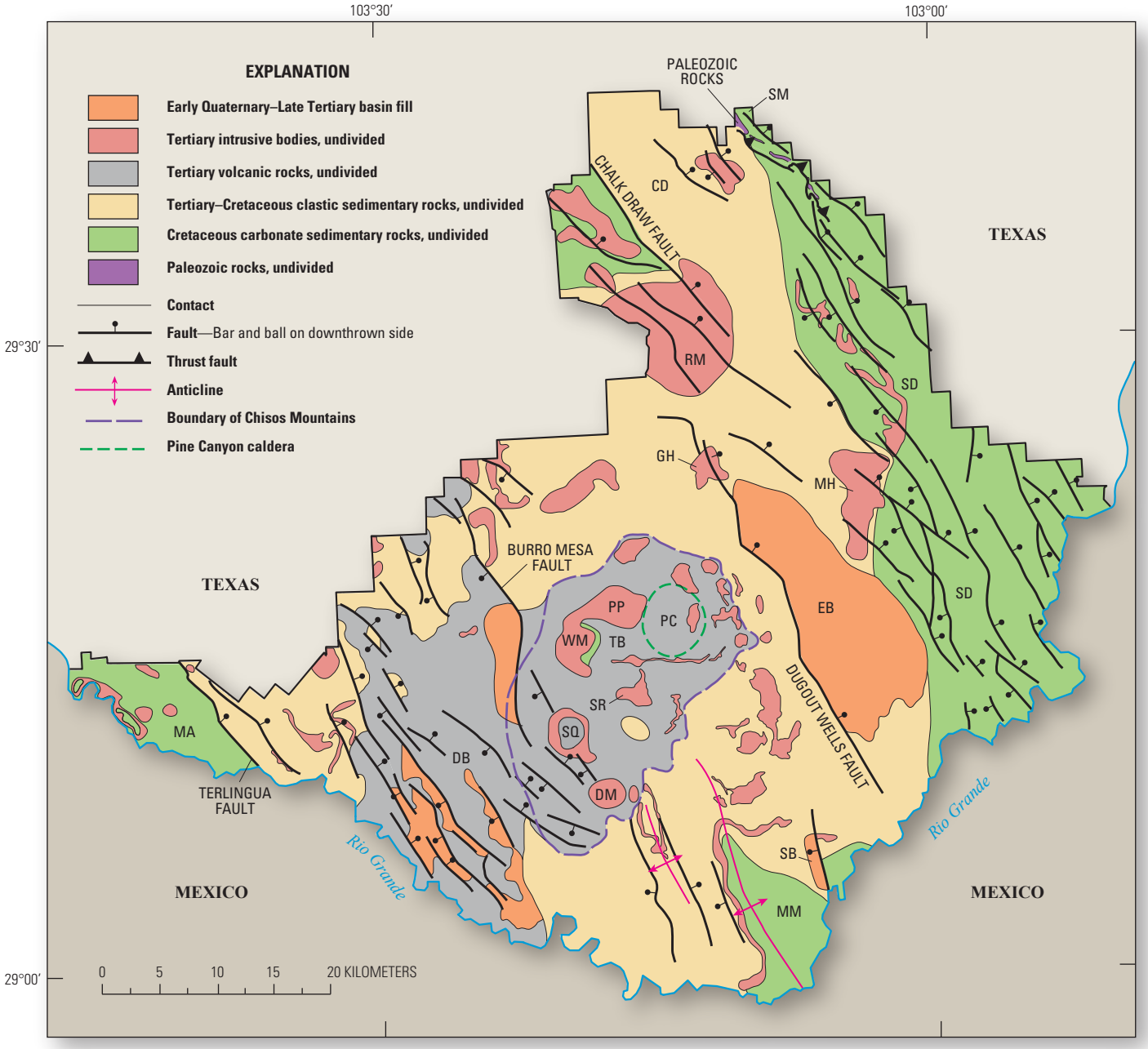

Figure 2. Generalized map of major structures and geographic features in BBNP. Features labeled on map include:

Chalk Draw basin, CD
Delaho bolson, DB
Dominguez Mountain, DM
Estufa bolson, EB
Grapevine Hills, GH
Mariscal Mountain, MM
Mesa de Anguila, MA
McKinney Hills, MH
Pine Canyon caldera, PC
Pulliam Peak, PP
Rosillos Mountains, RM
Santiago Mountains, SM
Sierra del Carmen, SD
Sierra Quemada, SQ
Solis basin, SB
South Rim, SR
The Basin, TB
Ward Mountain, WM

Prominent Researchers in the History of Big Bend Geology

Robert T. Hill

Robert T. Hill, U.S. Geological Survey geologist and father of Texas Geology, was one of the first to explore the Big Bend region in the 1899 survey of the canyons of the Rio Grande. Hill led a six man expedition from Presidio to Langtry, Texas, and published an article describing the survey in one of the first issues of Century Illustrated Magazine in 1901, titled "Running the cañons of the Rio Grande." Hill was hired by John Wesley Powell (first Director of the U.S. Geological Survey) in 1885. His expertise was stratigraphy of the Cretaceous rocks in Texas, and he discovered and defined the Comanchian series of the Lower Cretaceous system as a result of his Texas studies. In his career, he went on to author more than 100 publications on the geology of Texas and adjacent states, mineral deposits in Mexico, and the geology of Puerto Rico, Cuba, and Jamaica.

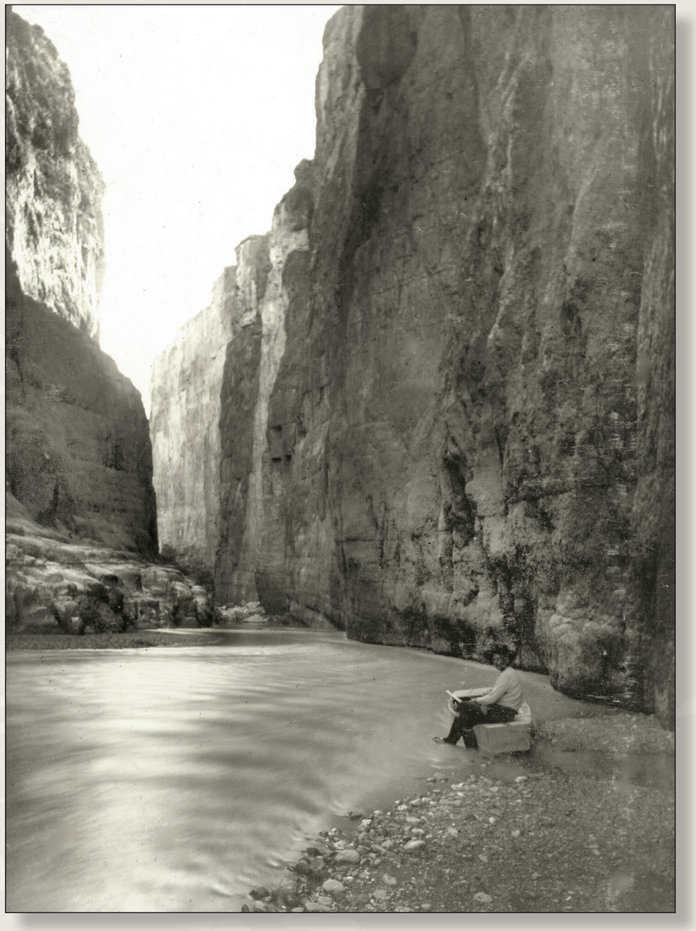

Member of the 1899 USGS expedition with boat in Santa Helena (Elena) Canyon, Big Bend National Park. The expedition was led by Robert T. Hill, USGS geologist.

Ross A. Maxwell

Ross A. Maxwell became the first superintendent of Big Bend National Park in 1944. As an effective administrator, Maxwell not only ran park operations, including the building of roads, but he also began mapping the park's geology. When he began mapping, the park had no paved roads, no electricity, and the nearest telephone was 100 miles away. Because no topographic maps existed then, the geologic information was superimposed on vintage planimetric maps that showed only approximate locations of roads, drainage patterns, and mountain peaks. By the late 1960s, Maxwell and his colleagues had published a remarkable geologic map and supporting text (Maxwell and others, 1967), and a geologic and cultural history of the park for the public (Maxwell, 1968). We recognize Ross A. Maxwell and his co-workers for their invaluable research contributions and map of Big Bend National Park.

Ross Maxwell, first superintendent of Big Bend National Park, shown here in the1980s.

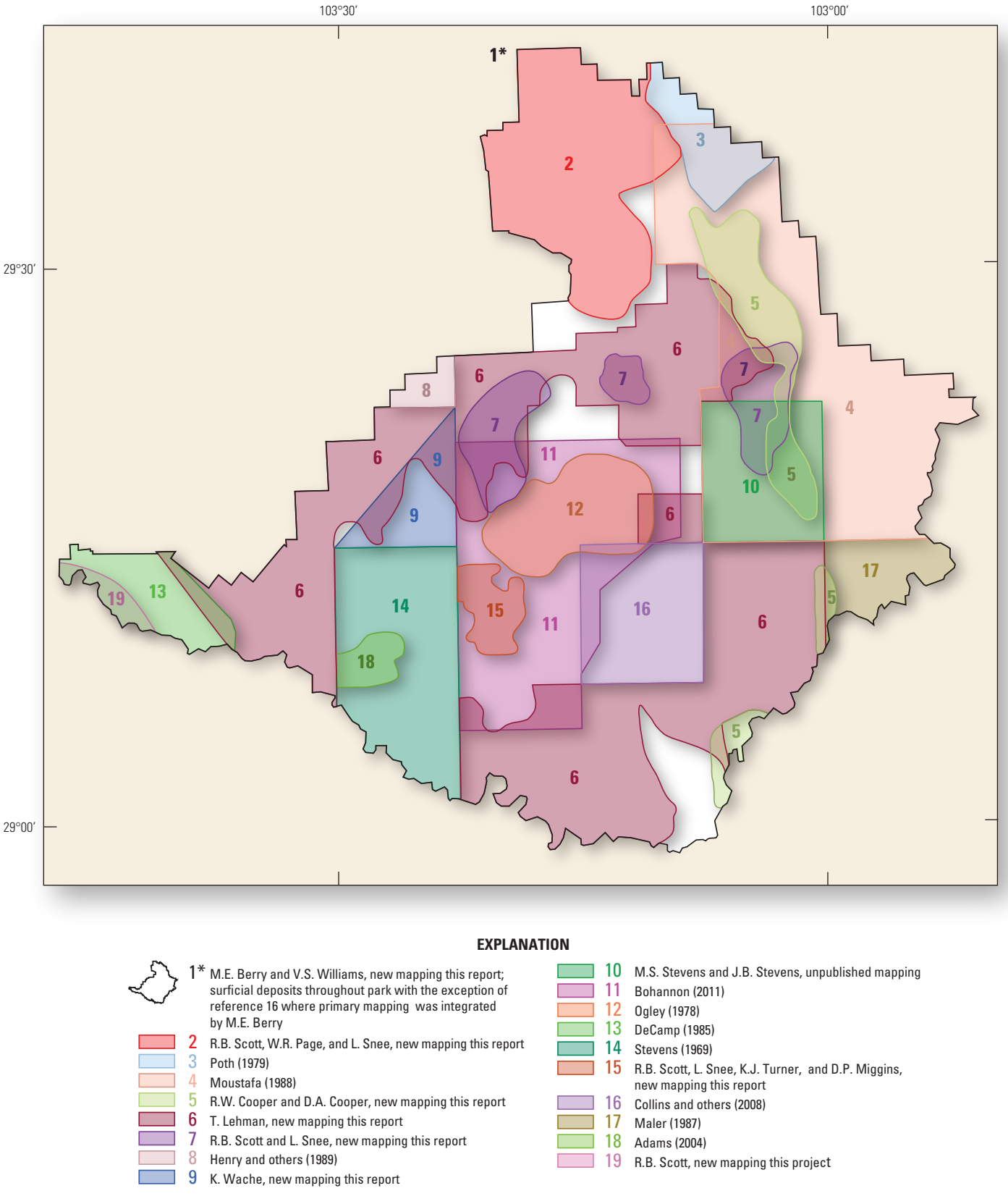

Figure 3. Index of geologic mapping used in map compilation.

Methods

The geologic map of BBNP (pl.) was compiled by combining geologic map data of many different authors from academia, Texas Bureau of Economic Geology, and USGS (fig. 3). Once existing mapping was digitally compiled, we evaluated the quality and consistency of each existing map by comparing it with digital orthophotographs, aerial photographs, and satellite imagery. Problem areas were identified and field checked, and unit contacts and structures were adjusted where necessary. In addition, as mapping was compiled into a comprehensive database, data gaps were identified and new mapping was completed in those areas.

The map includes incorporation of new geologic mapping of Upper Cretaceous to Eocene sedimentary rocks throughout BBNP (Lehman, 2002, 2004, 2007). New mapping was completed in the high Chisos Mountains that sheds new light on Sierra Quemada (Scott and others, 2007), and on the character of other volcanic features in this highly inaccessible, and rugged terrain (Bohannon, 2011). Other areas of new mapping include the recent northern addition to BBNP (the Harte Ranch section acquired in 1987), which includes parts of the Twin Peaks, Butterbowl, Persimmon Gap, and Bone Spring 7.5-minute quadrangles (R.B. Scott, W.R. Page, and L. Snee, unpub. mapping), and where little detailed mapping had been completed. Most of the new mapping for BBNP was carried out using traditional geologic mapping methods, which include extensive fieldwork and recording data using 1:40,000-scale color-infrared and black-and-white aerial photographs, and GPS technology. In most cases, mapping data were then transferred and georeferenced onto 1:24,000-scale topographic maps, and then converted to digital datasets.

The lack of detailed mapping of surficial deposits required extensive new mapping, which was completed for the entire BBNP with a combination of field and remote sensing techniques (Berry and Williams, 2004, 2007, 2008). Surficial geologic units were interpreted from stereoscopic pairs of 1:40,000-scale (color-infrared and black-and-white) aerial photographs, satellite imagery, and topographic data, and digitally mapped on color-infrared orthophotograph images with 1-meter ground resolution using VRone® mapping software; for some areas, a computerized PG-2 instrument in the Denver photogrammetry laboratory was used with 1:80,000-scale aerial photograph diapositive film to aid mapping. Surface morphology, tone, relative height above modern stream channel, and map pattern were used to interpret surficial geology from the imagery. Maps were printed on a topographic base and field checked, at which time soil, weathering, and pavement characteristics were used to refine interpretation of mapping units.

Material suitable for radiocarbon dating is scarce and Quaternary volcanic ashes have not been found in BBNP, so relative-age criteria were used to interpret age relations of the surficial deposits. Criteria used to evaluate relative age include relative height above the valley floor, which is higher for older surfaces where streams have incised; preservation state of depositional morphology, which is subdued through time by post-depositional processes; and amount of surface dissection, characteristics of desert pavement, soil development, and weathering, all of which tend to increase or change predictably through time. Stages of soil-carbonate morphology follow criteria outlined in Birkeland (1999), modified from Gile and others (1966, 1981) and Machette (1985). Age estimates for time divisions within the late Tertiary and Quaternary are based on the 2009 Geological Society of America Geologic Time Scale (Walker and Geissman, 2009), and supplemental information from Head and others (2008)[5], which place the base of the Quaternary at 2.6 Ma. This new mapping provides data critical in resource and ecosystem management activities in the park, including assessment, monitoring, inventory, groundwater studies, and in understanding the history of the Rio Grande.

Geologic mapping of volcanic and intrusive rocks was supported by $^{40}Ar/^{39}Ar$ and U-Pb isotopic age determinations and major and trace element analyses, and this report presents new age determinations in the appendix for 86 samples. To quickly access sample data in the appendix for discussion of the new isotopic age determinations in the report, we cross referenced the Map sample number listed in the first column of the table in the appendix. The new isotopic and geochemical data were critical in understanding and refining the complex volcanic stratigraphy and structure of BBNP, and will serve as a foundation for further geologic investigations. A more complete and comprehensive review of the new geochronologic and geochemical data for BBNP will be published at a later time.

[5]Pliocene, 5.3–2.6 Ma; early Pleistocene, 2.6 Ma–781,000 yr; middle Pleistocene, 781,000–126,000 yr; late Pleistocene, 126,000–11,700 yr; Holocene, 11,700–0 yr.

Oldest intermediate axial river deposits (Qiw3) of the Rio Grande preserved in isolated terrace 37 m above the Rio Grande floodplain; Sierra del Carmen in background. *(Photograph by Margaret E. Berry)*

Description of Map Units

Surficial Deposits

Eolian Deposits

Qe **Eolian sand (Holocene)**—Unconsolidated, moderately sorted, silty fine to medium sand, locally intermixed with small amounts of fine gravel likely introduced by surface wash or bioturbation. Very pale brown. Commonly forms small coppice dunes (nabkhas) around base of brushy vegetation; individual dunes too small to map separately. Thickness generally less than 1 m

Hillslope and Mass-Movement Deposits

Qrf **Rock fall deposits (Holocene and late Pleistocene)**—Generally unsorted, angular, cobble- to boulder-sized rock fragments forming talus on steep slopes. Thickness variable from about 2 m to more than 6 m

Qc **Colluvium and colluvial-fan deposits (Holocene and Pleistocene)**—Unconsolidated to moderately consolidated, unsorted to poorly sorted, unbedded to weakly bedded mixture of gravel, sand, silt, and clay, forming thin mantle or thicker fan-shaped accumulations of debris on the flanks of slopes. Cobble- to boulder-size clasts common. Clasts angular to subangular. Locally cemented by carbonate. Commonly ribbed and fluted due to various combinations of mass movement, rain splash, and wash processes active on slopes. Locally includes bedrock outcrops too small to map separately. Thickness variable from about 1 m to more than 6 m

Qls **Landslide deposits (Holocene and Pleistocene)**—Slumps, flows, and slides of bedrock, colluvium, and alluvium. Terrain typically hummocky or irregular with closed depressions and spires. Large areas of landslide deposits, such as at Chilicotal and Talley Mountains (Collins and others, 2007, 2008), represent multiple landslide events. Most likely Pleistocene in age. Thickness as much as 50 to 100 m

Spring Deposits

Qs **Spring deposits (Holocene and Pleistocene)**—Powdery to well-cemented, white, very pale-brown, light brownish-gray, or gray, fine-grained, spring-generated calcium carbonate mixed with fine sand and silt; locally nodular or laminated. Mapped mostly near Grapevine Spring and northwest of Kit Mountain. Thickness about 5 m near Grapevine Spring

Alluvial and Basin-Fill Deposits

Qaw **Active tributary wash and river deposits (latest Holocene)**—Unconsolidated gravel, sand, and silt deposited in active channels and flood plains of larger creeks and the Rio Grande. Light gray, light brownish gray, grayish brown, pale brown or very pale brown. In washes, deposits typically poorly to moderately sorted and poorly to moderately bedded. Cobble- and small boulder-size clasts common. Clasts subangular to subrounded, locally rounded. Braided channels and bar-and-swale topography common. Along the Rio Grande, deposits moderately to well sorted and moderately to well bedded, with subrounded to well-rounded clasts. Flood-plain deposits made up mostly of fine-grained sediment. Meander scroll topography common. Near Cottonwood Campground (west of Castolon), flood-plain deposits dating to within the last 17 years are at least 3.5 m thick (Dean and Schmidt, 2008)

Qyw1 **Younger of the young axial river deposits (Holocene)**—Differentiated from other types of alluvial deposits only along the Rio Grande. Forms low-level terraces generally within 3 m of active flood plain. Meander scroll topography commonly well preserved. Typically fine-grained deposits of unconsolidated to weakly consolidated sand and silt with pebble lenses and stringers. Near Boquillas Canyon, ^{14}C date on organic material from buried A horizon suggests that upper 2 m of alluvium at that locale was deposited within the last 3,000 yr (Mandel, 2002). Surfaces deflated locally by eolian processes, and covered in places by small dunes. Little or no pavement, varnish, or soil-carbonate development. Thickness 3 to 4 m or more

Qyw2 **Older of the young axial river deposits (Holocene to late Pleistocene)**—Differentiated from other types of alluvial deposits only along the Rio Grande. Unconsolidated to weakly consolidated, moderately to well-sorted, moderately to well-bedded gravel, sand, and silt forming low-level terraces generally 4–9 m above active flood plain. Limited preservation of meander scroll topography. Cobble- and small boulder-size clasts common; clasts typically subrounded to well rounded. Pavement moderately developed to densely packed and uniform with strong-brown, yellowish-red, dark reddish-brown, dark reddish-gray, and black varnish colors. Development of soil carbonate generally stage I^+ or less[6]. Thickness less than 1 m to about 4 m

Qya **Young alluvial deposits, undivided (Holocene to late Pleistocene)—**Pediment, fan, stream, and sheet-flow deposits. Unconsolidated to weakly consolidated, poorly to moderately sorted, poorly to moderately bedded gravel, sand, and silt. Cobble- and small boulder-size clasts common. Locally mostly silty sand or sandy silt with interspersed fine gravel. Clasts typically subangular to subrounded, locally angular or well rounded. Typically has low relative height where alluvial surfaces are incised. Elsewhere may veneer older deposits. Includes Qaw too narrow to map separately. Unit subdivided into Qya1 and Qya2 where divisions are evident and large enough to map separately. Thickness variable from less than 1 m to 8 m or more

Qya1 **Younger of the young alluvial deposits (Holocene)**—On or within several meters of valley floor. Occasionally flooded and (or) modified by sheet flow. Bar-and-swale topography and braided-channel morphology commonly well preserved. Surfaces deflated locally by eolian processes, and covered in places by dunes too small to map separately. Little or no pavement, varnish, or soil-carbonate development. Thickness variable from less than 1 m to 8 m or more

Qya2 **Older of the young alluvial deposits (Holocene to late Pleistocene)**—Typically elevated 3 m or more above valley floor. Limited preservation of bar-and-swale topography and braided-channel morphology. Surfaces commonly partly incised. Pavement weakly developed to densely packed and uniform. Pavement clasts lightly to well varnished with strong brown, yellowish-red, dark reddish-brown, and black varnish colors. Soil-carbonate development generally stage I or less. Thickness variable from less than 1 m to 8 m or more

Qiw **Intermediate axial river deposits, undivided (late and middle Pleistocene)**—Differentiated from other types of alluvial deposits only along the Rio Grande and upper Tornillo Creek. Weakly to moderately well-consolidated, moderately to well-sorted, moderately to well-bedded gravel, sand, and silt; sand locally crossbedded. In Rio Grande deposits, cobble- and small boulder-size clasts common to abundant. Clasts subrounded to well rounded. Some surface and subsurface clasts weathered. Unit subdivided into Qiw1, Qiw2, and Qiw3 where divisions are evident and large enough to map separately. Thickness commonly 3 to 4 m, but ranges from less than 1 m to more than 15 m

Qiw1 **Youngest intermediate axial river deposits (late Pleistocene)**—Terrace surfaces generally 12–18 m above Rio Grande flood plain. Surfaces typically broad and flat with a stage II soil-carbonate horizon, and a moderately to densely packed, uniform pavement. Pavement clasts moderately to well varnished; varnish colors typically strong brown, yellowish red, dark reddish brown, and black. Thickness commonly 3 to 4 m

Qiw2 **Older intermediate axial river deposits (late to middle Pleistocene)**—Terrace surfaces generally 18–25 m above Rio Grande flood plain. Surfaces typically broad and flat with a stage II to weakly cemented stage III soil-carbonate horizon 1 m or more thick, and a moderately to densely packed, uniform pavement. Pavement clasts moderately to well varnished; varnish colors typically strong brown, yellowish red and dark reddish brown. Thickness commonly 3 to 4 m

[6]In gravelly deposits, the progressive development of soil-carbonate morphology is described briefly as follows: Stage I—thin, discontinuous coatings of $CaCO_3$ are present on the bottom side of clasts. Stage II—$CaCO_3$ coatings are continuous around clasts; the soil matrix is mostly loose, but several clasts may be cemented together locally. Stage III—$CaCO_3$ is disseminated throughout the soil matrix, cementing the horizon and giving it a whitish color. Stage IV—thin laminar layers of almost pure $CaCO_3$ are present in the upper part of the horizon; the rest of the horizon is plugged with accumulated $CaCO_3$. For further discussion, see Birkeland (1999).

Qiw3 **Oldest intermediate axial river deposits (middle Pleistocene)**—Terrace surfaces generally 30–45 m above Rio Grande flood plain and about 40 m above upper Tornillo Creek flood plain. Surfaces vary from broad and flat to gently undulatory or irregular, with a stage I^+ to moderately-cemented stage IV soil-carbonate horizon, and a weak to well-formed uniform pavement. Where pavement well preserved, pavement clasts moderately to well varnished; varnish colors typically yellowish red and dark reddish brown. Thickness commonly 3 to 4 m

Qia **Intermediate alluvial deposits, undivided (late and middle Pleistocene)**—Pediment, fan, and stream deposits. Weakly to moderately well consolidated, poorly to moderately sorted, poorly to moderately bedded gravel, sand, and silt. Cobble- and small boulder-size clasts common to abundant. Clasts typically subangular to subrounded, locally angular or rounded. Typically has intermediate relative height where alluvial surfaces are incised. Surfaces typically uniform due to loss of bar-and-swale topography and braided channel morphology (smoothed by post-depositional surface processes); partly incised, and slightly rounded at the edges. Pavement weakly developed to densely packed and uniform. Varnish on pavement clasts ranges from almost none where pavement contains mostly limestone clasts, to moderately varnished with strong-brown, yellowish-red, and dark reddish-brown colors. Locally includes Qaw and Qya too narrow or small to map separately. Unit subdivided into Qia1 and Qia2 where divisions are evident and large enough to map separately. Seismic data indicate that on the northeast side of the Chisos Mountains, stacked alluvial sequences that include Qia and buried older alluvium (Qoa) reach total thicknesses in excess of 50 m (Monti, 1984). Thickness of Qia variable from less than 1 m to about 10 m

Qia1 **Younger of the intermediate alluvial deposits (late to middle Pleistocene)**—Typically has stage I–II soil-carbonate horizon 1–1.5 m thick. Less commonly has weak to moderately cemented stage III carbonate horizon 30–50 cm thick, especially where deposit contains mostly limestone clasts. Some surface clasts weathered and (or) split. Pediment surfaces generally 6–24 m above valley floor. Along Rio Grande, intertongues with, and grades into or overlaps Qiw1 and Qiw2 terraces. Thickness variable from less than 1 m to about 10 m

Qia2 **Older of the intermediate alluvial deposits (middle Pleistocene)**—Typically has weakly to moderately cemented stage III–IV soil-carbonate horizon 1 m or more thick. Weathered and (or) split surface and subsurface clasts common at some locales. Has higher relative height than Qia1 where alluvial surfaces are incised; pediment surfaces generally 12–40 m above valley floor. Along upper Tornillo Creek, grades to Qiw3 terrace. Thickness variable from less than 1 m to about 10 m

Qow **Old axial river deposits (middle to early? Pleistocene)**—Differentiated from other types of alluvial deposits primarily along the Rio Grande; mostly preserved as isolated terrace remnants 55 to 60 m above flood plain. Weakly to well-consolidated, poorly to moderately well sorted, moderately bedded gravel, sand, and silt; sand commonly cross-bedded. Pebble-, cobble-, and boulder-size clasts common to abundant. Clasts mostly subrounded to well rounded. Where preserved, soil has weakly cemented stage II^+–III soil-carbonate horizon; pavement moderately packed and uniform with strong-brown, yellowish-red, and dark reddish-brown varnish colors. Thickness typically 2 to 6 m

Qoa **Old alluvial deposits, undivided (middle to early? Pleistocene)**—Pediment, fan, and stream deposits. Typically moderately to well-consolidated, poorly to moderately sorted, poorly to moderately bedded gravel, sand, and silt. Cobble- and small boulder-size clasts common to abundant. Clasts typically subangular to subrounded, locally angular or rounded. Has higher relative height than Qia where alluvial surfaces are incised. Surfaces dissected into ridge and ravine (ballena) topography where gravel deposits are thick (in fans), or preserved as planar to gently undulatory remnants 30–50 m above valley floor where gravel deposits are thin (on pediments). Where preserved, soils have weakly to moderately cemented stage IV carbonate horizon 1–1.5 m or more thick. Weathered surface and subsurface clasts common. Pavement ranges from weakly developed to moderately packed and uniform. Varnish on pavement clasts ranges from none where pavement contains mostly limestone clasts, to moderately varnished with

yellowish-red and dark reddish-brown colors. Locally includes Qaw and Qya too narrow or small to map separately. Thickness variable from less than 1 m to about 15 m, but based on seismic data, may be as much as 30 m thick on the north side of the Chisos Mountains (Monti, 1984)

QTa **Very old alluvium (early Pleistocene and Pliocene)**—Mostly moderately to well-consolidated or indurated, poorly bedded, poorly to moderately sorted, alluvial-fan deposits of cobble gravel, sand and silt; clasts mostly subangular to subrounded. Also includes lesser amounts of moderately to well-consolidated, poorly to moderately sorted, poorly to moderately bedded, commonly crossbedded, gravelly stream deposits with subrounded to rounded clasts, and moderately consolidated, fine-grained deposits of possible playa-lake origin. Beds tilted near faults. Deposits eroded and deeply dissected to form ridge and ravine (ballena) topography. Surface soils, where preserved, have cemented stage III–IV carbonate morphology in horizons as much as 2 m thick. Includes informal Fingers formation (Burro Mesa area; Stevens, 1969, 1988; Stevens and Stevens, 1989), considered upper basin fill of the Delaho bolson (Lehman and Busbey, 2007), and informal Estufa Canyon formation (Stevens and Stevens, 1989, 2003; also called Estufa member by Thurwachter, 1984), comprising upper basin fill of Estufa bolson (lower Tornillo Creek area). In Sierra del Carmen, where very old alluvium has not been studied in detail, unit may also include some undifferentiated lower basin-fill deposits (Ta). Thickness 18 to 208 m for informal Fingers formation (Stevens, 1988), and about 284 m for informal Estufa Canyon formation (Stevens and Stevens, 1989)

Ta **Basin-fill deposits (Miocene)**—Alluvial-fan, stream, and playa deposits in fault-bounded basins (bolsons). Weakly to well-consolidated or indurated, poorly to moderately bedded, poorly to moderately sorted gravel, sand, silt, and clay. Formerly combined with Quaternary deposits by Maxwell and others (1967). Deeply dissected. Beds tilted by faulting; in Cerro Castellan area, dips as steep as 20°–35° reported (Maxwell and others, 1967). Clasts subangular to rounded. Near Castolon, deposits formally named Delaho Formation by Stevens and others (1969). Delaho Formation consists of pinkish- to brownish-buff siltstone, sandstone, mudstone, and gray conglomerate deposited in Delaho bolson (Stevens and Stevens, 1985, 1989). Lower (unnamed) member of Delaho Formation contains earliest Miocene vertebrate fossils of Castolon local fauna (Stevens and others, 1969; Stevens, 1977, 1991), and near De la Ho Spring, is interbedded near its base with thin basaltic flow dated by K-Ar method at 23.3 ± 0.6 Ma (Stevens, 1988; Stevens and Stevens, 1989). Upper Smoky Creek Member of Delaho Formation disconformably overlies lower member and contains few fossils but is proposed as late early Miocene (Stevens and Stevens, 1989) or middle? Miocene (Stevens, 1988) in age. In lower Tornillo Creek area, deposits named informal Banta Shut-in formation by Stevens and Stevens (1989, 2003; also called informal La Noria member by Thurwachter, 1984). Informal Banta Shut-in formation consists of pinkish- to reddish-buff sandstone and siltstone, red mudstone, and pinkish-gray conglomerate, deposited as lower basin fill in Estufa bolson. Contains late Miocene vertebrate fossils of the Screw Bean local fauna. Thickness about 670 m for Delaho Formation (Stevens, 1988), and 300 to 360 m for Banta Shut-in formation (Stevens and Stevens, 2003)

Tertiary Mass-Movement Deposits

Tgs **Gravity slide blocks (Miocene?)**—Blocks of Cretaceous limestone interpreted as gravity slide blocks (Maxwell and others, 1967; Poth, 1979) on southwest flank of the southern Santiago Mountains; age and origin unknown, but likely formed from uplift of Santiago Mountains related to Neogene basin-and-range faulting. Blocks consist mostly of Glen Rose Limestone, Boquillas Formation, and Buda Limestone, interpreted to have slid chiefly over Pen and Aguja Formations; stratigraphic order in blocks mostly preserved; 5 to 20 m thick

Undivided Surficial Deposits

QTu **Quaternary to Tertiary deposits, undivided (Holocene to Miocene)**—Shown in cross section only

Middle Tertiary Volcanic and Intrusive Rocks

Tv **Volcanic rocks, undivided (Oligocene)**—Volcanic rocks of unknown composition overlying units of South Rim Formation at northern end of Burro Mesa; about 60 m thick

Tirc **Intrusive complex at Rattlesnake Mountain (Oligocene)**—Black to greenish-black analcime-bearing monzonite sill; contains bodies of syenite related to in-place differentiation of monzonite liquid (Carmen and others, 1975). Monzonite comprises about 90 percent of intrusion; composed of 65–70 percent plagioclase and alkali feldspar, and ophitic augite, biotite, olivine, Fe-Ti oxides, analcime, and secondary minerals. Grain size varies from 0.5 mm at the chilled margin to 2–5 mm in the central zone. Syenite is lighter colored, medium to coarse hypoautomorphic to pegmatitic texture, composed of mostly alkali feldspar with lesser plagioclase, ophitic to subophitic pyroxene, amphibole, and accessory minerals (Carmen and others, 1975). K-Ar ages 28.6 ± 0.4 Ma and 27.9 ± 0.4 Ma (Henry and McDowell, 1986); sill about 80 m thick

Ti **Intrusive rocks, undivided (Oligocene to Eocene)**—Scattered intrusive bodies and dikes throughout park of unknown composition and includes intrusions of multiple compositions such as Pena Mountain (28.77 ± 0.08 Ma; appendix; 75; and 28.7 ± 0.4 Ma; appendix; 74), which is compositionally similar to intrusive complex at Rattlesnake Mountain (Tirc). Also shown in east end of cross section *B*-*B′* as undivided intrusive rocks

Tir **Rhyolitic and other felsic composition intrusive rocks, undivided (Oligocene to Eocene)**—Sills, dikes, and other irregular bodies with rhyolitic and other felsic compositions as defined below. Where chemical analysis available, includes rocks with SiO_2 greater than 63 percent (volatile-free), and where chemical analysis unavailable, composition based on determinations of Maxwell and others (1967) to include quartz syenite, quartz diorite, and granite. Unit mostly exposed southeast and northwest of Chisos Mountains. Isotopic age determinations range from 41.6 ± 0.4 Ma (Maverick Mountain; appendix; 85) to 28.1 ± 0.3 Ma (Tortuga Mountain; appendix; 72). Also includes intrusions at Chilicotal and Talley Mountains, Government Spring (33.0 ± 0.2 Ma; appendix; 84), Slickrock Mountain (31.7 ± 0.6 Ma; appendix; 80), Glenn Spring (30.22 ± 0.09 Ma; appendix; 77), and intrusion encompassing Paint Gap Hills and Croton Peak

Tia **Andesitic and other intermediate composition intrusive rocks, undivided (Oligocene to Eocene)**—Sills, dikes, and other tabular bodies with andesitic and other intermediate compositions as defined below. Where chemical analysis available, includes rocks with SiO_2 between 52 and 63 percent (volatile-free); where chemical analysis unavailable, composition based on determinations of Maxwell and others (1967) to include syenite, syenodiorite, diorite, and alkali syenite. Exposed north of Rosillos Mountains, north and west of Nugent Mountain (31.45 ± 0.18 Ma; appendix; 79), and southern end of Little Christmas Mountain

Tib **Basaltic and other mafic composition intrusive rocks, undivided (Oligocene to Eocene)**—Sills, dikes, and other tabular bodies with mafic compositions as defined below. Where chemical analysis available, includes rocks with SiO_2 less than 52 percent (volatile-free); where chemical analysis unavailable, composition based on determinations of Maxwell and others (1967) to include basalt, diabase, gabbro, syenogabbro, and trachydolerite. Includes intrusive bodies at Bone Spring, Dagger Flat, Mariscal Mountain, Cow Heaven Mountain, Mesa de Anguila, and north of Rosillos Mountains

Tfb **Basaltic flow (Oligocene)**—Lava flows overlying Burro Mesa Formation at Burro Mesa. Consists of several basaltic trachyandesite aa flows (Henry and others, 1989); microphenocrysts of highly altered olivine, biotite, minor amphibole; groundmass hypocrystalline with feldspar laths and altered olivine and opaques; dated at 29.53 ± 0.33 Ma and 29.10 ± 0.05 Ma (appendix; 1)

Burro Mesa Formation (Oligocene)—Includes rhyolite and Wasp Spring members, and related intrusive rocks, erupted from local vents in western BBNP (Henry and others, 1989; Holt, 1998; Adams, 2004). Descriptions from Becker (1976), Holt (1998), Adams (2004), and Benker (2005)

Tbr **Rhyolite member**—Blue-gray, rhyolitic ash-flow tuff and lava; contains anorthoclase and quartz phenocrysts and accessory minerals, including fayalite, arfvedsonite, acmite, and aenigmatite; upper part contains about 20 percent phenocrysts of anorthoclase with minor quartz and mafic inclusions (only present at Burro Mesa); rocks in lower part contain about 2 percent phenocrysts predominantly of alkali feldspar; lava often flow-banded and has ramp structures formed during emplacement of extrusive volcanic domes; dates range from 29.45 ± 0.08 Ma (appendix; 6) to 29.25 ± 0.07 Ma (appendix; 2); exposed at Burro Mesa, Goat and Kit Mountains, and in scattered outcrops between Castolon and Chisos Mountains; about 120 to 150 m thick at Burro Mesa

Tbw **Wasp Spring member**—Gray, yellowish-gray, and brownish-gray surge deposits, debris-flow breccia, and ash-flow tuff; unit has tuffaceous matrix with abundant lithic fragments, fiamme, and volcanic blocks and bombs; dates range from 29.48 ± 0.16 Ma (appendix; 10) to 29.27 ± 0.07 Ma (appendix; 7); thickest exposures in southern Burro Mesa area along Blue Creek; about 30 to 100 m thick

Tbi **Intrusive rocks, undivided**—Light-gray to blue-gray rhyolite, associated with plugs, domes, and dikes; mostly holocrystalline, fine- to medium-grained groundmass, and variably porphyritic with up to 15 percent phenocrysts of quartz and alkali feldspar commonly as glomerocrysts; interstitial arfvedsonite within groundmass; dike north of Blue Creek Ranch dated at 29.09 ± 0.07 Ma (appendix; 12), and intrusion west of Burro Mesa Pouroff dated at 29.03 ± 0.12 Ma (appendix; 11)

Tt **Trachytic lava, undivided (Oligocene)**—Black and dark-brown porphyritic trachyte, trachyandesite, and basaltic trachyandesite lava; basaltic trachyandesite groundmass has trachytic texture composed of plagioclase laths, opaque minerals, and altered pyroxene; phenocrysts include plagioclase and alkali-feldspar glomerocrysts, and altered pyroxene; trachyte and trachyandesite groundmass are intergranular to intersertal and composed of feldspar, clinopyroxene, and opaque minerals; phenocrysts include glomerocrysts of alkali feldspar with minor plagioclase and clinopyroxene. Trachyandesite likely stratigraphically below trachyte, relative stratigraphy of basaltic trachyandesite unknown; trachyandesite from Tuff Canyon dated at 30.42 ± 0.06 Ma (appendix; 15); trachyte from Goat Mountain dated at 30.29 ± 0.05 Ma (appendix; 14) and from Blue Creek Ranch area dated at 30.23 ± 0.11 Ma (appendix; 13). Present in southwestern part of BBNP north and west of Punta de la Sierra southward to Sierra de Chino where previously mapped as Tule Mountain Trachyandesite Member of Chisos Formation by Maxwell and others (1967); about 100 to 250 m thick

Sierra Quemada related rocks (Oligocene)—Intrusive complex in southern part of Chisos Mountains composed primarily of rhyolitic intrusive rocks (Duex and Tucker, 1989; Duex and others, 1994; Duex, 2007; Scott and others, 2007)

Tqd **Sierra Quemada ring dike**—Pink, mildly altered, porphyritic rhyolite with 20 to 30 percent phenocrysts and glomerocrysts of altered alkali feldspar and quartz; fine- to medium-grained groundmass with micrographic to granophyric texture; U-Pb zircon age of 29.93 ± 0.40 Ma (appendix; 21)

Tqi **Sierra Quemada intrusive rocks, undivided**—Pink rhyolite, dark-gray gabbro, and medium-gray syenite intrusive bodies; rhyolite typically in dike-like intrusions and similar in composition to ring dikes (Tqd); gabbro intrusions contain plagioclase, pyroxene, and alteration minerals, including epidote, sulfide, and possibly fibrous arfvedsonite; syenite is porphyritic and arfvedsonite-bearing and has glomerocrystic feldspar with resorbed edges; U-Pb zircon ages range from 31.09 ± 0.48 Ma (appendix; 23) to 29.06 ± 0.91 Ma (appendix; 19)

Tqv **Sierra Quemada vent breccia**—Light-pink, extremely lithic-rich volcanic breccia with minor rhyolitic ash matrix; lithic clasts consist of volcanic rocks, Cretaceous limestone, and Paleozoic rocks, and range in size from microscopic to Cretaceous limestone blocks 200 m in length; greater than 150 m thick in central part of Sierra Quemada

Dominguez Mountain related rocks (Oligocene)—Mafic to intermediate intrusive and volcanic complex to east of Punta de la Sierra, in southern Chisos Mountains (Maxwell and others, 1967; Bohannon, 2011). Extensive dike swarm associated with complex is best exposed on west side where dikes appear to merge upward with trachytic lavas (Tt) (Bohannon, 2011)

Tdm **Dominguez Mountain mafic lava flows**—Unstudied dark-gray to black lava flows and mafic tuff in core of Dominguez Mountain; flows are of basaltic to andesitic composition; in places, metamorphosed to dense hornfels

Tdd **Dominguez Mountain dike swarm**—Dikes consist of wide range of compositions, including granite, rhyolite, syenite, trachyte, gabbro, and basalt. Intermediate dikes are abundant, particularly southwest of volcanic center where they pass upward into trachyte flows at Punta de la Sierra. Most rocks are porphyritic; mapped as a discrete unit where dike-on-dike intrusion forms a wide body; maximum dike thickness about 10 m

Tdi **Dominguez Mountain intrusive rocks, undivided**—Light-gray to pale yellowish-brown rhyolite to dacite porphyry, but also includes more mafic compositions; rhyolite is fine-grained, vuggy, and contains sparse white subhedral feldspar phenocrysts. Intermediate to mafic composition intrusions are coarse-grained and porphyritic olivine syenodiorite and syenogabbro (Maxwell and others, 1967)

South Rim Formation (Oligocene)—Includes Emory Peak rhyolite, Boot Rock, and Pine Canyon rhyolite informal members and related intrusive rocks. Descriptions from Maxwell and others (1967), Barker and others (1986), Benker (2005), and White and others (2006)

Tse **Emory Peak rhyolite member**—Gray, welded, devitrified, rhyolite ash-flow tuff, lava, and vitrophyre erupted from intracaldera and extracaldera vents; lava is holocrystalline and with minor granophyric texture, and contains up to 12 percent euhedral anorthoclase and 12 percent quartz; ash-flow tuff and vitrophyre are eutaxitic with up to 2 percent phenocrysts of alkali feldspar; accessory minerals include biotite, magnetite, monazite, and zircon. Exposed at Emory Peak and in Blue Creek Ranch area. Dates range from 32.25 ± 0.07 Ma (appendix; 27) to 31.93 ± 0.13 Ma (appendix; 24); about 100 m thick

Tsb **Boot Rock member**—Gray to pinkish-gray quartz trachyte to rhyolite ash-flow tuff, lava flows, and maar surge breccia, erupted from intracaldera and extracaldera vents of the Pine Canyon caldera (Barker and others, 1986; White and others, 2006); lava has trachytic texture and ash-flow tuff is pilotaxitic to eutaxitic; contains less than 10 percent euhedral to subhedral anorthoclase and quartz phenocrysts, and trace amounts of clinopyroxene, ilmenite, and magnetite (Benker, 2005). Intracaldera units contain subangular quartz trachyte and rhyolite lithic fragments; overlies Pine Canyon rhyolite member (Tsp) in Pine Canyon caldera area. Extracaldera units poorly to non-welded, and consist mostly of breccia and ash-flow tuff; exposed in South Rim area and northern Burro Mesa. Dated at 32.33 ± 0.07 Ma (appendix; 29) and 32.17 ± 0.09 Ma (appendix; 28); about 100 to 120 m thick

Tsp **Pine Canyon rhyolite member**—Brown to light brownish-gray, densely welded, intracaldera rhyolitic tuff with pilotaxitic to eutaxitic texture; contains 2 to 7 percent euhedral to subhedral anorthoclase phenocrysts, and minor fayalite, apatite, hedenbergite, and ilmenite (Barker and others, 1986; Benker, 2005; White and others, 2006); exposed within Pine Canyon caldera; dated at 32.33 ± 0.07 Ma (appendix; 31) and 32.11 ± 0.23 Ma (appendix; 30); thickness from 300 to greater than 500 m

Tsr **Outflow deposits, undivided**—Includes unstudied outflow deposits, which may include Boot Rock and (or) Emory Peak rhyolite members; exposed west of Pulliam Peak and near Blue Creek Ranch

Tsd **Ring dike**—Reddish-brown to tan rhyolite with granophyric groundmass; contains 5 to 7 percent phenocrysts of quartz and sanidine and glomerocrysts of highly altered sanidine. Unit includes Hayes Ridge ring dike with a U-Pb zircon age of 32.6 ± 0.3 Ma, and an $^{40}Ar/^{39}Ar$ age on K-feldspar of 31.99 ± 0.32 Ma (appendix; 32); about 20 to 400 m thick

Tsi **Intrusive rocks, undivided**—Consists of pre- and post-caldera intrusive rocks; 1 to 7 percent phenocrysts of highly to mildly altered alkali feldspar, unaltered alkali feldspar, quartz with resorbed edges, and clinopyroxene, orthopyroxene, and euhedral arfvedsonite; groundmass varies from trachytic texture, with interstitial poikilitic alkali feldspar, to granular and micrographic texture; interstitial arfvedsonite common. Unit includes intrusions at Ward Mountain and Pulliam Peak (32.4 ± 0.4 Ma; appendix; 37), K-bar area (32.4 ± 0.3 Ma; appendix; 36), Nugent Mountain (31.5 ± 0.3 Ma, appendix; 33), Lone Mountain, Panther Spring, and other smaller intrusions in The Basin area

Tigh **Fayalite syenite of Grapevine Hills (Oligocene)**—Gray, fine- to medium-grained syenite; consists of euhedral phenocrysts of alkali feldspar, quartz, fayalite, and pyroxene; minor granophyric and porphyritic texture with phenocrysts of carlsbad-twinned alkali feldspar. U-Pb zircon age of 31.9 ± 0.2 Ma, and an $^{40}Ar/^{39}Ar$ age on K-feldspar at 31.62 ± 0.30 Ma (appendix; 81); about 200 m thick

Timh **Fayalite syenite of McKinney Hills (Oligocene)**—Blue to blue-green, fine-grained syenite; consists of subhedral phenocrysts of alkali feldspar, quartz, fayalite, augite, plagioclase, and hornblende. U-Pb zircon age of 32.2 ± 0.3 Ma (appendix; 83); individual bodies range from about 200 to 400 m thick

Tirm **Syenite of Rosillos Mountains (Oligocene)**—Blue to blue-green, fine- to medium-grained syenite; consists of euhedral to subhedral phenocrysts of alkali feldspar, augite, fayalite, and quartz. U-Pb zircon age of 32.1 ± 0.2 Ma (appendix; 82); about 200 to 600 m thick

Chisos Formation (Oligocene and Eocene)—Includes younger and older parts (table 1) described below. Rocks of younger part of Chisos Formation (Tcy) are widely exposed in western BBNP, but they also are exposed in the northeastern Chisos Mountains where they flank the Pine Canyon caldera, and unconformably overlie rocks of the older part of the Chisos Formation. Rocks of older part are restricted to the Chisos Mountains, east of Sierra Quemada and Burro Mesa

Tcy **Younger part, undivided (Oligocene and Eocene)**—Gray, white, red, pink, and brown tuffaceous clay, mudstone, sandstone, siltstone, tuff, conglomerate, and some lacustrine limestone. In western BBNP, base of unit defined by Alamo Creek Basalt, and variably includes lava and ash-flow members described below (Tcac, Tcas, Tcbm, Tcme, and Tctm). In Chisos Mountains, consists mostly of tuffaceous sedimentary rocks and most lava and ash-flow members present in western BBNP are absent, but base of unit is locally defined by Ash Spring Basalt Member north of Pulliam Bluff and west of Panther Spring, and between Ward Mountain and Burro Mesa; in most places in Chisos Mountains, however, tuffaceous sedimentary rocks of unit unconformably overlie sedimentary rocks of older part of Chisos Formation. Contains Eocene mammal and turtle bone fragments, and fresh water gastropods (Maxwell and others, 1967). $^{40}Ar/^{39}Ar$ ages on sanidine range from 42.31 ± 0.10 Ma (appendix; 62) to 32.96 ± 0.06 Ma (appendix; 38), and U-Pb zircon ages at 45.3 ± 0.7 Ma (appendix; 63) and 42.6 ± 0.4 Ma (appendix; 62). About 400 to 600 m thick

Tctm **Tule Mountain Trachyandesite Member (Oligocene)**—Brownish-gray porphyritic trachyte to trachyandesite lava; phenocrysts and glomerocrysts consist of skeletal plagioclase, alkali feldspar, clinopyroxene, and orthopyroxene. Exposed at Burro Mesa, Tule Mountain, and Sierra Aguja. $^{40}Ar/^{39}Ar$ ages on groundmass concentrate range from 33.88 ± 0.54 Ma (appendix; 40) to 33.18 ± 0.10 Ma (appendix; 39). About 20 to 60 m thick

Tcbm **Bee Mountain Basalt Member (Oligocene)**—Dark-gray, fine- to medium-grained, vesicular to nonvesicular, basalt to basaltic trachyandesite lava; includes phenocrysts of plagioclase, olivine, and clinopyroxene. Vesicles often filled with secondary minerals of calcite, zeolite, and microcrystalline quartz. In southwestern BBNP, consists of several flows above and below Mule Ear Spring Tuff Member. Dates range from 34.03 ± 0.17 Ma (appendix; 52) to 33.07 ± 0.15 Ma (appendix; 41); about 90 m thick in Blue Creek Ranch area, and 160 m at Bee Mountain and south of Cerro Castellan (Maxwell and others, 1967)

Tcme **Mule Ear Spring Tuff Member (Oligocene)**—Gray, brown, and red, densely to poorly welded, silicified ash-flow tuff; phenocrysts of alkali feldspar, biotite, and clinopyroxene. Generally overlain and underlain by tuffaceous sedimentary units, but in places in contact with Bee Mountain Basalt Member (Tcbm) above or below. Dates range from 33.67 ± 0.09 Ma (appendix; 47) to 33.64 ± 0.08 Ma (appendix; 43); about 2 to 3 m thick

Tcl **Undifferentiated lava flows (Eocene)**—Lava flows east of Burro Mesa mapped by Maxwell and others (1967) as undifferentiated lava; lava is dark gray, porphyritic with fine-grained groundmass; phenocrysts include large plagioclase laths up to 2 cm in length, and completely altered pyroxene and olivine. Dated at 38.87 ± 0.09 Ma (appendix; 53). About 20 m thick

Tcas **Ash Spring Basalt Member (Eocene)**—Dark-gray, porphyritic, fine-grained basaltic to trachyandesitic lava, with large white plagioclase laths from 1 to 2 cm long, and equant plagioclase grains and glomerocrysts; also contains olivine and pyroxene. $^{40}Ar/^{39}Ar$ age on groundmass concentrate of 40.92 ± 0.07 Ma (appendix; 58). Exposed in northern and western Chisos Mountains, and in Tule Mountain and Kit Mountain areas. About 30 m thick

Tcac **Alamo Creek Basalt Member (Eocene)**—Dark-gray, dense, fine-grained basalt to trachybasalt, and basaltic trachyandesite to trachyandesite; scoriaceous in places. Consists of several flows; locally, some of the flows are porphyritic and contain plagioclase phenocrysts and glomerocrysts, but in other places, such as the Alamo Creek area, lacks visible phenocrysts. Dates range from 47.09 ± 0.33 Ma (appendix; 71) to 44.41 ± 0.22 Ma (appendix; 64). Defines base of Chisos Formation in western BBNP; about 30 to 60 m thick

Older part, undivided (Eocene)—Includes 3 informal units of Bohannon (2011) described below. Restricted to Chisos Mountains, east of Sierra Quemada and Burro Mesa. Unconformably overlies Aguja Formation in southern Chisos Mountains, and Black Peaks Formation on eastern flank of Chisos Mountains

Tco **Older part, undivided**—Shown in cross section only and includes units described below

Tcstr **Sandstone, tuff, and rhyolite unit**—Brown sandstone with accessory tuffaceous sandstone and rhyolite. Bedding is mostly parallel with even bedding surfaces and uniform bed thickness maintained over large distances. Many beds cross-stratified internally, others are more massive. Some beds have a conglomeratic base with clasts typically of limestone. Sand grains are mostly quartz; fragments of tuff and glass shards are abundant in places. Present in Fresno Creek area, south of Hayes Ridge, and around perimeter of Pine Canyon caldera; 690 m thick

Tcks **Siltstone unit**—Greenish, purplish, and gray siltstone, probably derived from Upper Cretaceous Javelina Formation (Kj), and white to brown quartz-rich beds that are probably altered and silicified air-fall tuff beds; unit altered to hornfels near Juniper Canyon. Intertongues with map unit Tcstr; thickness is variable with a maximum of 175 m near Juniper Canyon on the east flank of Chisos Mountains

Tcrt **Rhyolite tuff unit**—Light-pink to light-gray rhyolite tuff; fine-grained to very fine grained; in discontinuous, irregular beds a few centimeters to a few tens of centimeters thick; characteristically contains small (1–2 cm) medium-gray globular concretions. Most glass shards altered to clay. Also includes silt and clay with parallel, continuous, and even bedding, and interbedded layers of air-fall tuff and siltstone; tuff and siltstone beds are parallel to one another and are 3–50 cm thick, and bedding surfaces are even and beds are uniform in thickness. Beds of each lithology are internally laminated. Sandy lenses as thick as 1–2 m occur locally. Disconformably overlies metamorphosed Aguja Formation; present between Fresno Creek and Dominguez Mountain. About 65 m thick

Tx **Christmas Mountains related volcanic rocks (Eocene)**—Orangish-gray air-fall and ash-flow tuff, lava, and debris flows associated with initial eruptive events of the Christmas Mountains caldera complex; tuff is rhyolitic with up to 30 percent pumice, alkali feldspar phenocrysts, and sparse biotite; lava is porphyritic quartz trachyte with up to 20 percent alkali feldspar phenocrysts and altered pyroxene; groundmass has trachytic texture composed of alkali feldspar and interstitial to poikilitic quartz. K-Ar dates range from 42.8 ± 0.9 to 41.2 ± 0.9 Ma (Henry and others, 1989). About 246 m thick at Little Christmas Mountain, and about 40 m thick at Dogie Mountain

Lower Tertiary to Lower Cretaceous Sedimentary Rocks

Tc **Canoe Formation (Eocene)**—Light-gray, reddish-gray, brownish-gray, and yellowish-gray sandstone and conglomeratic sandstone, purple and gray tuffaceous mudstone and claystone, gray to whitish-gray nodular tuff, basaltic lava, and minor limestone at top of unit. Tuffaceous sediments and tuff dominate upper part of formation; base includes 10-m-thick Big Yellow Sandstone Member (Maxwell and others, 1967), consisting of fine- to coarse-grained sandstone; conglomeratic at base. Vertebrate fossils (Maxwell and others, 1967; Runkel, 1988; Busbey and Lehman, 1989; Lehman and Busbey, 2007), including a wide variety of mammals, some crocodile and turtle bones, and petrified wood. Unit mostly exposed in Tornillo Flat, but includes several small exposures in Estufa Spring and Dawson Creek areas. About 350 m thick

Thh **Hannold Hill Formation (Eocene)**—Mostly gray and red mudstone, and gray to reddish-brown conglomeratic sandstone; also contains some lignite beds and calcareous nodules. Unit subdivided into following units (Beatty, 1992), from top to base: upper mudstone, upper conglomeratic sandstone, lower mudstone, and Exhibit Sandstone Member, a basal conglomeratic sandstone. Exhibit Sandstone Member consists of conglomeratic sandstone with clasts of Cretaceous limestone, chert, sandstone, oyster shell fragments, and petrified wood. Unit contains abundant vertebrate fossils (Maxwell and others, 1967; Hartnell, 1980; Busbey and Lehman, 1989; Lehman and Busbey, 2007). Unit exposed in Tornillo Flat area where it is unconformable with overlying Canoe Formation, and as much as 70 m thick

TKbp **Black Peaks Formation (Paleocene to Upper Cretaceous)**—Mostly variegated gray, black, red, and white mudstone, and interbedded white, light-gray, grayish-brown, and yellowish-gray, medium- to coarse-grained, partly conglomeratic sandstone; also includes freshwater limestone about 65 m above base containing gastropods and pelecypods. Sandstone contains reddish-brown "cannonball" concretions. Upper contact with Hannold Hill Formation disconformable; base of formation is marked by conglomeratic, crossbedded sandstone. Formation contains vertebrate fossils, including dinosaur, turtle, and crocodile bones, fish scales and bones, Paleocene mammals, and petrified logs and wood fragments (Maxwell and others, 1967; Schiebout, 1974; Schiebout and others, 1987; Busbey and Lehman, 1989; Lehman and Busbey, 2007). About 300 to 400 m thick

Kj **Javelina Formation (Upper Cretaceous)**—Variegated, gray, brown, red, and purple calcareous mudstone, and yellowish-gray, yellowish-brown, and dark-brown, lenticular, crossbedded, partly conglomeratic sandstone. Mudstone contains calcareous nodules associated with paleosol zones; unit contains vertebrate fossils (Maxwell and others, 1967; Busbey and Lehman, 1989; Lehman and Busbey, 2007) and petrified wood; tuff bed in middle part of formation dated at 69.0 ± 0.9 Ma (Lehman and others, 2006); formation conformable with overlying Black Peaks Formation, and is about 100 to 200 m thick

Ka **Aguja Formation (Upper Cretaceous)**—Consists of six informal members described below in descending order (Lehman, 1985): (1) upper shale member is light- to dark-gray and reddish shale and mudstone, and interbedded light-brown to reddish-brown sandstone near top; mudstone is carbonaceous and lignitic, and contains some petrified tree stumps; (2) Terlingua Creek sandstone is light-gray, calcareous, fine- to medium-grained sandstone, and some light-gray shale and lignite interbeds; (3) middle shale member is light-gray to dark-gray, calcareous, carbonaceous, and lignitic shale; (4) Rattlesnake Mountain sandstone member is mostly light-gray, fine-grained, calcareous sandstone; sandstone is ripple marked and trough crossbedded, and contains oysters and *Ophiomorpha* burrows; (5) lower shale member is light-gray to dark-gray, laminated, silty, carbonaceous shale, and some brown and gray sandstone and siltstone; contains some coal and lignite, and reddish-brown concretions and oysters; and (6) basal sandstone member consists of yellowish-gray to dark reddish-brown, fine-grained, calcareous sandstone; contains some conglomeratic beds near base with light-gray claystone clasts derived from underlying Pen Formation. Formation contains vertebrate fossils and petrified tree stumps (Maxwell and others, 1967; Busbey and Lehman, 1989; Lehman and Busbey, 2007). Mafic pyroclastic deposits in uppermost part of formation dated at 76.9 ± 1.2 Ma (Breyer and others, 2007; Befus and others, 2008). Upper contact with Javelina Formation is gradational and placed at the top of sandstone beds in the Aguja, which are overlain by predominantly variegated mudstone of the Javelina. Combined maximum thickness about 100 to 280 m thick

Kp **Pen Formation (Upper Cretaceous)**—Mostly light-gray, yellowish-gray, and yellowish-brown claystone, and some sandstone and chalk; claystone is calcareous and sandy. Unit contains yellowish-gray to dark-brown concretions, up to 1 m in diameter, some which form layers, and others that are isolated; concretions are sandy and fossiliferous. Formation includes sandstone beds, up to 1.5 m thick, which increase in number and thickness upward; sandstone beds near top of formation contain gastropods and bivalves. Upper contact with Aguja Formation is gradational and intertonguing with Aguja sandstone units. Formation contains ammonites, pelecypods, and gastropods. Forms slope and about 100 to 230 m thick

Kb **Boquillas Formation, undivided (Upper Cretaceous)**—Thin-bedded, medium-gray, light-gray, yellowish-gray, and brownish-gray limestone, shale, claystone, marl, chalk, and very minor siltstone and sandstone. Contact with overlying Pen Formation gradational (Lehman, 1985); contact with underlying Buda Limestone is sharp and disconformable, and marked by a distinctive color change from gray tones in Buda Limestone to light-brown tones in the lowermost Boquillas Formation. Formation contains abundant inoceramids, as well as ammonites, echinoids, cephalopods, foraminifera, and fish bones. Unit subdivided into San Vicente and Ernst Members in areas along the western flank of Sierra del Carmen, and near Sierra San Vicente and Mariscal Mountain, but in other areas of BBNP, unit mapped undivided. About 220 to 245 m thick

Kbs **San Vicente Member**—Medium-gray, finely crystalline, thin-bedded limestone, and brownish-gray and yellowish- to light-gray claystone, calcareous shale, marl, and chalk. Limestone is argillaceous and chalky; claystone is calcareous and contains some clay minerals including kaolinite, montmorillonite, and illite; about 145 m thick

Kbe **Ernst Member**—Mostly medium-gray, finely crystalline, thin-bedded silty limestone, and brownish-gray to light-brown calcareous shale, and some siltstone, claystone, and marl. Top of member marked by brown-weathering limestone and shale beds that contain *Allocrioceras hazzardi* Zone (Cooper, 2000; Cooper and others, 2007, 2008); about 75 to 100 m thick

Kbd **Buda Limestone and Del Rio Clay, undivided (Upper Cretaceous)**—Unit shown in cross section only

Kbu **Buda Limestone (Upper Cretaceous)**—Consists of an upper cliff-forming limestone, a middle slope-forming marly limestone, and a lower cliff-forming basal limestone; upper limestone thicker than lower limestone. Upper and basal limestones are white to light-gray, finely crystalline, partly burrowed, massive bedded, and have distinctive conchoidal fractures; middle marly limestone is light gray, nodular, and dense. Formation contains gastropods and pelecypods. Contact with overlying Boquillas Formation is unconformable. Exposed in southern Santiago Mountains, Sierra del Carmen, Mariscal Mountain, and Mesa de Anguila; about 20 to 30 m thick

Kdr **Del Rio Clay (Upper Cretaceous)**—Pale-red, yellowish-gray, and light-gray claystone, interbedded dark yellowish-orange to moderate yellowish-brown, thin-bedded to laminated limestone, and some yellowish-brown, friable sandstone; formation is limonitic. Limestone contains abundant benthic foraminifera (*Haplostiche texana* most common) and ammonite shell fragments. Contact with overlying Buda Limestone is sharp. About 36 m thick in Dog Canyon area, 30 m thick in the Mesa de Anguila area, and only about 1.5 m thick in Sierra Del Carmen near the Rio Grande, where basal parts of formation are absent (Maxwell and others, 1967)

Kse **Santa Elena Limestone (Lower Cretaceous)**—Light-gray, thin- to thick-bedded, finely crystalline limestone and some yellowish-gray marly limestone, and brown chert nodules; contains abundant silicified rudistids and some gastropods. Forms massive cliffs and exposed in Sierra del Carmen, Mariscal Mountain, and Mesa de Anguila; about 225 m thick

Ksp **Sue Peaks Formation (Lower Cretaceous)**—Upper part is light-gray nodular, thin-bedded limestone and interbedded yellowish-gray shale. Middle part is a 6-m-thick massive gray limestone ledge. Lower part is yellowish-gray marly shale and lesser amounts of thin-bedded, nodular limestone. Unit contains gastropods, echinoids, and ammonites. Unit forms slope between the more resistant Santa Elena Limestone above and the Del Carmen Limestone below. About 76 m thick in Sierra del Carmen and 80 m thick in Santa Elena Canyon

Kdc **Del Carmen Limestone (Lower Cretaceous)**—Massive cliff-forming, light-gray to yellowish-gray, finely crystalline limestone and brown chert layers and nodules. Unit contains rudistids and ammonites. Sharp contact with underlying Telephone Canyon Formation. About 100 m thick in Sierra del Carmen and Santiago Mountains, and 144 m thick in Mesa de Anguila area

Ktm **Telephone Canyon Formation and Maxon Sandstone, undivided (Lower Cretaceous)**—Telephone Canyon Formation is alternating yellowish- to brownish-gray nodular limestone and yellowish-gray marl; contact with overlying Del Carmen Limestone sharp and disconformable. Maxon Sandstone is reddish-weathering, fine-grained, calcareous, silty sandstone; lower and upper contacts gradational with underlying Glen Rose Limestone and overlying Telephone Canyon Formation (Poth, 1979); Maxon reported to be about 3 m thick in BBNP (Maxwell and others, 1967). Combined unit forms slope between more resistant Glen Rose Limestone below and Del Carmen Limestone above; exposed in Santiago Mountains, Sierra del Carmen, and Santa Elena Canyon area; about 20 to 45 m thick

Kgr **Glen Rose Limestone (Lower Cretaceous)**—Most of unit consists of alternating resistant limestone and less resistant marl beds. Limestone is medium to light gray, finely to medium crystalline, and mostly thick bedded, and includes interbeds of light-brown marl; contains pelecypods, gastropods, and echinoids. Basal 20 m of unit consists of pale-red pebble to cobble conglomerate and interbedded gray and red sandstone, and pale-red claystone. Conglomerate is crudely bedded with some clast imbrication and graded bedding; clasts are subangular to subrounded and consist mostly of gray sandstone, siltstone, and mudstone derived from underlying Tesnus Formation. A 10-m-thick nodular limestone unit above basal conglomerate and clastic beds contains a distinctive coquina of the oyster *Exogyra quitmanensis*. Unit exposed in Santiago Mountains where it unconformably overlies Pennsylvanian–Mississippian Tesnus Formation, and in Sierra del Carmen; about 100 to 150 m thick

Paleozoic Rocks

Pzu **Paleozoic rocks, undivided (Lower Pennsylvanian through Ordovician)**—Mapped where individual units could not be subdivided. Includes parts of units described below, but some exposures may include parts of older units including the Lower Ordovician Marathon Limestone and Alsate Shale (Maxwell and others, 1967); exposed in southern Santiago Mountains and southeast of Dog Canyon. Unit shown in cross section as Paleozoic rocks, undivided

IPMt **Tesnus Formation (Lower Pennsylvanian and Upper Mississippian)**—Shale, sandstone, and siltstone. Shale is black, brown, and gray, and sandstone and siltstone is light gray to light brown. Pebble conglomerate at base of unit about 0.3 m thick and consists of subangular chert clasts derived from Caballos Novaculite below; unconformable with underlying Caballos Novaculite. Unit exposed in Persimmon Gap area; about 150–200 m thick; incomplete thickness

MOu **Mississipian to Ordovician rocks, undivided**—Includes the Caballos Novaculite (Mississippian to Silurian) and Maravillas Formation (Upper and Middle Ordovician). Caballos Novaculite is novaculite, chert, and some shale. Upper part is black to brown thin-bedded to laminated chert with interbeds of brown silicious shale. Lower part is light-gray to white novaculite that forms resistant ledge; Caballos Novaculite unconformable with underlying Maravillas Formation and about 20 m thick. Maravillas Formation includes limestone and alternating chert, and interbedded shale. Upper 10 to 12 m includes Persimmon Gap Shale of Wilson (1954), which consists of interbedded reddish-weathering shale and black chert of Late Ordovician age. Below Persimmon Gap Shale is alternating limestone and interbedded chert. Limestone is medium gray, finely to medium crystalline, and thin bedded; some beds contain silicified brachiopod, crinoid, and bryozoan fragments; limestone beds contain Late Ordovician conodonts including *Amorphognathus ordovicicus*, *Belodina*, *Oistodus venustus*, *Panderodus gracilis*, *Panderodus unicostatus*, and *Phragmodus undatus* (Page and Harris, 2007). Chert is black and thin bedded to laminated. Exposed in Persimmon Gap area of Santiago Mountains; about 60 to 80 m thick; base not exposed

Stratigraphy

Paleozoic Rocks

Paleozoic rocks in the park are exposed near Persimmon Gap (fig. 1), and include the upper part of the Middle to Upper Ordovician Maravillas Formation, the Lower Silurian to lowermost Mississippian Caballos Novaculite, and part of the Upper Mississippian-Lower Pennsylvanian Tesnus Formation. Maxwell and others (1967) reported some exposures of flaggy limestone and shale in the Santiago Mountains southeast of Persimmon Gap that they tentatively identified as parts of Lower Ordovician Marathon Limestone and Alsate Shale. Because these rocks lack positive identification, and they may include parts of the units listed below, they were mapped on the plate as Paleozoic rocks, undivided (Pzu). Paleozoic rocks are well exposed in the Marathon Basin north of the map area (Barnes, 1979; Anderson and others, 1982), and like the Persimmon Gap section, they are deformed by northwest directed thrust faults related to the Paleozoic Ouachita-Marathon-Sonora orogeny (Maxwell and others, 1967; Poole and others, 2005).

The Middle and Upper Ordovician Maravillas Formation consists of chert, limestone, and some shale and interbedded chert at the top (Persimmon Gap Shale of Wilson, 1954). The Persimmon Gap Shale was originally mapped with the Caballos Novaculite by Maxwell and others (1967), but because of its Late Ordovician age, it probably shares greater affinity to the Maravillas Formation. The limestone beds in the Maravillas contain silicified brachiopods, crinoids, and bryozoans, and conodonts, including representatives of *Amorphognathus ordovicicus* Branson & Mehl, *Belodina* sp. (of Late Ordovician morphotype), *Oistodus venustus* Stauffer, *Panderodus gracilis* Branson & Mehl, *Panderodus unicostatus* Branson & Mehl, *Periodon aculeatus* Hadding (likely reworked), *Phragmodus undatus* Branson & Mehl, and *Protopanderodus insculptus* Branson & Mehl (Page and Harris, 2007). These taxa are known from many collections of Late Ordovician age in North America from the eastern Appalachians westward through the Great Basin.

Alternating limestone and chert beds in the Maravillas Formation at Persimmon Gap. *(Photograph by William R. Page)*

With the exception of the panderodids, most of the conodonts are incomplete to fragmentary and include a mix of shallow- to deep-water taxa that indicate relatively high-energy post-mortem transport basinward. The Maravillas Formation was likely deposited in a deep-water, basinal environment based on the fragmented and reworked nature of the fauna in combination with the occurrence of both shallow and deep water forms (McBride, 1989; Poole and others, 2005; Page and Harris, 2007).

The Caballos Novaculite consists of novaculite and some shale, and is Silurian to Mississippian in age based primarily on radiolarians (Noble, 1994; Poole and others, 2005). Because the Caballos Novaculite is only 20 m thick in the map area, we combined it with the Maravillas Formation on the plate (MOu). The formation forms a resistant ledge in the Persimmon Gap area, and like the Maravillas Formation, was deposited in a deep-water environment (Poole and others, 2005).

The Mississippian–Pennsylvanian Tesnus Formation consists of shale, siltstone, and sandstone, and it locally includes a pebble conglomerate (consisting mainly of Caballos Novaculite clasts) at the base. The age of the Tesnus Formation is based mainly on conodonts identified from the formation in the Marathon Basin (Ellison and Powell, 1989); fossil plants of Pennsylvanian age were also reported from the formation in the Marathon Basin (Maxwell and others, 1967). The Tesnus Formation is synorogenic flysch deposited in front of the advancing Marathon orogenic belt (Poole and others, 2005). The top of the formation is not exposed in BBNP.

Lower Cretaceous to Lower Tertiary Sedimentary Rocks

The Glen Rose Limestone (Kgr) consists of a basal clastic sequence of conglomerate, sandstone, and claystone, and an overlying sequence of alternating limestone and marl beds that make up a majority of the formation. A distinctive oyster coquina (*Exogyra quitmanensis)* is present about 5 m above the top of the clastic sequence near the Persimmon Gap area; the lower part of the formation is not exposed in the Santa Elena Canyon area, so the extent of this coquina marker horizon is unknown southward in BBNP. The formation also contains other pelecypods, gastropods, and echinoids. The carbonate rocks of the Glen Rose were deposited in a shallow, open-shelf environment (Smith, 1981), and the lower clastic units were interpreted as nearshore facies resulting from northward retrogradation of the coastal environments (Maxwell and others, 1967). The Glen Rose Limestone unconformably overlies Paleozoic rocks in the region, and is gradationally overlain by the Maxon Sandstone and (or) Telephone Canyon Formation.

The Maxon Sandstone and Telephone Canyon Formation were mapped as a combined unit (Ktm), and they generally form a reddish-colored slope separating the cliff-forming Glen Rose (Kgr) and Del Carmen (Kdc) Limestones. The Maxon Sandstone is not recognized everywhere in the park likely due to a facies change from calcareous sandstone to marl or limestone, southward across BBNP (Maxwell and others, 1967). In the Santiago Mountains southeast of Persimmon Gap, the Maxon Sandstone is calcareous, silty sandstone that grades upward into marl and nodular limestone of the Telephone Canyon Formation (Poth, 1979). The echinoid *Enallaster* sp. and snail *Turritella* sp. are some of the more common fossils in the Telephone Canyon Formation (Maxwell and others, 1967). The Maxon Sandstone and Telephone Canyon Formation interrupted carbonate shelf deposition of the Glen Rose Limestone, and represented an influx of terriginous clastic sediments derived from uplift in the Marathon region of Texas (Smith, 1981).

The Del Carmen Limestone (Kdc) was named by Maxwell and others (1967) for prominent exposures in the Sierra del Carmen of BBNP, but it is also exposed at Mesa de Anguila. The formation is characterized by massive cliffs of limestone that contain discontinuous layers and nodules of chert. The formation resulted from transgression across the carbonate-shelf interior (Smith, 1981), and contains abundant rudistids that formed in reefs along the shelf. The formation also contains gastropods, echinoids, and foraminifera. Maxwell and others (1967) noted a complete section of the formation in Telephone Canyon, Sierra del Carmen, where upper and lower cliff-forming, rudistid-bearing limestones are separated by a middle, less-resistant marly limestone. The Del Carmen Limestone is similar in appearance to the Santa Elena Limestone (Kse), and Poth (1979) described criteria to differentiate the units; he reported that the Santa Elena generally has a finer-grained texture and lighter color tones than the Del Carmen, and fossils and rudistid bioherms in the formation are better preserved than the Del Carmen.

The Sue Peaks Formation (Ksp) was named for exposures in the Sue Peaks area of the Sierra del Carmen (Maxwell and others, 1967), and the unit forms a slope between the cliff-forming Del Carmen Limestone below and the Santa Elena Limestone above. Maxwell and others (1967) observed a three-part subdivision for the formation in the Sierra del Carmen, consisting of a lower marly shale, a middle massive limestone ledge, and an upper thin-bedded limestone. In the

Caves and other dissolution features forming in the Del Carmen Limestone, Boquillas Canyon area. *(Photograph by Kenzie J. Turner)*

Santa Elena Limestone in Boquillas Canyon area. (*Photograph by Kenzie J. Turner)*

Santa Elena Canyon area, the base of the unit is covered, but the upper part differs from the Sierra del Carmen sections because it contains more marl than limestone. The formation is abundantly fossiliferous, and contains gastropods, echinoids, and ammonites.

The Santa Elena Limestone (Kse) was named by Maxwell and others (1967) for the prominent cliffs on the northwest side of Mesa de Anguila in the Santa Elena Canyon area of BBNP. The formation is also exposed in Sierra del Carmen, Mariscal Mountain, and north of the Rosillos Mountains. Like the Del Carmen Limestone (Kdc), the formation contains silicified rudistids, gastropods, and foraminifera, and nodules and layers of chert, and was deposited in a carbonate shelf environment. The formation contains marl beds mostly in the upper part, which form less resistant intervals between the more resistant, dense limestone beds.

The Del Rio Clay (Kdr) consists of claystone, laminated limestone, and some sandstone, and generally forms yellowish-, orange-, and reddish-covered slopes. Deposition of the Del Rio Clay represented another influx of clastic sediment from areas to the north. The formation is observed to thin southeastward across BBNP, from about 20 to 30 m thick in southern Santiago Mountains, northern Sierra del Carmen, and Mesa de Anguila, to less than 1 m thick in the southern Sierra del Carmen. Maxwell and others (1967) attributed the thickness variation to absence of basal parts of the formation indicated by missing faunal zones, due to a possible combination of non-deposition and (or) post-depositional erosion.

The Buda Limestone (Kbu) consists of a cliff-forming, massive-bedded limestone at the top and base, and a slope-forming nodular marly limestone unit in the middle. Thickness of the unit decreases southward across BBNP, where part of the upper member of the unit was subject to post-depositional erosion. The unit is distinctive due to its whitish-colored, conchoidally fractured limestone, and represents a transgressional lime mudstone, deposited in a deep shelf environment above mixed clastic and carbonate sediments of the Del Rio Clay (Kdr).

The Boquillas Formation (Kb) includes the lower Ernst (Kbe) and upper San Vicente (Kbs) Members (Maxwell and others, 1967), and consists mainly of thin-bedded limestone, calcarenite, and interbedded shale, claystone, marl, siltstone, and very minor sandstone. Maxwell and others (1967) reported some bentonitic clay and minor tuff beds mostly in the San Vicente Member (Maxwell and others, 1967), but in general, there are very few indicators of volcanic activity as compared with equivalent units of the Cretaceous Western Interior Seaway. The presence of thin layers of pure kaolinite in the San Vicente Member is enigmatic (Cooper and others, 2004). There is a general upward increase in marl and shale beds in the formation. Cooper and others (2007, 2008) reported the formation was deposited during a global sea level rise, and they investigated and correlated important ammonite and inoceramid zones with established zones in other parts of the Cretaceous Western Interior Seaway (Cobban and others, 2008; Cooper and others, 2008). The identified invertebrate assemblages range from the upper lower Cenomanian near the base of the Ernst Member to at least middle Santonian near the top of the San Vicente Member. Maxwell and others (1967) originally defined the contact between the Ernst and San Vicente Members at the top of beds containing the ammonite *Coilopoceras* sp., but Cooper and others (2005, 2007, and 2008) redefined the top of the Ernst at the top of the *Allocriceras hazzardi* zone (Cooper, 2000), about 50 m below the previously defined contact, based on the presence of distinctive brown-weathering limestone, more easily identified for mapping purposes.

The Pen Formation (Kp), named by Maxwell and others (1967), is a distinctive slope-forming claystone unit that has poor expression due to weathering. Sandstone units increase upward in the formation. The unit is entirely marine and facies indicate shallowing-upward, progradational deposition in a shallow carbonate shelf environment (Lehman, 1985). The formation contains ammonites, pelecypods, and gastropods, and it also contains sandy, fossiliferous concretions. The contact with the overlying Aguja Formation (Ka) is gradational and placed at the base of the first substantial sandstone above marine claystone of the Pen Formation (Lehman, 1985). The Pen Formation intertongues with the Aguja Formation as represented by the McKinney Springs Tongue (Lehman, 1985), a wedge of marine claystone within the Aguja in the McKinney Hills and in the Mariscal and Cow Heaven Mountains area, which is separated from the main part of the Pen by basal sandstone and the Rattlesnake Mountain sandstone member of the Aguja.

Distinctive alternating layers of limestone, claystone, and shale in the Boquillas Formation, Hot Springs area. *(Photograph by William R. Page)*

Yellow slope-forming claystone of the Pen Formation near the west entrance of Big Bend National Park; Maverick Mountain in background. *(Photograph by Daniel P. Miggins)*

The Aguja Formation (Ka) records the beginning of a shift from marine to continental deposition, and includes deposits of meandering stream channels, flood plains, swamps, lakes, and deltas in a coastal plain environment, and open to restricted marine environments (Lehman, 1985). The formation consists of sandstone and interbedded carbonaceous and calcareous shale, and lignite. Lehman (1985) defined six informal members of the Aguja Formation (see Description of Map Units); the individual members are not mapped separately across BBNP because of their limited extent, complex facies changes, and intertonguing relations with adjacent units in the region. For example, the basal sandstone member is thickest and best developed in the eastern part of BBNP, compared to exposures in western BBNP where the member consists of thinner sandstone beds separated by shale beds; the McKinney Springs tongue of the Pen Formation (Kp) is better developed in the eastern part than the western part of the park where it is partly equivalent to the lower and middle shale members of the Aguja Formation; and the Rattlesnake Mountain sandstone member is present in western BBNP but absent in eastern BBNP. The Aguja Formation is widely exposed in BBNP; it thins northeastward across the park and is gradational with both the underlying Pen Formation and the overlying Javelina Formation (Kj). Continental deposits of the Aguja contain abundant vertebrate fossils including dinosaur, turtle, and crocodile remains; marine units contain ammonites, oysters, and fish scales and bones (Lehman and Busbey, 2007). Breyer and others (2007) reported an age of 72.6 ± 1.5 Ma (U-Pb) for a mafic pyroclastic deposit in the uppermost part of the formation along the eastern flank of the Rosillos Mountains, and Befus and others (2008) reported an age of 76.9 ± 1.2 Ma for a similar deposit at about the same stratigraphic interval near Pena Mountain.

Sandy concretions in the Aguja Formation southwest of Pena Mountain. *(Photograph by Daniel P. Miggins)*

Paleontology in the History of Big Bend National Park

Photograph of Work Projects Administration (WPA) field crew at dinosaur bone excavation site in Aguja Formation (1938). Significant and diverse fossil collections are an important part of the natural history of Big Bend National Park, including numerous Cretaceous dinosaur and crocodile remains, Paleocene–Oligocene mammals, and unique assemblages of Miocene vertebrate fauna. Dinosaur bones were first discovered in the Big Bend area in the early 1900s, and fossil collections in the park were made from quarries in the 1930s by the WPA, the American Museum of Natural History, and the Texas Memorial Museum. Important Tertiary mammal fossils were discovered in the park in the 1950s, and paleontologic investigations continue in the park to this day.

A "Super-Croc"

The fossilized remains of gigantic crocodiles have been discovered in the Aguja Formation in the south-central part of the Big Bend National Park. These are among the largest crocodiles ever known. With lengths of 40–50 feet and jaws studded with 6-inch teeth, these powerful predators were extraordinarily equipped to feed upon a variety of dinosaurs. Just like modern day crocodilians, *Deinosuchus riograndensis* probably hunted by ambush... lying submerged near shore, and violently seizing large dinosaurs as they foraged amid the vegetation of Big Bend's ancient swamps *(National Park Service)*.

Variegated mudstone and sandstone of the Black Peaks Formation, capped by the Alamo Creek Basalt Member of the Chisos Formation in the Alamo Creek area. *(Photograph by Kenzie J. Turner)*

Maxwell and others (1967) named the Javelina Formation (Kj) for exposures in the Javelina Creek area of Tornillo Flat. The formation consists of variegated mudstone and lenticular sandstone. The mudstone represents overbank and lacustrine deposits, and the sandstone was deposited in meandering channels in a fluvial flood-plain environment. The mudstone contains calcareous nodules and carbonaceous layers reflecting paleosol development (Lehman, 1985). The Javelina contains abundant vertebrate fossils and petrified wood, and lacustrine deposits in the upper part of the formation are known for their pterosaur assemblage, discovered in northern Tornillo Flat (Pterodactyl ridge; Lehman and Busbey, 2007). The Javelina is gradationally overlain by the Black Peaks Formation. Lehman and others (2006) reported an age of 69.0 ± 0.9 Ma (U-Pb) for a tuff bed in the middle part of the Javelina Formation.

The Black Peaks Formation (TKbp) was named by Maxwell and others (1967) for exposures at Hannold Draw in Tornillo Flat, near McKinney Hills. The formation was originally interpreted as entirely Paleocene (Maxwell and others, 1967), but subsequent studies indicated that the Cretaceous-Tertiary boundary is likely in the lower part of the formation (Lehman and Busbey, 2007). The Black Peaks contains fluvial sandstone and flood-plain deposits of mudstone, and is lithologically and depositionally similar to the Javelina Formation (Kj) (Lehman, 1985). Subtle differences help to distinguish between the two formations (Lehman, 1985; Lehman and Busbey, 2007); the Black Peaks Formation contains distinctive black mudstone color bands absent in the Javelina Formation, and a regionally extensive marker bed with abundant petrified logs, informally known as “the log jam sandstone,” is present in the Black Peaks throughout BBNP (Lehman and Busbey, 2007). The Black Peaks Formation was originally mapped only in the Tornillo Flat area of BBNP (Maxwell and others, 1967), but new mapping by Lehman (unpub. mapping; this report) shows a much wider distribution south and west of the Chisos Mountains (pl.) where it was formerly mapped mostly as Javelina Formation.

The Hannold Hill Formation (Thh) was named by Maxwell and others (1967) for exposures in Tornillo Flat. Maxwell and others (1967) mapped the formation in the area between Pulliam Peak and Grapevine Hills, but Lehman (unpub. mapping; this report) identified exposures in those areas as Black Peaks Formation (TKbp), and noted that the distribution of the formation is restricted to Tornillo Flat. The formation consists of four units recognized by Beatty (1992); they include, from base to top, a basal conglomerate (Exhibit Sandstone Member), a lower mudstone, an upper conglomeratic sandstone, and an upper mudstone. Maxwell and others (1967) originally mapped the base of the formation at about 100 m below the base of the Exhibit Sandstone Member. Beatty (1992) later placed the contact at the base of the Exhibit Sandstone because it is a more practical contact for mapping purposes. The revised lower contact was utilized by Lehman (unpub. mapping; this report) as it was not possible to identify the basal contact as defined by Maxwell and others (1967), in any exposures other than the type section. The Fossil Bone Exhibit in northern BBNP is in the Exhibit Sandstone Member, and contains a unique assemblage of vertebrate fossil mammals, especially *Coryphydon*.

The Canoe Formation (Tc) was named by Maxwell and others (1967) for exposures in Tornillo Flat. The formation contains the basal Big Yellow Sandstone Member, a distinctive, 10-m-thick, yellowish-weathering fluvial sandstone, which unconformably overlies variegated mudstone of the Hannold Hill Formation (Thh). Maxwell and others (1967) noted that the Canoe Formation thins northwestward across Tornillo Flat. Most of the formation consists of tuffaceous mudstone, claystone, sandstone, siltstone, tuff beds, and basalt flows, indicating initiation of widespread volcanism in BBNP (Runkel, 1990; Lehman, 1991). Wilson and Runkel (1989) correlated the Canoe Formation with part of the Chisos Formation based on mammalian fauna. Maxwell and others (1967) suggested that the lava flows in the upper Canoe Formation may be time equivalent with the Alamo Creek Basalt Member (Tcac) of the Chisos Formation. Runkel (1990) further identified basalt flows at two horizons in the formation in Tornillo Flat; the lower flow was referred to as basalt A (fig. 4), which he interpreted to be time equivalent to the Alamo Creek Basalt, and the upper flow, referred to as basalt B, he interpreted to be time equivalent with the Ash Spring Basalt. Geochronological studies on the Canoe basalts are needed to confirm these correlations.

Big Yellow Sandstone Member of the Canoe Formation in Tornillo Flat. *(Photograph by William R. Page)*

Table 1. Stratigraphic table comparing units of the Chisos Formation in this report with units of Maxwell and others (1967) in BBNP, and Henry and Davis (1996) in adjacent Big Bend Ranch State Park. Gray shading represents undivided tuffaceous sediments of Chisos Formation; note the older part of the Chisos Formation in this report is older than the Chisos Formation of Maxwell and others (1967), and the Chisos Group of Henry and Davis (1996).

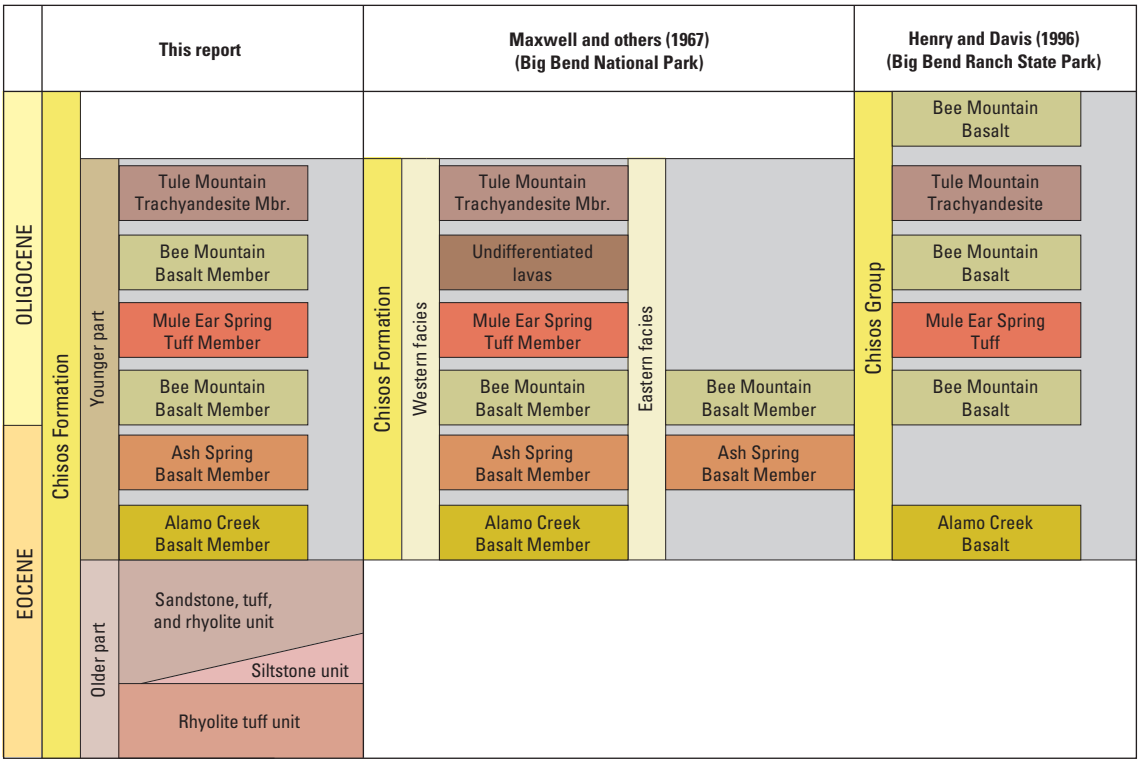

Middle Tertiary Volcanic Rocks

Chisos Formation

The Chisos Formation was originally named Chisos beds by Udden (1907) from exposures in the Chisos Mountains to include a thick section of tuffaceous sedimentary rocks, tuff, and lava. Maxwell and others (1967) subsequently raised the rank of these rocks to the Chisos Formation, and they described a western and eastern facies for the formation that varied significantly in thickness and lithology. The eastern and western facies were interpreted as interfingering, age-equivalent strata characterized by dramatic facies and thickness changes from western BBNP to the Chisos Mountains. The geographic boundary between the eastern and western facies of the Chisos Formation extends from Dominguez Mountain, northward to the east side of Sierra Quemada, and between Burro Mesa and the northwest flank of the high Chisos Mountains. Maxwell and others (1967) defined the western facies rocks to contain undifferentiated tuffaceous sedimentary units with mappable lava flows; these flows were designated as members of the formation and included (in ascending order), the Alamo Creek Basalt (Tcac), Ash Spring Basalt (Tcas), Bee Mountain Basalt (Tcbm), Mule Ear Spring Tuff (Tcme), and the Tule Mountain Trachyandesite Members (Tctm). The base of their western facies rocks is defined by the Alamo Creek Basalt Member, which generally overlies eroded Black Peaks Formation (TKbp). Maxwell and others (1967) described the eastern facies rocks as much thicker than the western facies, and characterized these rocks as mostly tuffaceous sedimentary units that lacked many of the interbedded lava flows of the western facies.

Henry and Davis (1996) noted that the tuffaceous sedimentary rocks and volcanic flows that Maxwell and others (1967) defined as the western facies of the Chisos Formation were widespread, mappable units in the Big Bend Ranch State Park area (Henry and Davis, 1996), west of BBNP, and they raised the rank of the formation to group status, and raised the rank of the members of Maxwell and others (1967) to formations with the exception of the Ash Spring Basalt (Tcas), which was not present. They defined the age of the group to be constrained between about 47 and 33 Ma, and that the 32.7-Ma Mitchell Mesa Rhyolite (Henry and Davis, 1996; Henry and others, 1998), similar in age to the South Rim Formation in BBNP, overlies the group.

We retained formational rank for the Chisos because of unresolved stratigraphic issues and lack of consensual definition for the unit across the BBNP region. Table 1 compares units of the Chisos Formation used in this report with units of the Chisos defined by Maxwell and others (1967) for the BBNP area, and Henry and Davis (1996) and Henry and others (1998) in the adjacent Big Bend Ranch State Park.

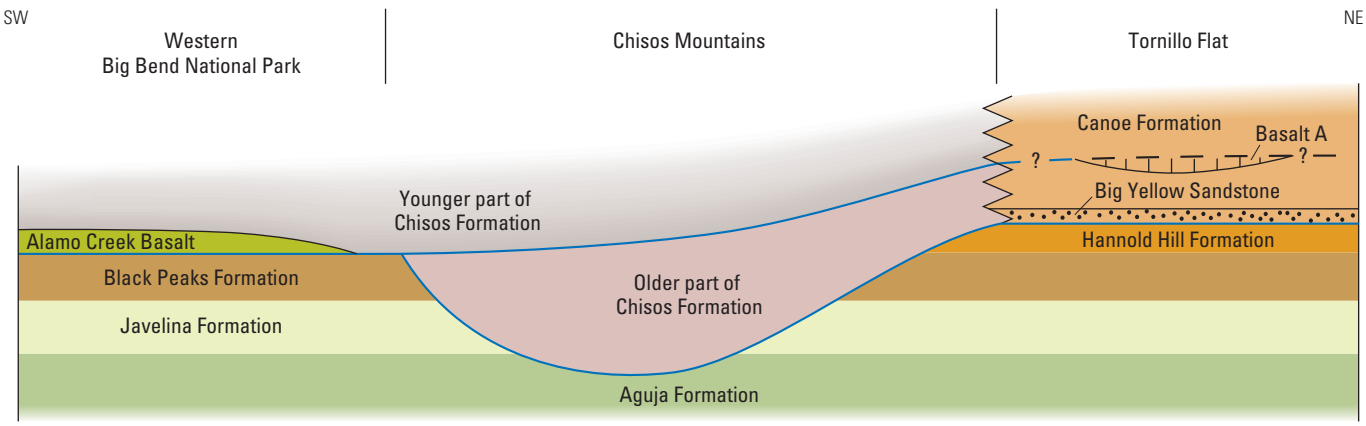

Figure 4. Diagrammatic relationships between the older and younger parts of the Chisos Formation, Canoe Formation, and underlying Tertiary–Cretaceous sedimentary rocks, from southwest to northeast across BBNP. Rocks of the older part of the Chisos Formation were deposited into a local basin in the Chisos Mountains area, which pre-dated deposition of the younger part of the Chisos Formation. Major unconformities are shown in blue. Basalt A in the Canoe Formation is time equivalent with the Alamo Creek Basalt Member of the Chisos Formation (Runkel, 1990).

Undivided Older and Younger Parts of the Chisos Formation

In this report, we subdivided the Chisos Formation into older and younger parts (table 1). Rocks of the older part are restricted to the Chisos Mountains, east of Sierra Quemada and Burro Mesa, and are equivalent to the Fresno Creek facies of the Chisos Formation of Bohannon (2011). The older part of the Chisos is lithologically equivalent to the lower part of the eastern facies of Maxwell and others (1967), but they interpreted their eastern and western facies as the same age, in contrast to our interpretation of the older part as pre-dating their eastern and western facies (table 1; fig. 4). The older part also pre-dates the Chisos Group of Henry and Davis (1996), as they did not recognize any rocks in the Chisos older than the Alamo Creek Basalt (Tcac).

Rocks of the older part of the Chisos Formation were further subdivided into a basal rhyolite tuff unit (Tcrt), and an upper sandstone, tuff, and rhyolite unit (Tcstr) of Bohannon (2011). Bohannon (2011) also mapped a siltstone unit (Tcks) which intertongues with map unit Tcstr, and is interpreted to pinch out westward, and thicken eastward to the southeast flank of the Chisos Mountains near Juniper Creek. The basal unit (Tcrt) is exposed in the Tortuga Mountain area, mostly between Dominguez Mountain and Fresno Creek, and consists of tuff and tuffaceous mudstone with some sandstone lenses and concretions. Although the unit unconformably overlies the Cretaceous Aguja Formation (Ka), it is folded in the same manner as the underlying Cretaceous units (Bohannon, 2011). The next youngest unit (Tcstr) contains sandstone, tuffaceous sandstone, and rhyolitic tuff beds. Some of the sandstone beds are conglomeratic at the base, and the rock is mottled. The unit does not appear to be affected by Laramide folding as much as the basal unit.

Lithologic, stratigraphic, and structural data indicate rocks of the older part were deposited into a local basin in the Chisos Mountains area (fig. 4), prior to deposition of rocks of the younger part of the formation (including the Alamo Creek Basalt, Tcac), and during a transitional period from near the end of Laramide deformation to the beginning of widespread volcanism in BBNP. The older part of the Chisos is correlative with the lower part of the Canoe Formation (Tc, fig. 4) (Runkel, 1990) below Canoe basalt A of Runkel (1990), which he interpreted as time equivalent with the Alamo Creek Basalt (fig. 4). Rocks of the older part of the Chisos are much thicker (about 900 m thick in the Chisos Mountains) than equivalent strata of the lower Canoe Formation (about 70 to 80 m thick in Tornillo Flat), suggesting that the high Chisos Mountains were the basin depocenter for these rocks, while thinner equivalent strata of the Canoe in the Tornillo Flat area were likely deposited near the northeastern basin margin. Rocks of the older part of the Chisos are absent west of Sierra Quemada and the Burro Mesa fault, suggesting these areas represent the southwestern basin margin.

Rocks of the younger part of the Chisos Formation (Tcy) are widely exposed in western BBNP, but they also are exposed in the Chisos Mountains (pl.). Rocks of the younger part are equivalent to the Smoky Creek facies of the Chisos Formation of Bohannon (2011), and to the western facies of the Chisos of Maxwell and others (1967) in western BBNP, and to the upper part of their eastern facies in the Chisos Mountains. The Chisos Group of Henry and Davis (1996) mostly corresponds to our younger part of the Chisos in western BBNP, except their sequence lacks the Ash Spring Basalt (Tcas), and has Bee Mountain Basalt (Tcbm) flows above the Tule Mountain Trachyandesite (Tctm) (table 1).

In western BBNP, tuffaceous sedimentary rocks of the younger part are variably interbedded with the lava and ash-flow members of the Chisos, and the base of the younger part is defined by the Alamo Creek Basalt (Tcac, fig. 4). In most areas of the Chisos Mountains, however, tuffaceous sedimentary rocks of the younger part unconformably overlie tuffaceous sedimentary rocks of the older part of the Chisos Formation (fig. 4), and lack the lava flow members present in the western part of the park. However, the base of the younger part is locally defined by the Ash Spring Basalt Member (Tcas) between Ward Mountain and Burro Mesa, and north of Pulliam Bluff and west of Panther Spring (pl.). The occurrence of the Ash Spring Basalt at the base of the younger part of the Chisos in this area likely resulted from non-deposition and pinching out of the Alamo Creek Basalt and undivided sedimentary rocks below Ash Spring Basalt. Alternatively, these rocks may have been removed along some pre-Ash Spring Basalt unconformity. Rocks of the younger part of the Chisos are thicker in western BBNP (more than 600 m thick) compared to the Chisos Mountains (about 400 m thick) (cross section *B–B′*); reduced thicknesses for these rocks in the Chisos Mountains is partly due to erosion during doming associated with early development of the Pine Canyon caldera (Barker and others, 1986).

Rocks of the younger part of the Chisos Formation (Tcy) are conspicuously much lighter in color than those in the older part, primarily owing to the abundance of white to very light-gray tuff. The younger part contains rocks of diverse lithologies including tuffaceous sandstone, mudstone and claystone, conglomerate, tuff, and some lava and limestone. Most of these rocks in western BBNP are above the Alamo Creek Basalt Member (Tcac) and below the Bee Mountain Basalt Member (Tcbm), but they are also present at different stratigraphic horizons above the Bee Mountain Basalt.

(Facing page top). Gray and red tuffaceous mudstone and sandstone, tuff, conglomerate, and dark-gray lava flows in the upper part of the Chisos Formation west of Round Mountain and Mule Ear Peaks. *(Photograph by Daniel P. Miggins)*

(Facing page bottom). Light-gray tuff, tuffaceous mudstone and sandstone of the upper Chisos Formation with local discontinuous conglomerate beds; same area as previous photograph. *(Photograph by Daniel P. Miggins)*

Lava and Ash-Flow Members of the Younger Part of the Chisos Formation

The Alamo Creek Basalt Member (Tcac) is a composite of multiple flows in western BBNP, and extends westward into the Big Bend Ranch State Park area and southward into Mexico. The unit is well exposed in the Trap Mountain, Round Mountain, and Black Mesa areas (pl.). In most areas of BBNP, the Alamo Creek forms the base of the Chisos Formation and unconformably overlies the Black Peaks Formation (TKbp), but tuff beds of the Chisos have been identified below the Alamo Creek locally in the Dogie Mountain area (T. Runkel and C. Henry, written commun., 2010). Stewart (1984) and Carmen and others (2003) reported the unit to consist of as many as nine chemically and petrographically distinct lava flows that originated from multiple sources in Mexico and the Big Bend region, including some within BBNP. Major element composition of the Alamo Creek indicates two common classifications, basalt to trachybasalt, and basaltic trachyandesite to trachyandesite (fig. 5). Henry and McDowell (1986) reported K-Ar ages for the Alamo Creek ranging from 46.9 to 39.7 Ma, and Schucker and Nelson (1988) reported a K-Ar age of 46.5 Ma. Most new $^{40}Ar/^{39}Ar$ ages for the Alamo Creek Basalt range between 47 and 46 Ma (appendix; 71–64).

The Ash Spring Basalt (Tcas) consists of two or more flows in BBNP, and was named by Maxwell and others (1967) for exposures in the Ash Spring area, north of Pulliam Peak in the Chisos Mountains, and between Ward Mountain and Burro Mesa. Scattered outcrops of the unit are also exposed west of Burro Mesa, north of Kit and Goat Mountains, westward to the Tule Mountain area, and Maxwell and others (1967) identified an unmapped outcrop at Casa Grande. Identification of the Ash Spring is difficult due to similar appearance and composition with the Alamo Creek Basalt Member (Tcac). Major element classification overlaps the Alamo Creek with most Ash Spring Basalt classified as basaltic trachyandesite to trachyandesite (fig. 5). Furthermore, trace element data do not differentiate the two units. Henry and McDowell (1986) reported a K-Ar age from the type locality of 34.5 ± 1.7 Ma, and Schucker and Nelson (1988) obtained a K-Ar age of 44.5 ± 1.8 Ma from the unit north of Goat Mountain. New $^{40}Ar/^{39}Ar$ ages determined on groundmass concentrate from the Ash Spring Basalt are 40.92 ± 0.07 and 40.38 ± 0.35 Ma (appendix; 58), but these ages are younger than constraining tuff ages elsewhere. Single crystal sanidine $^{40}Ar/^{39}Ar$ ages of 42.31 ± 0.10 Ma (appendix; 62) from tuff below the Ash Spring Basalt southwest of the Burro Mesa Pouroff (fig. 1), and 41.41 ± 0.07 Ma (appendix; 59) and 41.75 ± 0.11 Ma (appendix; 60) from tuff that overlies the Ash Spring on the northeast side of Burro Mesa, and north of Tule Mountain (fig. 1), respectively, suggest an age around 41 to 42 Ma.

Bee Mountain Basalt Member of Chisos Formation overlying white tuffaceous sediments of the Chisos Formation at Kit Mountain; uppermost pinkish-weathering bed is Mule Ear Spring Tuff Member of the Chisos Formation. *(Photograph by Daniel P. Miggins)*

The Bee Mountain Basalt Member (Tcbm) is composed of multiple lava flows ranging from basalt to basaltic trachyandesite (fig. 6). These lava flows extend from the Chisos Mountains westward to the Bofecillos Mountains in Big Bend Ranch State Park (Maxwell and Dietrich, 1970; McKnight, 1970; Henry and others, 1998), and southward into Mexico (Maxwell and others, 1967). The thickest sections of the unit in BBNP are at Bee Mountain and southeast of Castolon. Maxwell and others (1967) originally restricted the unit to below the Mule Ear Spring Tuff Member (Tcme) in BBNP; however, Bee Mountain lava flows are present above the Mule Ear Spring Tuff in places within BBNP (Turner and others, 2008). Henry and Davis (1996) also noted Bee Mountain lava flows at several horizons above the Mule Ear Spring west of BBNP. In BBNP, most Bee Mountain lava flows above the Mule Ear Spring are more evolved than the flows below, with higher silica and total alkalis (fig. 6), lower Hf/Ta, and higher La/Yb ratios (fig. 7). However, some of the stratigraphically highest Bee Mountain flows above the Mule Ear Spring appear less evolved with lower silica and total alkalis and higher Hf/Ta ratios (figs. 6 and 7) than other flows above the Mule Ear Spring Tuff; parental magma of these uppermost flows may have originated from a source of similar composition and (or) depth as the source for flows below the Mule Ear Spring Tuff. Henry and others (1986) reported a K/Ar age of 34.5 ± 1.8 Ma for the unit. $^{40}Ar/^{39}Ar$ ages determined for this report range between 34.03 ± 0.17 and 33.37 ± 0.48 Ma (appendix; 52–49) for the lower flows (below the Mule Ear Spring); dates on the upper flows (above the Mule Ear Spring) are 33.68 ± 0.09 Ma (appendix; 42) and 33.07 ± 0.15 Ma (appendix; 41).

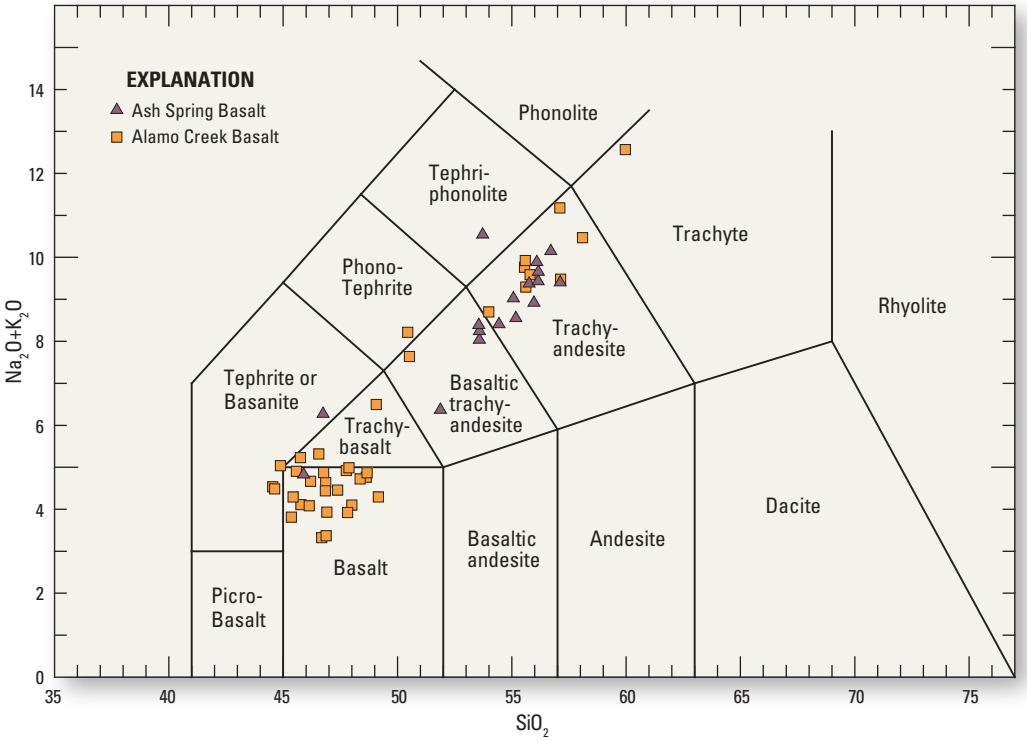

Figure 5. Total alkali-silica diagram of Le Maitre and others (1989) for Ash Spring Basalt and Alamo Creek Basalt Members of the Chisos Formation. Analyses normalized to volatile-free and total iron as FeO derived by multiplying total iron (Fe_TO_3) by 0.8998.

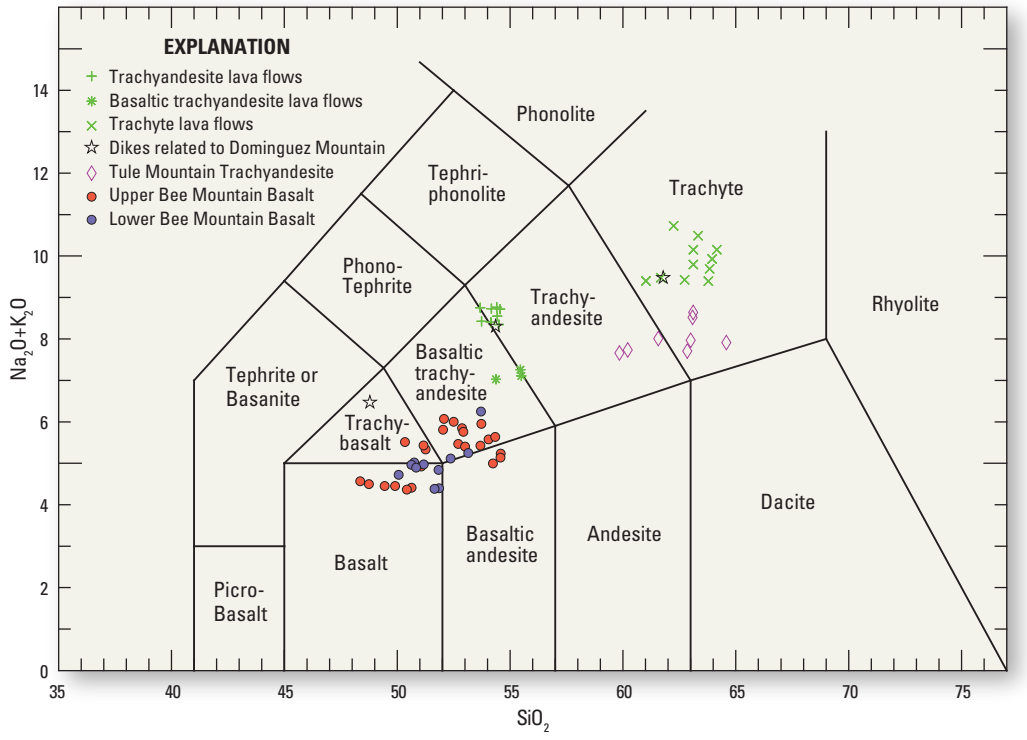

Figure 6. Total alkali-silica diagram of Le Maitre and others (1989) for lavas including the Bee Mountain Basalt and Tule Mountain Trachyandesite Members of the Chisos Formation trachytic lava that is divided into classifications, and possibly related dikes of the Dominguez Mountain dike swarm. Analyses normalized to volatile-free and total iron as FeO derived by multiplying total iron (Fe_TO_3) by 0.8998.

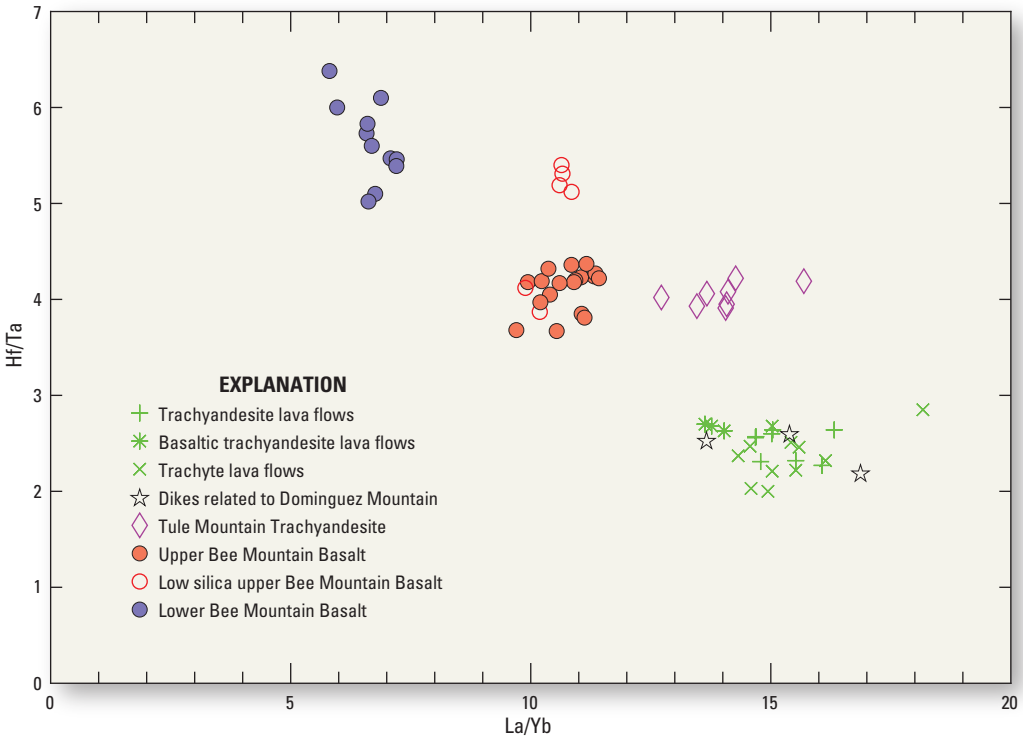

Figure 7. High Field Strength Element (HFSE) ratio plot for the Bee Mountain Basalt and Tule Mountain Trachyandesite Members of the Chisos Formation trachytic lava that is divided into classifications as in figure 6, and dikes related to the Dominguez Mountain dike swarm. The general progression is from mafic and less evolved in the upper left to silicic and more evolved in the lower right.

The Mule Ear Spring Tuff Member (Tcme) is a distinctive ash-flow tuff exposed in western BBNP, and it extends westward to the Bofecillos Mountains in Big Bend Ranch State Park (McKnight, 1970; Henry and others, 1998), and southward into Mexico. The unit is well exposed in the Goat, Kit, and Trap Mountain areas, and north and south of Cerro Castellan. Gregory (1981) correlated a tuff in the El Matadero Formation in Chihuahua, Mexico, with the Mule Ear Spring, and subsequently, the unit has been recognized and mapped in other areas of Chihuahua and parts of Coahuila, Mexico (Chuchla, 1981; Gunderson and others, 1986; Ritter and Cepeda, 1991). Henry and others (1998) reported an $^{40}Ar/^{39}Ar$ age of 33.76[7] ± 0.19 Ma for the Mule Ear Spring in BBNP. Five new laser-fusion ages (appendix 47–43); from BBNP indicate an average age of 33.65 Ma, which agrees with the age determination from Henry and others (1998). Previous studies have suggested Sierra Quemada was the source of the Mule Ear Spring Tuff (Ogley, 1978; Henry and Price, 1986; Duex and Tucker, 1989; Duex and others, 1994), but Scott and others (2007) demonstrated that intrusive rocks at Sierra Quemada are about 2.5 m.y. younger than the Mule Ear Spring Tuff. Furthermore, compositional comparison shows the Mule Ear Spring Tuff has a smaller negative Eu anomaly and is depleted in rare earth elements and high field strength elements (Zr, Hf, and Ta) relative to Sierra Quemada ring dikes and other intrusions.

The Tule Mountain Trachyandesite Member (Tctm) is the uppermost lava flow member of the Chisos Formation in western BBNP (Maxwell and others, 1967). Turner and others (2008) reported rocks previously mapped by Maxwell and others (1967) as the Tule Mountain Trachyandesite Member in a large area of BBNP, extending from Kit Mountain and Punta de la Sierra southward to Sierra de Chino, are much younger (30.4 to 30.2 Ma; appendix; 15–13), and have different major and trace element composition than the Tule Mountain Trachyandesite Member (figs. 6 and 7). These newly recognized rocks are not part of the Chisos Formation, and are mapped in this report as trachytic lava, undivided (Tt). Confirmed exposures of the Tule Mountain Trachyandesite Member in BBNP are at Burro Mesa, where it is overlain by a tuff of the Boot Rock member (Tsb) of the South Rim Formation (32.33 Ma; appendix; 29); at Tule Mountain, where it overlies the Mule Ear Spring Tuff (33.67 Ma); and at Sierra Aguja. Rocks from these localities are trachyandesite to trachyte (fig. 6) and compositionally similar to the Tule Mountain Trachyandesite in the Fresno Canyon area of Big Bend Ranch State Park (Henry and Davis, 1996; Henry and others, 1998). New $^{40}Ar/^{39}Ar$ dates for this report show age variance for the unit in BBNP, but the most stratigraphically compatible ages are 33.18 ± 0.10 Ma (appendix; 39) for a sample collected at Sierra Aguja, and 32.71 ± 0.24 Ma (appendix; 40) for a sample from Tule Mountain.

[7] Age is corrected to a neutron fluence monitor age for Fish Canyon Tuff sanidine of 28.02 Ma (Renne and others, 1998) to allow comparison with newly derived ages in appendix; correction of age following methods described at www.earth-time.org.

Table 2. Stratigraphic table comparing units of the South Rim and Burro Mesa Formations in this report with the South Rim Formation of Maxwell and others (1967) and Barker and others (1986).

	This report*		Barker and others (1986)		Maxwell and others (1967)		
			Western BBNP	Chisos Mountains	Western BBNP	Chisos Mountains
OLIGOCENE	Burro Mesa Formation	Rhyolite member	South Rim Formation: Burro Mesa Rhyolite member	Burro Mesa Rhyolite member	South Rim Formation: Burro Mesa Riebeckite Rhyolite	Burro Mesa Riebeckite Rhyolite
		Wasp Spring member	Wasp Spring Flow Breccia		Wasp Spring Flow Breccia	
	South Rim Formation	Emory Peak rhyolite member	absent		absent	
		Boot Rock member		Lost Mine Member		Lost Mine Rhyolite
				Boot Rock member		Wasp Spring Flow Breccia
		Pine Canyon rhyolite member		Pine Canyon Rhyolite**		Brown Rhyolite

* Modified stratigraphy from Urbanczyk and White (2000) and Benker (2005)
** Ogley (1978) first renamed Brown Rhyolite to Pine Canyon Rhyolite

Revision of South Rim Formation and Definition of Burro Mesa Formation

We revised the South Rim Formation in this report based on results of petrologic, geochemical, and petrographic studies subsequent to the original work of Maxwell and others (1967), and new geochronologic analyses completed for this report. Table 2 compares units of the South Rim and Burro Mesa Formations in this report with units of the South Rim defined by Barker and others (1986) and originally by Maxwell and others (1967). The most significant revisions are removal of rocks equivalent to the Burro Mesa Riebeckite Rhyolite and Wasp Spring Flow Breccia from the South Rim Formation of Maxwell and others (1967), and definition of the Burro Mesa Formation as a separate unit from the South Rim Formation (table 2). These revisions were originally recommended by Benker (2005) and White and others (2006) based on more comprehensive and updated geochemical and petrographic data, and on new geochronologic data presented by Miggins and others (2004, 2007, and 2008) (appendix). We further designate two informal members of the Burro Mesa Formation, a lower and more locally restricted Wasp Spring member (Tbw) (formerly Wasp Spring Flow Breccia of the South Rim Formation of Maxwell and others, 1967; Wasp Spring member of South Rim Formation of Barker and others, 1986; Wasp Springs member of the Burro Mesa Formation of Benker, 2005), and an upper more widespread rhyolite member (Tbr) (formerly Burro Mesa Riebeckite Rhyolite of the South Rim Formation of Maxwell and others, 1967; Burro Mesa rhyolite member of South Rim Formation of Barker and others, 1986; and Burro Mesa rhyolite member of the Burro Mesa Formation of Benker, 2005). The Wasp Spring and rhyolite members are lithologically equivalent to the Wasp Spring Flow Breccia and Burro Mesa Riebeckite Rhyolite, respectively, as originally defined and mapped in their type areas in western BBNP by Maxwell and others (1967).

Fundamental reasons for exclusion of the Burro Mesa units from the South Rim Formation are the 3-Ma age difference between these units and the South Rim Formation, and restriction of these units to western BBNP. Miggins and others (2004, 2007, and 2008) conducted new geochronologic analyses for this report indicating the Burro Mesa units range from 29.48 to 29.25 Ma (appendix; 10-2), compared to rocks of the South Rim Formation, which range from 32.33 to 31.93 Ma (appendix; 31-24). This indicates that Burro Mesa units are not related to the South Rim Formation and Pine Canyon caldera, as originally proposed by Maxwell and others (1967).

The Burro Mesa Formation rocks were originally included in the South Rim Formation by Maxwell and others (1967) because of compositional and petrographic similarities. However, Benker (2005) identified differences in trace element composition and subtle petrographic differences between the formations. Burro Mesa units generally show light rare earth element enrichment and depletion of Ba, Sr, Ti, and K relative to South Rim Formation units (Benker, 2005). Petrographic comparison indicates the Burro Mesa units contain an abundance of feldspar compared to South Rim Formation units (Benker, 2005).

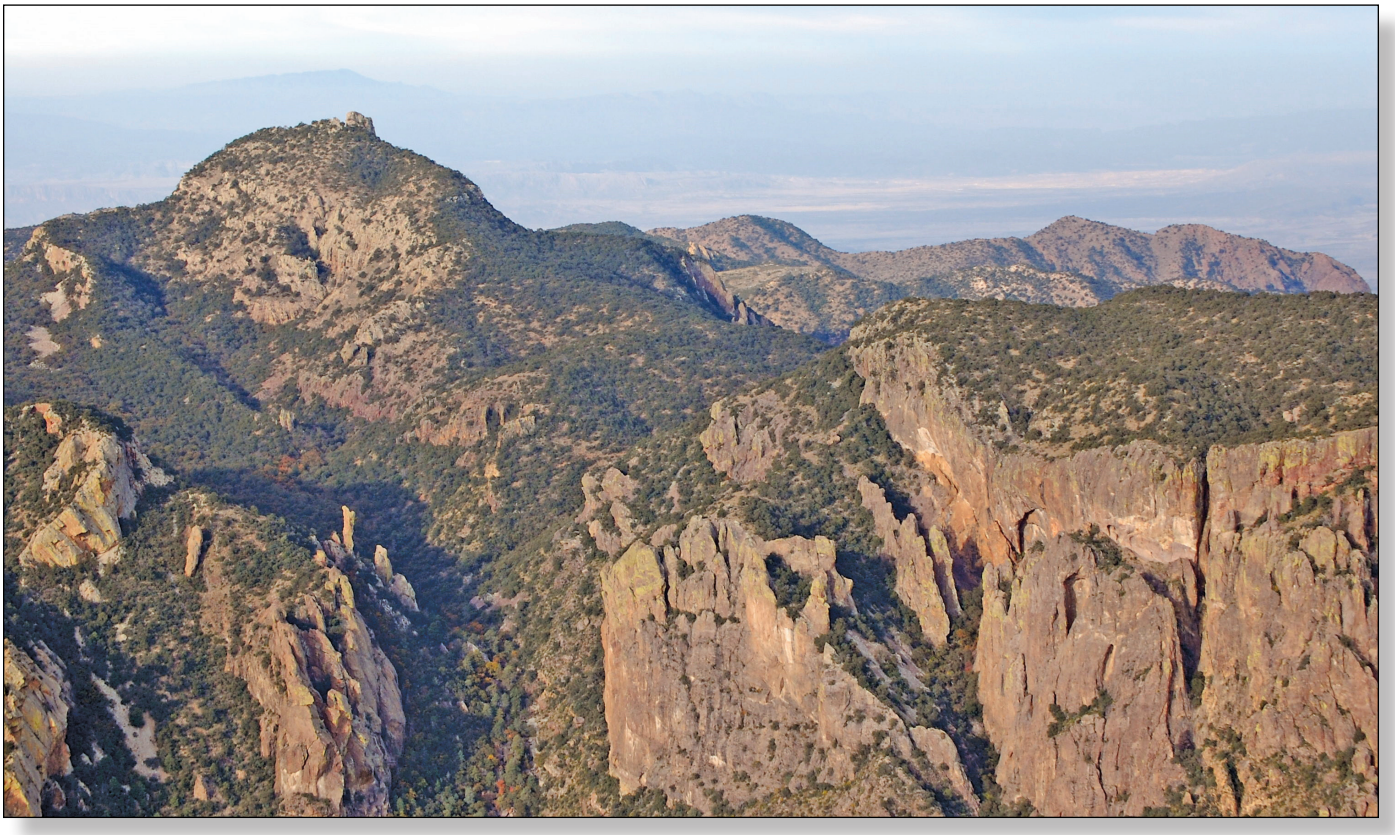

Aerial view of Emory Peak (high peak on left) and Toll Mountain (flat-topped mountain on right), exposing volcanic units of the South Rim Formation. *(Photograph by Don Corrick)*

Units of the South Rim Formation are here restricted to eruptive rocks of the Pine Canyon caldera magmatic system (Ogley, 1978; Barker and others, 1986, Benker, 2005; White and others, 2006), and units of the Burro Mesa Formation were erupted from multiple vents in western BBNP (Holt, 1998; Parker, 2002; Adams, 2004). We revised the South Rim Formation to include the following informal members (from base to top), the Pine Canyon rhyolite member (Tsp), Boot Rock member (Tsb), and Emory Peak rhyolite member (Tse). The term Pine Canyon rhyolite was introduced by Ogley (1978) to replace the Brown rhyolite of Maxwell and others (1967), and to signify it as the main caldera-filling unit of the Pine Canyon caldera. The term was subsequently used by Barker and others (1986) (table 2), Benker (2005), and White and others (2006), therefore we propose the name for consistency and to indicate a genetic link to the caldera. The name Boot Rock member was proposed as an informal member of the South Rim Formation by Barker and others (1986) to replace units formerly mapped as the Wasp Spring Flow Breccia by Maxwell and others (1967) in the South Rim, The Basin, and Pine Canyon areas of the high Chisos Mountains (table 2). We combined the Lost Mine Rhyolite (originally named by Maxwell and others, 1967) with the Boot Rock member, based on recent studies by Benker (2005). He reported that trachytic and rhyolitic rocks of the Lost Mine Rhyolite show no petrographic or geochemical difference from the quartz trachytes to rhyolites of the Boot Rock member, and field evidence indicated no clear distinction between the two units. In addition, Ogley (1978) and Barker and others (1986) did not identify the Lost Mine Rhyolite at the type locality as defined by Maxwell and others (1967). The Emory Peak rhyolite is the upper member of the South Rim Formation, and the name was introduced by Urbanczyk and White (2000) for exposures in their type area of Emory Peak to replace units formerly mapped as Burro Mesa Riebeckite Rhyolite at Emory Peak by Maxwell and others (1967) and Barker and others (1986).

(Facing page) Aerial view of South Rim, comprised of thick outflow units of the South Rim Formation. *(Photograph by Don Corrick)*

South Rim Formation

The Pine Canyon rhyolite member (Tsp) is the primary fill of the Pine Canyon caldera (Ogley, 1978; Barker and others, 1986), and its known distribution is limited to within the caldera boundary (pl.; cross section *B*–*B′*). The unit is a peralkaline rhyolite composed of multiple cooling units of densely welded vitrophyre to welded ash-flow tuff. Aeromagnetic data indicate the Pine Canyon rhyolite is reversely magnetized (Drenth and Finn, 2007), and these data help to estimate its thickness within the caldera. Thickness estimates based on geophysical modeling for the unit range from about 400 m to over a kilometer (Drenth and Finn, 2007); Ogley (1978) reported a minimum thickness of 300 m for the unit.

The Boot Rock member (Tsb) consists of quartz trachyte and rhyolite lava, tuff, and maar-type surge deposits erupted from vents around the caldera following collapse (Barker and others, 1986; Urbanczyk and White, 2000). The Boot Rock member is widely exposed in the Pine Canyon caldera, and in the South Rim area; many of these exposures were originally mapped as the Wasp Spring Flow Breccia and Lost Mine Rhyolite by Maxwell and others (1967). Distal outflow tuff of the Boot Rock member is exposed as far west as Burro Mesa (pl.). The tuff at Burro Mesa has similar age (appendix; 29), rare earth element concentration, magnitude of negative Eu anomaly, and high field strength element concentration as samples from the South Rim and Pine Canyon caldera areas reported by Benker (2005) and White and others (2006). The Pine Canyon rhyolite and the Boot Rock members share a common magma source and are interpreted to have evolved primarily through crystal fractionation of a mafic melt with alkali basalt composition (Benker, 2005; White and others, 2006). Multiple intrusive bodies external to the caldera, such as Nugent and Lone Mountains, have similar composition to the Boot Rock and Pine Canyon rhyolite members, and are likely related to the caldera's parental magma.

The Emory Peak rhyolite member (Tse) consists of lava, rheomorphic tuff, and vitrophyre erupted from intracaldera and extracaldera vents. The unit is exposed at Emory Peak and in the Blue Creek Ranch area. The Emory Peak rhyolite in the Blue Creek Ranch area is the same age (appendix; 25) as rocks at Emory Peak, and has similar peralkalinity, REE concentrations, and a large negative Eu anomaly consistent with analyses reported by Benker (2005) and White and others (2006). Numerous intrusions, including the Hayes Ridge ring dike, and Ward Mountain and Pulliam Peak intrusion, among others, are compositionally similar to the Emory Peak rhyolite (White and others, 2006). Parental magma of the Emory Peak rhyolite is interpreted to not be cogenetic with magma that produced the Pine Canyon rhyolite and Boot Rock members, but likely developed contemporaneously from partial melting of a lower crustal source (Benker, 2005; White and others, 2006).

View from Lost Mine trail along the rim of the Pine Canyon caldera, looking southward toward Elephant Tusk. *(Photograph by Daniel P. Miggins)*

Trachytic Lava, Undivided

Lava flows mapped as trachytic lava, undivided (Tt), formerly mapped by Maxwell and others (1967) in areas of BBNP as Tule Mountain Trachyandesite Member (Tctm) of the Chisos Formation, are mostly exposed from Kit Mountain to Punta de la Sierra, and southward to Sierra de Chino. The lava flows consist of three compositional groups: basaltic trachyandesite, trachyandesite, and trachyte (fig. 6). Although scatter is present in the high field strength elements, likely due to crustal contamination, observed similarities in trace-element chemistry suggest a genetic relationship between the groups (fig. 7). Geochronology indicates the trachyandesite is 30.42 Ma (appendix; 15), slightly older than the trachyte dated at 30.29 Ma (appendix; 14) and 30.23 Ma (appendix; 13), and at Triangulation Station Mountain the trachyte overlies a 30.40 Ma tuff (appendix; 18). Henry and others (1986) reported a K-Ar age of 29.3 ± 1.5 Ma from Smoky Creek near the Rio Grande, which is within analytical error of dates on the trachyte. The trachyte group is exposed in the Blue Creek Ranch, Goat Mountain, Round Mountain, and Sierra de Chino areas, and probably at Punta de la Sierra. The trachyandesite group is exposed in a belt west of the trachyte group, on the southwest flank of Burro Mesa, Bee Mountain, Tuff Canyon, and southeast of Cerro Castellan. The basaltic trachyandesite group is only identified between Cerro Castellan and Sierra de Chino.

A possible source for the undivided trachytic lava may be the volcanic complex at Dominguez Mountain. Two dikes in the Sierra de Chino area, which are interpreted to be associated with the Dominguez Mountain dike swarm (Tdd), are compositionally similar to the trachyandesite and trachyte groups (figs. 6 and 7). Furthermore, some dikes of the Dominguez Mountain dike swarm appear to merge upward into the trachytic flows capping the eastern cliffs of Punta de la Sierra (Bohannon, 2011). The flows at Punta de la Sierra appear to be in the same stratigraphic position as elsewhere, and are underlain by two tuffs that are around 30 Ma (appendix; 16, 17). Further investigations of volcanic and intrusive rocks at Dominguez Mountain, the dike swarm, and flows capping Punta de la Sierra are needed to confirm Dominguez Mountain as the source for the trachytic lava.

(Below) Southeastern point of Punta de la Sierra showing trachyitic lava (dark-gray rock capping mountain peak), dike swarm (light-brown, sub-vertical dikes in central part of mountain) cross-cutting sediments of the Chisos Formation, and Alamo Creek Basalt Member of the Chisos Formation (dark-gray basalt flow near base of photograph). *(Photograph by Robert G. Bohannon)*

(Facing page) Tuff Canyon after rainstorm; dark-gray rock in the lower part of the photograph is trachyitic lava (Tt), and overlying light-gray to tan rocks forming rim are outflow units of the Burro Mesa Formation. *(Photograph by Blake Trester)*

Goat Mountain along Ross Maxwell Drive; rocks of the Burro Mesa Formation form the steep cliffs in the upper part of the mountain. *(Photograph by Daniel P. Miggins)*

Burro Mesa Formation

Maxwell and others (1967) originally included the Burro Mesa Riebeckite Rhyolite and Wasp Spring Flow Breccia as members of the South Rim Formation (table 2). Although they defined and mapped these units in type sections in western BBNP, they also mapped these units in the Chisos Mountains. Barker and others (1986) restricted the Wasp Spring Flow Breccia and Burro Mesa rhyolite to areas south and west of the Chisos Mountains (table 2), with the exception of one outcrop of Burro Mesa at Emory Peak, mapped in this report as the Emory Peak rhyolite (Tse) (Urbanczyk and White (2000). Becker (1976), Henry and others (1989), and Benker (2005) noted compositional differences, and Miggins (2004, 2008) documented age differences between Burro Mesa rocks in their type area and in the Chisos Mountains. Barker and others (1986) and Henry and others (1989) reported the distribution of the Wasp Spring Flow Breccia and Burro Mesa Riebeckite Rhyolite south and west of the Chisos Mountains could not have erupted from a single vent, and multiple source vents for those units have been identified (Holt, 1998; Parker, 2002; Adams, 2004). In this report, the newly defined Burro Mesa Formation includes a lower more restricted Wasp Spring member (Tbw), and an upper more widespread rhyolite member (Tbr). Numerous new $^{40}Ar/^{39}Ar$ ages for the Burro Mesa Formation range from 29.48 to 29.25 Ma (appendix; 10–2).

Rocks of the Burro Mesa Formation are exposed at Burro Mesa, Goat and Kit Mountains, and in scattered outcrops between Castolon and the Chisos Mountains. The Wasp Spring member (Tbw) consists of surge deposits, and air-fall and ash-flow tuff, and most beds contain abundant lithic fragments and fiamme. The member is one of the more recognizable volcanic units in BBNP because it forms brightly colored orange to yellow cliffs near Burro Mesa Pouroff and at Cerro Castellan. The rhyolite member (Tbr) consists of lava flows and ash-flow tuff, which were erupted from local maar-type rhyolite lava domes (Holt, 1998; Parker, 2002; Adams, 2004). Extrusive rocks of the formation were erupted from vents at Burro Mesa, Kit and Goat Mountains, Cerro Castellan, and Horseshoe Canyon to name a few (Holt, 1998; Adams, 2004). Rhyolitic intrusive bodies in southwestern BBNP are compositionally identical and time equivalent (appendix; 11, 12) to Burro Mesa extrusive rocks; these rocks are mapped on the plate as map unit Tbi.

Burro Mesa from pouroff parking lot, showing light-brown, orange, and yellow-weathering deposits of the lower Wasp Spring member of the Burro Mesa Formation, overlain by thick, dark-brown flows of the upper rhyolite member. *(Photograph by Robert B. Scott)*

Alluvial Deposits

Late Tertiary to Quaternary Basin Fill

During the Miocene, Pliocene, and early part of the Pleistocene, alluvial-fan, stream, and playa deposits accumulated in fault-bounded basins (bolsons), formed by basin-and-range extensional faulting. Two main basins in the park are the Delaho bolson, on the west side near Castolon, and the Estufa bolson on the east side in the lower Tornillo Creek area (fig. 2).

Basin fill deposited in the Delaho bolson has been deeply eroded and dissected such that only disconnected remnants remain. The older part of the fill, mapped as Ta in this report, is made up of debris-flow, fluvial-channel, and sheet-flow deposits of the Delaho Formation (Stevens and others, 1969; Stevens and Stevens, 1989). The unnamed lower member of the Delaho Formation contains a diverse vertebrate fauna of large and small mammals, tortoises, and lizards of earliest Miocene age (Castolon local fauna; Stevens and others, 1969; Stevens, 1977, 1991), and is interbedded near its base with a thin basaltic flow yielding a K-Ar age of 23.3 ± 0.6 Ma (Stevens, 1988; Stevens and Stevens, 1989), indicating that deposition in the Delaho bolson began in the earliest Miocene. The Smoky Creek Member of the Delaho Formation disconformably overlies the lower member and represents a later stage of sediment deposition in the bolson. Because the Smoky Creek Member contains few fossils, timing of its deposition is poorly constrained, but estimates of late early Miocene (Stevens and Stevens, 1989) and middle? Miocene (Stevens, 1988) have been proposed. The youngest sediments attributed to the Delaho bolson are gravelly alluvial-fan deposits in the Burro Mesa area (Lehman and Busbey, 2007), named the informal Fingers formation by Stevens (1969, 1988) and mapped as QTa in this report. No fossils have been found in these coarse-grained deposits, and their age is unknown, but Stevens and Stevens (1989), who have done most of the work on bolson deposits in the park, consider them possibly Blancan (North American mammal age), which they associate with a Pliocene-Pleistocene geologic age (Stevens and Stevens, 1989, 2003).

Basin fill in the Estufa bolson is less deeply eroded and dissected than in the Delaho bolson, and in places along the western edge of the Estufa bolson, the fill sequence is largely intact. The older part of the fill, named the informal Banta Shut-in formation by Stevens and Stevens (1989, 2003) and mapped as Ta in this report, is made up of fine-grained, distal alluvial-fan and playa deposits interbedded with coarser-grained, mid-fan deposits. The formation contains large and small mammals, tortoises, lizards, snakes, and toads of late Miocene age (Screw Bean local fauna; Stevens and Stevens, 1989, 2003), indicating that deposition began much later in the Estufa bolson than in the Delaho bolson. The upper Miocene section is overlain unconformably by a younger sequence of fill made up of gravelly alluvial-fan deposits, referred to as the informal Estufa Canyon formation by Stevens and Stevens (1989, 2003) and mapped as QTa in this report. The informal Estufa Canyon formation is considered correlative to the informal Fingers formation of the Delaho bolson (Stevens and Stevens, 1989); as with the informal Fingers formation, its age is unknown, but is considered possibly Pliocene–Pleistocene (Maxwell and others, 1967; Stevens and Stevens, 1989, 2003). Based on lithologic characteristics, gravels of the informal Estufa Canyon formation previously were correlated to an isolated outcrop of calcareous silt near Grapevine Spring (Maxwell and others, 1967); elephant teeth found in the calcareous silt suggest a Pleistocene age for that deposit (Lonsdale and others, 1955). However, we interpret the calcareous silt as part of a Pleistocene spring deposit that post-dates deposition of the upper bolson fill. Some beds within the gravelly alluvial-fan deposits have been tilted near faults, or are offset, indicating that basin-bounding faults were still active at the time upper bolson fill was being deposited.

(Top) Informal Estufa Canyon (QTa) and **(Bottom)** Banta Shut-in (Ta) Formations of Estufa bolson. *(Photographs by Margaret E. Berry)*

Rio Grande Integration History

Long-term aggradation represented by the bolson deposits was followed by degradation that resulted in the erosion of large volumes of rock and sediment from the Big Bend landscape during the Quaternary. This shift from aggradation to degradation was probably due to declining rates of fault activity and the establishment of the Rio Grande as an integrated drainage network. Since its establishment, the fluvial system in the BBNP region has been dominated by long-term incision, punctuated by episodes of aggradation that were likely related to fluctuations in climate and river hydrology.

The timing of river integration is still debated. Although some workers think that integration of the Rio Grande through the Big Bend region occurred relatively recently, around 700 ka (middle Pleistocene; Pazzaglia and Hawley, 2004), others suggest that the Rio Grande was through-flowing by the end of the Pliocene or beginning of the Pleistocene (Gustavson, 1991; Dickerson and Muehlberger, 1994), an interpretation more consistent with the surficial geology of BBNP. The ancestral Rio Grande is thought to have expanded its drainage southward by aggrading basins along its course; as basins filled with sediment, drainages breached divides and spilled into the next lower basin downstream (Henry, 1998; Connell and others, 2005). This southward growth of the river system is thought to have been facilitated by slowing rates of regional extension in the southeastern Basin-and-Range, such that rates of deposition exceeded rates of tectonic subsidence (Connell and others, 2005). Work by Gustavson (1991) suggests that around 2.25 Ma, the ancestral Rio Grande breached the drainage divide at the southern end of the Hueco bolson, in western Texas (northwest of BBNP). Based on the extent to which Hueco bolson fill was subsequently eroded, breaching of this divide may have integrated the northern segment of the Rio Grande with an ancestral southern segment of the river, such that the Rio Grande became through-flowing to the Gulf of Mexico at that time (Gustavson, 1991; Mack and others, 2006).

Extensive erosion of the Big Bend landscape inverted the topography of both the informal Fingers formation of the Delaho bolson (Burro Mesa) and the informal Estufa Canyon formation of Estufa bolson (for example, Hannold Hill area), which now stand in relatively high relief even though they were deposited in basins. The oldest alluvial deposits that post-date erosional inversion of the bolson deposits have strong calcic soils with cemented, stage IV carbonate horizons that probably took several hundred thousand years or longer to form (Machette, 1985), indicating that the gravel deposits on which the soils formed were deposited in the middle (or early?) Pleistocene (Berry and Williams, 2008). Given the amount of erosion required to invert the bolson topography prior to deposition of these gravels, in an environment where rates of erosion were probably relatively low, it is likely that long-term degradation of the Big Bend landscape associated with integration of the fluvial system began well prior to 700 ka (middle Pleistocene), and could be consistent with timing around 2.25 Ma (early Pleistocene).

Endangered Rio Grande Silvery Minnow in Big Bend National Park

(Above) The Rio Grande, its flood plain (densely vegetated), and late Pleistocene terrace (Qiw1, elevated surface to left of flood plain) upstream of Boquillas Canyon (carved in Santa Elena Limestone, background). U.S. is on the left side of river; Mexico is on the right side. Foreground is a remnant of the Qiw2 terrace. *(Photograph by Margaret E. Berry)*

Scientists with the USGS Texas Water Science Center collaborate with scientists at the National Park Service in Big Bend National Park, U.S. Fish and Wildlife Service, and the Mexican Maderas del Carmen and Cañon de Santa Elena protected areas to evaluate available habitat of the federally endangered Rio Grande silvery minnow. USGS scientists conduct field mapping studies of available habitat over a range of river flow critcial to spawning and dispersal of various life stages of this species.
—J. Bruce Moring, USGS Biologist, Texas Water Science Center (Austin)

The Rio Grande silvery minnow.

Pleistocene and Holocene Landscape Development

Evidence that extensive erosion in BBNP continued throughout much of the Quaternary is provided by the multiple levels of pediment surfaces prominent in the park (fig. 8). The highest pediment level, considered middle (or early?) Pleistocene in age based on its relative age characteristics, is generally 30–50 m above the valley floor (Qoa). Below the highest level are more extensively preserved, intermediate pediment surfaces, generally 12–40 m (Qia2) and 6–24 m (Qia1) above the valley floor, that probably were formed during the middle and late Pleistocene. Still younger surfaces, generally 3 m or more above the valley floor, are probably late Pleistocene to Holocene in age (Qya2). This extensive erosion of the Big Bend landscape during the Quaternary probably contributed to the destabilization of bedrock slopes, which resulted in large, multi-event landslides in several areas of the park, such as those at Chilicotal and Talley Mountains (Collins and others, 2007, 2008) and the northwest mountain front of the Chisos.

Periodic changes in climate and river hydrology during the Quaternary interrupted long-term incision of the river system with episodes of aggradation (Dethier, 2001; Connell and others, 2005), represented in BBNP by multiple levels of coarse-gravel terrace deposits along the Rio Grande and its tributary streams. The highest level is preserved in isolated remnants roughly 55–60 m above the Rio Grande flood plain (Qow), and is likely middle (or early?) Pleistocene in age based on soil development and geomorphic relations (Berry and Williams, 2008). Three intermediate levels present along the Rio Grande, roughly 30–45 m (Qiw3), 18–25 m (Qiw2), and 12–18 m (Qiw1) above the Rio Grande flood plain are probably middle and late Pleistocene in age. Whereas remnants of the two higher intermediate levels are fairly local in their extent, the lowest intermediate terrace forms a broad, flat remnant surface that can be traced all along the stretch of Rio Grande that flows through the park. The lowest terrace levels, about 4–9 m (Qyw2) and 3 m or less (Qyw1) above the active flood plain, are likely late Pleistocene to Holocene, and Holocene in age. In contrast to the coarse gravels that characterize the Pleistocene and late Pleistocene to Holocene terrace deposits, fine-grained sand and silt predominate the Holocene deposits.

In recent times (last 100 years), the Rio Grande has changed dramatically from a broad sandy riverbed to a narrow channel with steep banks and flood plain heavily vegetated by invasive plant species (Purchase, 2002; Dean and Schmidt, 2008). Irrigation diversions and the construction of dams upstream have reduced flow and the occurrence of floods to the point where the river has been unable to transport its sediment load (Purchase, 2002). These factors, combined with increased bank roughness and decreased channel capacity, caused by the invasion of non-native vegetation, have resulted in significant aggradation of the flood plain and narrowing of the active channel (Dean and Schmidt, 2008).

(Above) Tamarisk (salt cedar) in flood plain of the Rio Grande near Santa Elena Canyon. Tamarisk is an invasive plant species that chokes out native plants, and reduces the diversity of native plant and animal species in the riparian habitat. *(Photograph by Daniel P. Miggins)*

Figure 8 (Facing page). Examples of pediment sequences in BBNP. Labels mark surfaces of thin, gravel-rich, Quaternary-age alluvial deposits that cap Cretaceous-age bedrock made up of yellowish-brown sandstone and yellowish-brown and maroon clay: Qoa, old alluvial deposits; Qia2, older of the intermediate alluvial deposits; Qia1, younger of the intermediate alluvial deposits; Qya2, older of the young alluvial deposits; Qya1, younger of the young alluvial deposits; Qaw, active tributary wash and river deposits. *A*, View looking southwest across Alamo Creek towards Santa Elena Canyon, a deep gorge cut by the Rio Grande through Cretaceous-age limestone. *B*, View looking north (toward the Chisos Mountains) in the Reed Camp area. *(Photographs by Margaret E. Berry)*

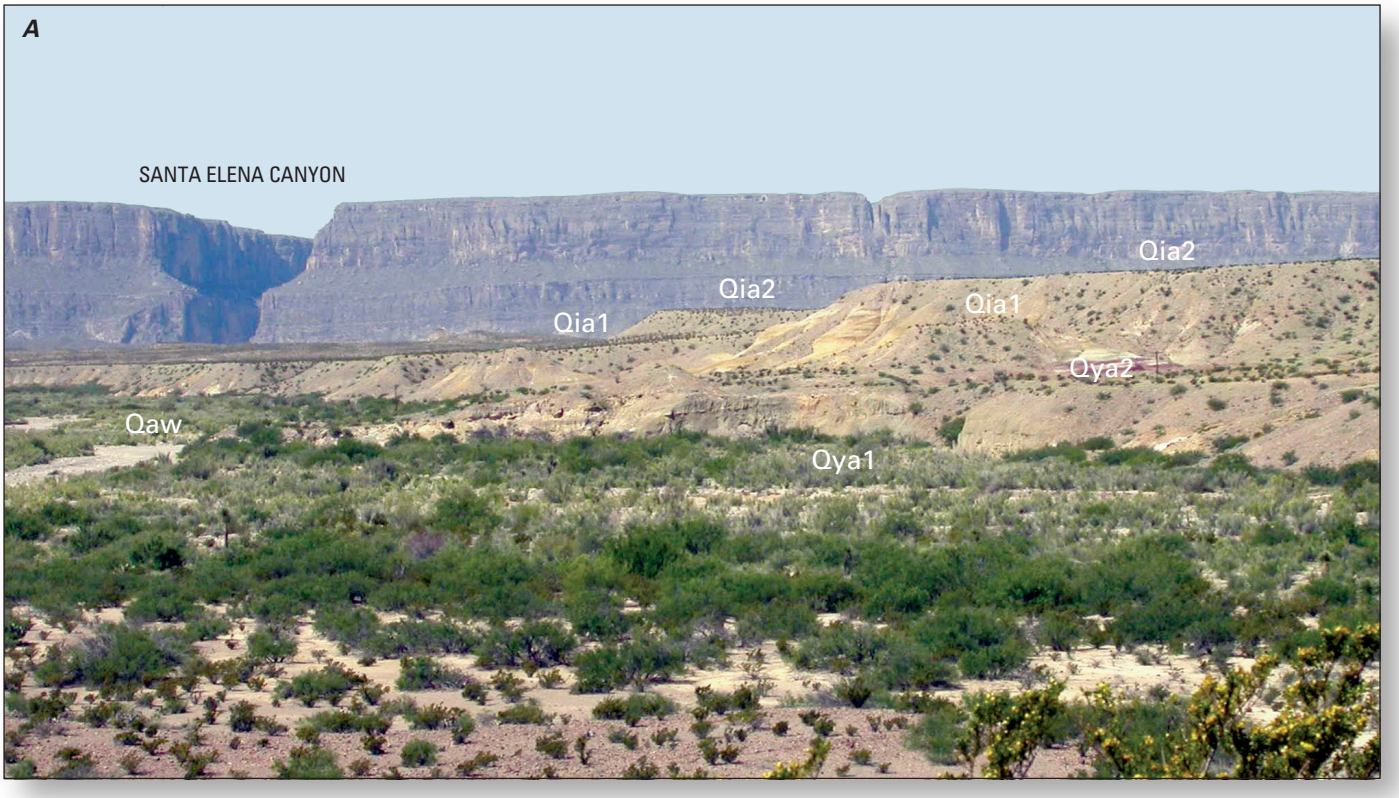
A
SANTA ELENA CANYON
Qia2
Qia2
Qia1
Qia1
Qya2
Qaw
Qya1

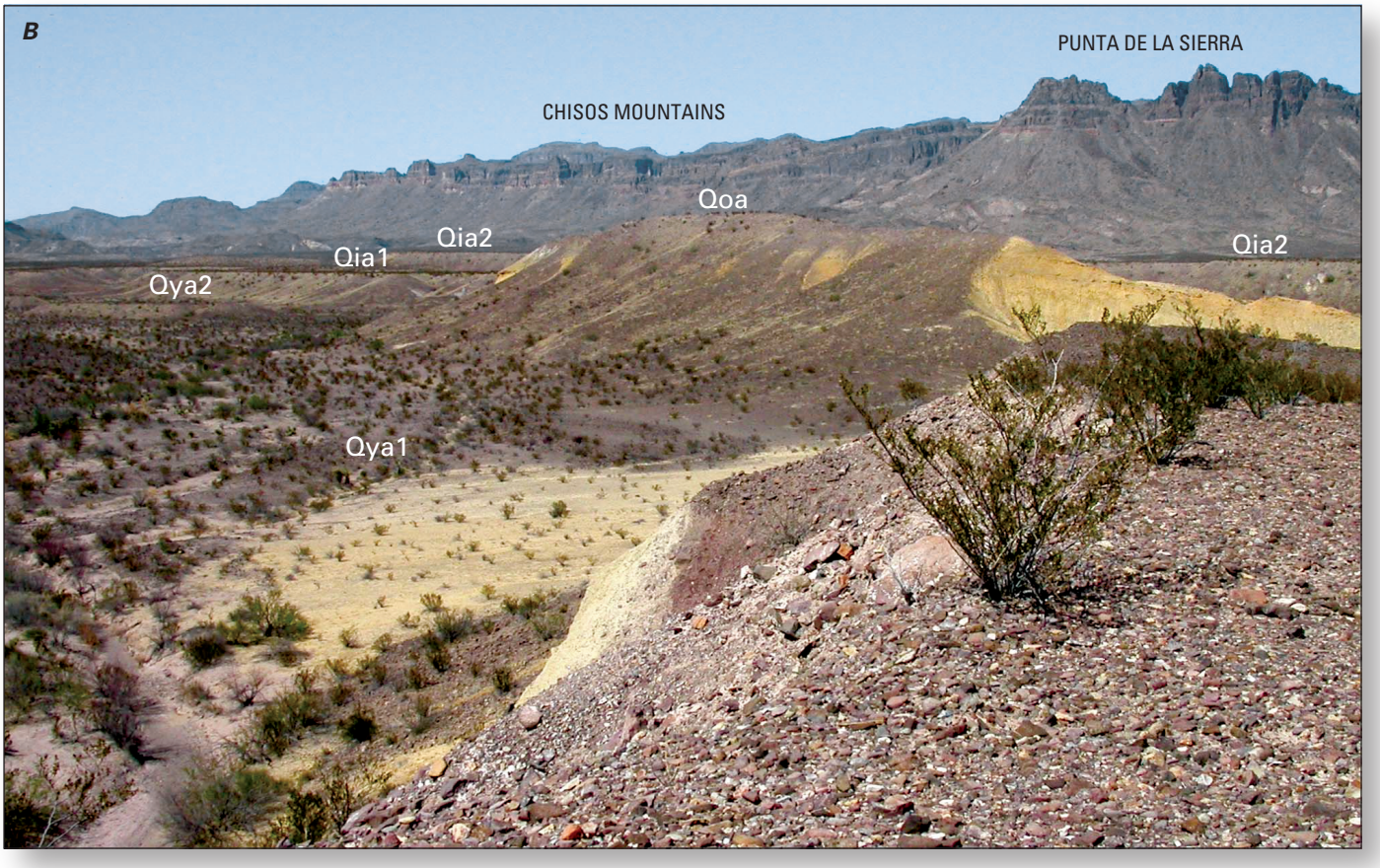
B
PUNTA DE LA SIERRA
CHISOS MOUNTAINS
Qoa
Qia2
Qia1
Qia2
Qya2
Qya1

Structure

Proterozoic Rifting

Although the oldest recorded tectonism in BBNP is related to the late Paleozoic Marathon orogeny, Proterozoic rifting and protocontinental plate collision events likely had a profound influence in shaping BBNP's landscape (Muehlberger, 1980; Dickerson, 1980; Page and others, 2008). These older events have been interpreted to have established the northwest trend of major structural features that characterize the park today (fig. 2).

The Texas lineament (Albritton and Smith, 1957; Muehlberger, 1980; Dickerson, 1980) is a zone of proposed northwest-striking basement faults extending from Presidio, Tex., southward into the Big Bend area, and into Mexico (fig. 9). The zone is deeply buried and Dickerson (1980) and Muehlberger (1980) speculated that faults of the lineament formed from rifting events as long ago as 1,500–1,000 Ma, and they emphasized that faults in the zone have been reactivated during subsequent tectonic events, including the late Paleozoic Marathon orogeny, Late Cretaceous–early Tertiary Laramide orogeny, and late Tertiary basin-and-range faulting.

Rifting between the North American and South American plates was proposed to have occurred about 800–550 Ma along the southern edge of the North American continent (Thomas, 1991; Poole and others, 2005), and produced northwest-striking transform faults interpreted to have laterally offset the southern continental margin (fig. 9). In the southern Texas part of the continental margin, the synrift transform faults were reported to be episodically active from about 600 to 570 Ma, and apparently established a tectonic fabric in the continental crust that persisted at least through Paleozoic time (Poole and others, 2005), and probably well into the Cenozoic in the BBNP region as indicated by the prominent northwest-trending structural grain. The postulated position of the rift zone and offsetting transform faults shown in figure 9 is based on data points (Poole and others, 2005) indicating the location of stable North American continental basement rocks relative to South American volcanic-plutonic arc rocks. The relationship between the Neoproterozoic transform faults and faults of the Mesoproterozoic Texas lineament is unclear; although, they both are subparallel (fig. 9), postulated to have formed during rifting events at the southern continental margin, and they separate stable North American plate continental basement rocks from less stable, rifted South American plate volcanic and plutonic rocks.

Paleozoic Marathon Orogeny

During the Paleozoic, BBNP was near the southern edge of the North American continent and was the site of shallow marine shelf deposition and complex interactions between the North American and South American tectonic plates (fig. 10). The oldest structures in the park are thrust faults associated with the Middle Mississippian to Early Permian Marathon orogeny (Poole and others, 2005). The Marathon orogenic belt (fig. 10) is one segment of the larger Ouachita-Marathon-Sonora orogenic belt (Poole and others, 2005) that extends along the Paleozoic continental margin from Mississippi and Arkansas (Ouachita segment), through Texas (Marathon segment), and into Chihuahua and Sonora, Mexico (Sonora segment). A regional synthesis of the Paleozoic tectonic history of BBNP and Trans-Pecos, Texas, is summarized in Muehlberger and Dickerson (1989).

In west Texas, deep-water ocean basin rocks originally deposited south of the Big Bend area were thrust northwestward onto the North American continent during the convergence between the North and South America plates (fig. 10). Paleozoic rocks of the Marathon belt are well exposed to the north of BBNP in the Marathon Basin, where they are deformed by northeast-striking, northwest-vergent thrust faults and folds (Anderson and others, 1982; Barnes, 1979). Remnants of the Marathon orogenic belt are exposed in the Persimmon Gap area in northern BBNP (fig. 1), but elsewhere in the park, the record of the orogenic events is overprinted by later structures and buried by younger deposits. These remnants are characterized by small outcrop belts containing Paleozoic rocks (fig. 2) and northwest-directed thrust faults (Maxwell and others, 1967). Paleozoic rocks of the Marathon orogenic belt include, from base to top, the Middle and Upper Ordovician Maravillas Formation, Silurian to Mississippian Caballos Novaculite, and Mississippian to Pennsylvanian Tesnus Formation. The Maravillas Formation and Caballos Novaculite are pre-Marathon orogenic, allochthonous, deep-water basin rocks, and the Tesnus Formation is synorogenic flysch deposited into the Pedregosa foreland basin, in front of the advancing Marathon orogenic belt. Several northwest-vergent thrust faults duplicate the Paleozoic section and juxtapose rocks of the Maravillas Formation above the Tesnus Formation (Maxwell and others, 1967). The Paleozoic thrust block at Persimmon Gap was subsequently deformed during the Late Cretaceous–early Tertiary Laramide orogeny, which juxtaposed the Paleozoic thrust block with Cretaceous sedimentary rocks above and below. Preserved northwest vergent thrust faults of the Paleozoic Marathon orogeny and their relationship with later southwest vergent Laramide faults are shown in detailed geologic maps of the Persimmon Gap area (Maxwell and others, 1967; Poth, 1979).

Following Paleozoic deformation, the Marathon orogenic highlands eroded during Triassic and Jurassic time. The absence of Triassic- and Jurassic-age rocks in BBNP reflects this period of erosion, which is characterized locally in the park, in the Persimmon Gap area, by a major unconformity separating rocks of the Lower Cretaceous Glen Rose Limestone above from rocks of the Mississippian–Pennsylvanian Tesnus Formation below.

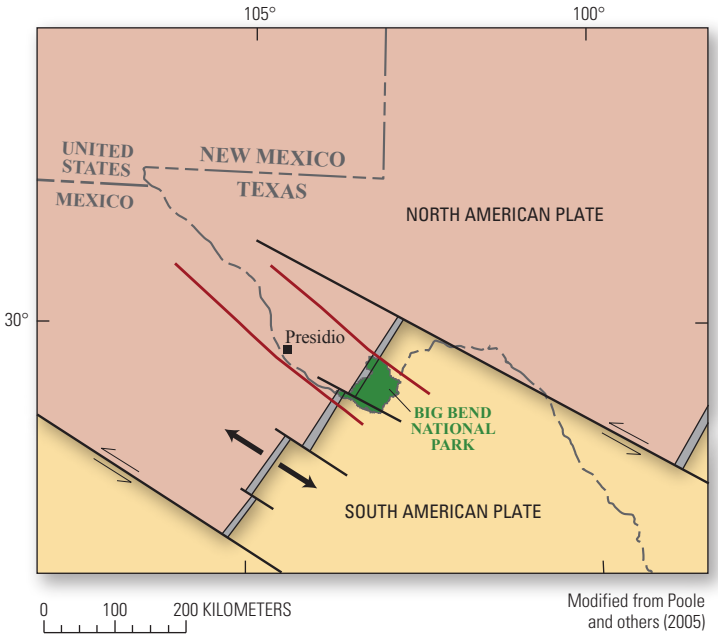

Figure 9. Map showing transform faults and lineaments related to Proterozoic rifting along the southern North American continental margin. Solid black lines are Neoproterozoic transform faults (Thomas, 1991; Poole and others, 2005); arrows show relative motion of continental plate offset; gray double-banded line is interpreted rift zone between North and South American plates; solid red lines are Texas lineament (Muehlberger, 1980); dark green area is BBNP.

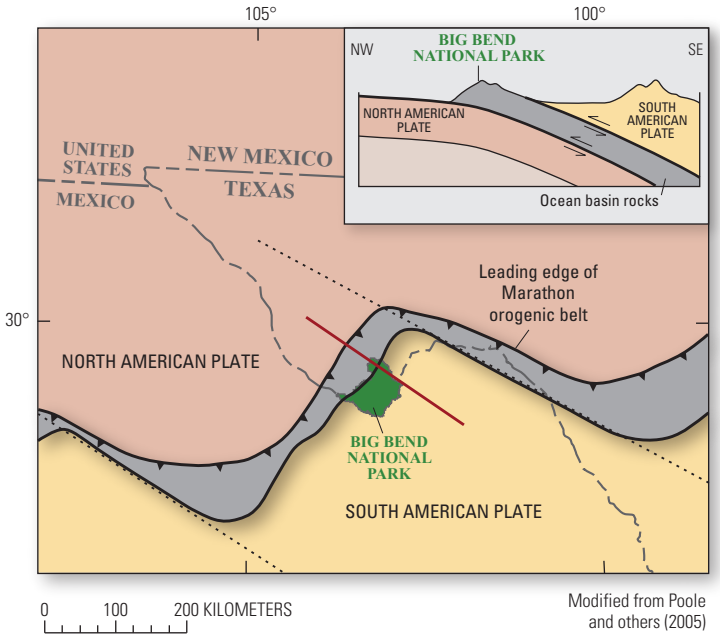

Figure 10. Map showing location of Paleozoic Marathon orogenic belt (gray), formed from convergence between the North and South American plates. Dotted black lines are traces of Proterozoic transform faults shown in figure 9; solid red line is approximate line of section for inset figure; dark green area is BBNP.

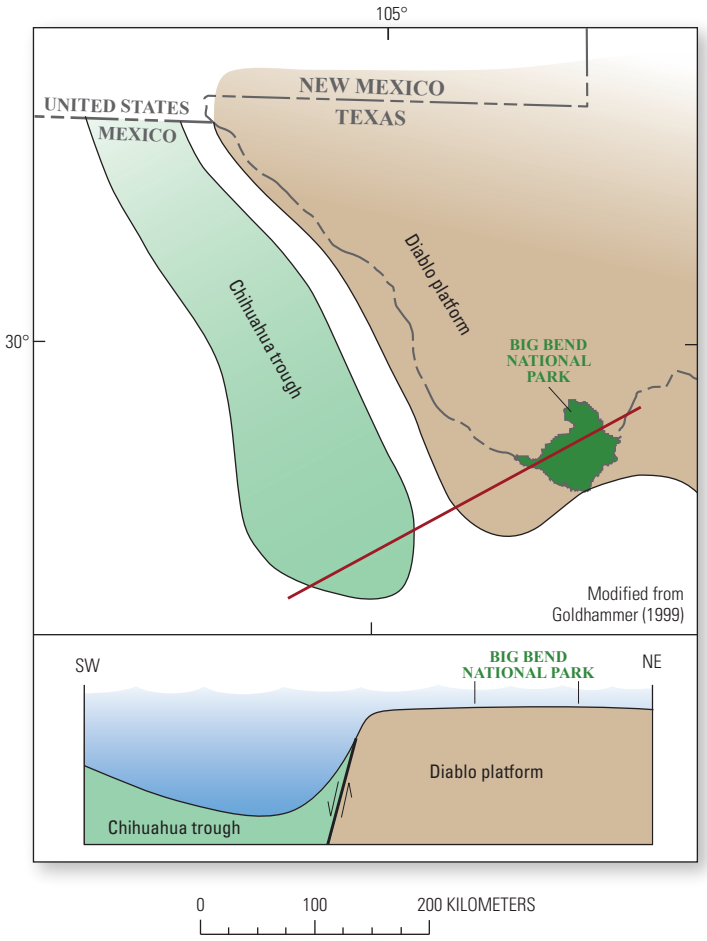

Figure 11. Map showing location of the Diablo platform and the Chihuahua trough, features that formed in the Big Bend area during Late Triassic through Late Cretaceous rifting between North and South America. Solid red line is approximate line of section for inset figure; dark green area is BBNP.

Triassic to Cretaceous Rifting

From the Late Triassic into the Late Cretaceous (about 200–85 Ma), the BBNP area experienced subtle effects of rifting, or seafloor spreading, between North and South America; this rifting controlled the opening of the Gulf of Mexico (Muehlberger, 1980; Muehlberger and Dickerson, 1989; Lehman and Busbey, 2007). During rifting, BBNP was part of the Diablo platform (fig. 11) (Henry, 1998; Goldhammer, 1999), where sediments of Lower and Upper Cretaceous limestone and shale units were deposited in a shallow, open-marine shelf environment. These units include, from base to top, the Glen Rose Limestone, Maxon Sandstone, Telephone Canyon Formation, Del Carmen Limestone, Sue Peaks Formation, Santa Elena Limestone, Del Rio Clay, Buda Limestone, Boquillas Formation, and Pen Formation.

Southwest of the platform, an ocean basin known as the Chihuahua trough formed in association with the opening of the Gulf of Mexico (fig. 11) (Muehlberger, 1980; Muehlberger and Dickerson, 1989; and Lehman and Busby, 2007). Development of the trough resulted from Late Triassic rifting, and faulting along its margin with the Diablo platform (fig. 11) controlled subsidence of the trough from the Jurassic to Late Cretaceous time (Lehman and Busbey, 2007). Cretaceous rocks in the Chihuahua trough are much thicker than time-equivalent rocks of the Diablo platform. Lehman and Busbey (2007) reported that trough rocks of the Ojinaga Formation (found outside of BBNP) are about six times thicker than equivalent platform rocks of the Boquillas Formation in BBNP.

Deposition of the Upper Cretaceous Aguja and Javelina Formations in BBNP indicate a significant shift from marine to continental deposition. This change in depositional regime, coupled with thickness similarities between equivalent trough and platform rocks, indicate the trough had filled and major subsidence had ended by Late Cretaceous time (Lehman and Busbey, 2007).

Late Cretaceous–Early Tertiary Laramide Orogeny

The Late Cretaceous–early Tertiary Laramide orogeny was a period of contractional deformation that produced monoclinal uplifts, basins, and faults and folds from northeast-southwest compression broadly related to subduction of the Farallon plate at the western edge of North America (fig. 12). The plate convergence formed the Cordilleran overthrust belt, which extends from Canada to Mexico in the intermountain region of western North America, and the Laramide foreland east of the overthrust belt (fig. 12). The two provinces are temporally and structurally distinct, and thin-skinned Cretaceous deformation of the overthrust belt generally pre-dated thick-skinned, basement-involved deformation of the Laramide foreland (Dickinson and others, 1988). The Chihuahua tectonic belt, southwest of BBNP (fig. 12), represents the frontal edge of the overthrust belt in the region. Structures in BBNP likely formed in the Laramide foreland from vertical uplift along basement-involved transpressional faults, and broad folding, similar to other structures in the foreland of Wyoming, Colorado, New Mexico, and Arizona (Muehlberger, 1980).

The major Laramide structures in BBNP include the Mesa de Anguila monocline, an uplifted monocline on the southwest margin of the park; the Sierra del Carmen-Santiago Mountains monocline, an uplifted and thrust-faulted monocline bounding the eastern part of the park; and the Tornillo basin (Lehman, 1991), which developed between the uplifted monoclines (fig. 12). Major Laramide folds in BBNP include the Mariscal Mountain and Cow Heaven anticlines (fig. 12). Thrust faults in BBNP are mostly southwest-vergent and include the Santiago thrust (Poth, 1979; Cobb, 1980; Cobb and Poth, 1980) in the southern Santiago Mountains (cross section *A–A′*), and small-scale thrusts at Mariscal Mountain (Maxwell and others, 1967) and in the southern Sierra del Carmen (Maler, 1987).

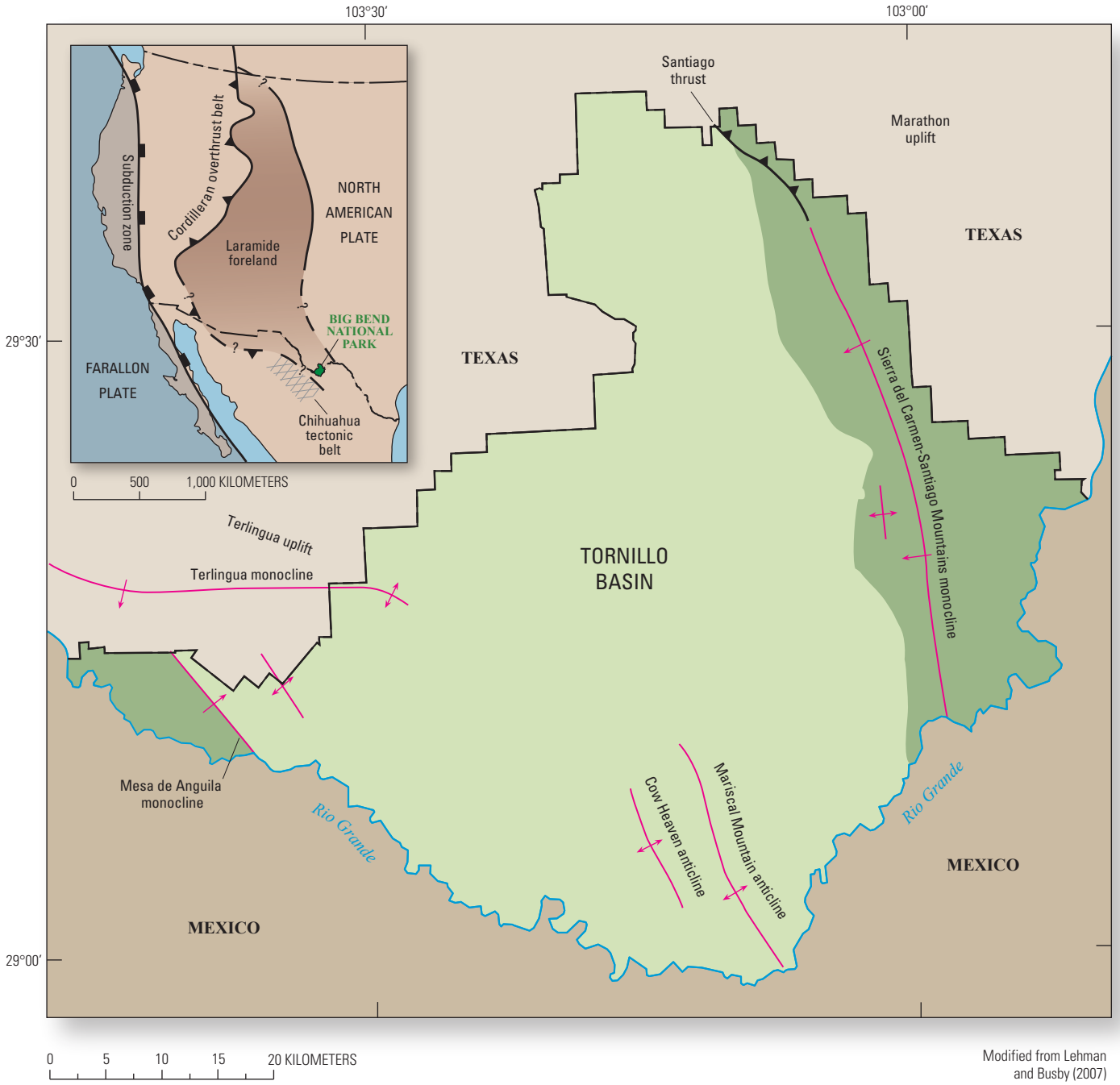

Figure 12. Generalized map of the major structures that formed in the BBNP area during the Laramide orogeny. Inset map shows location of North American and Farallon plates, subduction zone along the western North American continental margin, Cordilleran overthrust belt, and Laramide foreland in western North America, BBNP in dark green, and Chihuahua tectonic belt southwest of BBNP.

Northwest view of the southern Santiago Mountains, extending from Dog Canyon area to Persimmon Gap. Shown in foreground are outcrops of Buda Limestone (ledge) and overlying Boquillas Formation (slope), which are in the lower plate of the Santiago thrust fault. The main ridge of southern Santiago Mountains is composed mostly of the Lower Cretaceous Glen Rose Limestone, which forms the upper plate of the Santiago thrust fault. Shown along main ridge is scar from 1987 rock slide. *(Photograph by Kenzie J. Turner)*

The Mesa de Anguila monocline was described by DeCamp (1981, 1985) as a northeast-directed monoclinal flexure that formed from northeast-directed Laramide compression of the Chihuahua tectonic belt against the stable Diablo platform in the BBNP area. DeCamp (1981, 1985) discussed evidence for left-lateral strike-slip faults at Mesa de Anguila and speculated that these faults largely accommodated uplift of the monocline during the Laramide. The monocline and strike-slip faults were interpreted as an eastern extension of the much broader Terlingua uplift (fig. 12), west of BBNP (Erdlac, 1990). The age of the Terlingua uplift is reported to be between 68 and 50 Ma, and it was interpreted as a push-up block, or transfer zone, which primarily accommodated left-lateral shearing related to northeast-directed Laramide compression (DeCamp, 1981, 1985; Muehlberger, 1989; Muehlberger and Dickerson, 1989; Erdlac, 1990).

The Sierra del Carmen-Santiago Mountains monocline (cross sections *B–B′* and *C–C′*) forms the southwestern margin of the much broader Marathon uplift (fig. 12) (Lehman, 1991; Ewing, 1991), a Laramide dome, which uplifted and exposed deformed Paleozoic strata northeast of BBNP. The monocline is thrust-faulted in the Santiago Mountains by the Santiago thrust fault (Cobb, 1980; Cobb and Poth, 1980), a southwest-directed thrust which juxtaposes mainly Lower Cretaceous rocks in the upper plate above the Upper Cretaceous Aguja and Pen Formations in the lower plate (cross section *A–A′*). The thrust extends southward into the Dagger Flat area, where it dies out into a series of range blocks containing several monoclines formed during the Laramide (Moustafa, 1988), that were later domed by middle Tertiary intrusions, and faulted by late Tertiary normal faults. Maler (1987) mapped some small-scale, southwest-directed thrust faults in the southern Sierra del Carmen, northwest of Boquillas Canyon (pl.), and like the Santiago thrust, they are southwest vergent and juxtapose Lower Cretaceous rocks in the upper plate above Upper Cretaceous rocks in the lower plate.

Dickerson (1980) interpreted the Sierra del Carmen-Santiago Mountains monocline as a raised basement ridge that was uplifted during the Laramide along reactivated basement-cored faults. Muehlberger (1980) proposed the Sierra del Carmen-Santiago Mountains monocline to have formed by vertical uplift from upthrusting and drape folding, and described it as a typical Laramide basement-involved uplift, similar to other basement-cored uplifts in the Laramide foreland. Lehman and Busbey (2007) also noted similarities between the uplift with other basement-cored uplifts in the Laramide foreland. Although the origin of basement-cored uplifts remains debatable in BBNP and other parts of the Laramide foreland, and whether they resulted from vertical or horizontal tectonism, or a combination of both, the Sierra del Carmen-Santiago Mountains monocline was attributed to horizontal compression and left-lateral shearing along major transpressional faults (Cobb and Poth, 1980; Muehlberger, 1980, 1989; Moustafa, 1988; Muehlberger and Dickerson, 1989; Maler, 1990), similar to the Terlingua uplift described by Erdlac (1990), west of BBNP. Other models of transpressional deformation associated with basement-cored uplifts in Laramide foreland of Colorado and New Mexico were described by Chapin and Cather (1983).

View near Persimmon Gap showing the approximate trace of the Santiago thrust fault (thick dashed line; arrow shows direction of movement on fault), and southwest-vergent, overturned anticline in the Lower Cretaceous Glen Rose Limestone (Kgr) in the upper plate of the thrust, above the Upper Cretaceous Pen Formation (Kp) in the lower plate. *(Photograph by Kenzie J. Turner)*

The Tornillo basin of Lehman (1991) formed between the Mesa de Anguila and Sierra del Carmen-Santiago Mountains monoclines (fig. 12). The basin is asymmetric with the deepest part adjacent to the western flank of the Sierra del Carmen-Santiago Mountains monocline. The synorogenic rocks that compose the basin fill are mostly fluvial deposits and include, from base to top, the Javelina, Black Peaks, and Hannold Hill Formations. Based on sedimentological and structural data, Lehman (1991) reported that Laramide deformation in the basin began with deposition of sediments of the Javelina Formation (70–65 Ma) and ended after the middle Eocene, with deposition of sediments of the Canoe Formation, about 50 Ma. The Canoe Formation unconformably overlaps folds as well as thrust and reverse faults in the Hannold Hill, Black Peaks, Javelina, and Aguja Formations (Lehman and Busbey, 2007).

Major Laramide folds in the Tornillo basin include the northwest-trending Mariscal Mountain and Cow Heaven anticlines (fig. 12). The Mariscal Mountain anticline is an asymmetric fold that is deformed by small-displacement thrust faults (pl.; cross section *C*–*C′*). Maxwell and Dietrich (1965), Maxwell and others (1967), and Bumgardner (1976) interpreted mafic sills, partly concordant with bedding planes in the anticline, were emplaced prior to Laramide folding based on field relations and preliminary K-Ar geochronology. Henry and McDowell (1986) reinterpreted the mafic sills were emplaced after Laramide folding based on field observations and on K-Ar age determinations for sill rocks at about 38 Ma (Henry and others, 1986), and paleomagnetic and geochronologic investigations by Harlan and others (1995) further supported the sills were emplaced at about 37 Ma, following Laramide folding. Our age determinations for the mafic sills at Mariscal Mountain were inconsistent, and we obtained a U-Pb zircon age as old as 46.5 ± 0.3 Ma, and an $^{40}Ar/^{39}Ar$ age as young as 36.11 ± 0.19 Ma (appendix; 86). All these ages for the mafic sills are compatible with widespread mafic magmatism which post-dated major episodes of Laramide folding throughout the BBNP region (Henry and others, 1986). The Cow Heaven anticline has mafic sills like Mariscal Mountain, and although these rocks were not dated, they probably were emplaced in a similar manner and time period as the sills at Mariscal Mountain. The Cow Heaven anticline is an asymmetric fold, with steep easterly dips (as great as 80°) along the east flank of the anticline (cross section *C*–*C′*).

North-northwest-trending folds in Cretaceous rocks are present in other parts of the park (pl.), such as those east of Terlingua Creek, near Slickrock Mountain, and southeast of McKinney Hills, and many of these are likely Laramide structures; however, some of the folded Cretaceous rocks are adjacent to Oligocene intrusions; therefore, it is difficult to determine if folds are Laramide, or are Laramide folds reactivated during Oligocene magmatism. Maxwell and others (1967) discussed probable Laramide folds in Cretaceous rocks in BBNP that they interpreted as refolded during Oligocene magmatism. Other folds deform volcanic and intrusive rocks in the Chisos Mountains, and formed primarily during Oligocene magmatism. Some examples include the Hayes Ridge anticline, attributed to collapse of the Pine Canyon caldera (Ogley, 1978), local folds formed from doming at Sierra Quemada (Scott and others, 2007), and folds adjacent to other domes, plutons, and intrusions.

Mafic sill (above thin brownish-weathering bed) in the Pen Formation (below brownish-weathering bed) at Mariscal Mountain. *(Photograph by Daniel P. Miggins)*

Middle Tertiary Volcanic and Intrusive Features

Pine Canyon Caldera

At about 32 Ma, the Pine Canyon caldera complex (fig. 2; pl.; cross section *B*–*B′*) erupted rocks of the South Rim Formation, which are mostly preserved in the high Chisos Mountains. Pre-eruptive development of the caldera began with doming of the country rock as a result of rising magma, as indicated by thinning of the Chisos Formation, and an angular unconformity between the Chisos and overlying South Rim Formation units around the perimeter of the caldera (Maxwell and others, 1967; Ogley, 1978; Barker and others, 1986). A down-sag style of collapse was interpreted for the caldera based on inward dips in the Chisos Formation and the apparent lack of ring faults (Ogley, 1978; Barker and others, 1986). Initial caldera subsidence accompanied eruption of the Pine Canyon rhyolite, causing the tuff to pond within the caldera (cross section *B*–*B′*). Following initial caldera development, rocks of the Boot Rock member erupted from multiple vents around the periphery of the caldera, and were deposited within the caldera, in the South Rim area, and as far west as Burro Mesa. Ponding of the Boot Rock member within the caldera suggests that collapse may have continued after eruption of the Pine Canyon rhyolite, or the caldera simply remained as a topographic low (Barker and others, 1986). Volcanic activity related to the Pine Canyon caldera concluded with eruption of the Emory Peak rhyolite from vents along the caldera periphery (Ogley, 1978; Barker and others, 1986; Benker, 2005; White and others, 2006).

Intrusive activity related to the Pine Canyon caldera magmatic system mainly occurred after caldera development (Ogley, 1978; Barker and others, 1986), and included emplacement of the Hayes Ridge ring dike (Ogley, 1978) and Ward Mountain-Pulliam Peak pluton (fig.2; pl.). Emplacement of these intrusions likely followed the main pulse of caldera-forming extrusive activity, based on deformed South Rim outflow deposits adjacent to the intrusion northwest of Pulliam Peak and on the west side of the South Rim (Maxwell and others, 1967). The Ward Mountain-Pulliam Peak intrusion uplifted Cretaceous strata, which are exposed adjacent to the intrusion in The Basin.

Recent analysis of aeromagnetic and gravity data revealed new details of the structure, igneous geology, and temporal evolution of the Pine Canyon caldera (Drenth and Finn, 2007). The primary intracaldera fill and oldest unit of the South Rim Formation, the Pine Canyon rhyolite, is reversely magnetized, and aeromagnetic data were used to estimate caldera fill thickness. Modeling of gravity and aeromagnetic data indicates that Pine Canyon rhyolite is probably thickest in the northeastern part of the caldera, where it may be greater than 1 km thick (Drenth and Finn, 2007). Lineaments interpreted from high-resolution aeromagnetic data (Drenth and Finn, 2007) suggest the presence of buried faults beneath the caldera fill (cross section *B*–*B′*), which may have led to increased subsidence in the northeast part of the caldera, allowing for thicker sections of caldera fill to accumulate there.

South-dipping units of the South Rim Formation along the southeast flank of the Pine Canyon caldera, near the mouth of Pine Canyon. *(Photograph by Don Corrick)*

Sierra Quemada

The Sierra Quemada dome and intrusive complex (fig. 2; cross section *B–B′*) is a strikingly circular feature in the southwest part of the Chisos Mountains (pl.). Previous workers interpreted Sierra Quemada as a caldera formed by eruption of the Mule Ear Spring Tuff Member of the Chisos Formation at 33.65 Ma (Ogley, 1978; Henry and Price, 1984; Duex and Tucker, 1989; Duex, 2007). However, Scott and others (2007) concluded that Sierra Quemada was most likely not a caldera, but was formed as rising magma domed the overlying country rock (cross section *B–B′*), followed by intrusion of a nearly continuous, circular rhyolitic ring dike (pl.) between about 31–30 Ma. No evidence for collapse or faults connecting gaps in the ring dikes was found. Intrusive activity was accompanied, or possibly preceded, by minor explosive venting, which is preserved as several irregularly shaped bodies of lithic-rich volcanic breccia. Lithic clasts consist of Chisos Formation volcanic rocks, some Paleozoic rocks, and blocks of Cretaceous limestone as large as 200 m in length. No outflow units were observed suggesting only a small volume of gaseous material erupted before venting ceased (Scott and others, 2007).

Dominguez Mountain

A small volcano formed at Dominguez Mountain with numerous vertical dikes radiating into the surrounding country rock (pl.), and the mountain still preserves the original cone shape of this volcano. The volcano has not been studied in detail, but good descriptions exist for the rocks that compose the volcano and dikes (Maxwell and others, 1967). Small granitic, intrusive bodies surround the volcano at Dominguez Mountain, and its interior is a mixture of layered flows and dense dike swarms. The layered rocks dip gently outward from the volcanic center and likely originated as lava flows forming the flanks of the volcanic buildup (Bohannon, 2011). The dike swarm cuts the layered rocks vertically and forms large bodies of rock in which dikes intrude other dikes to the extent that country rock is nearly absent. The dikes include both mafic and intermediate rock types, with intermediate types being more prevalent. Most dikes radiate outward from the volcanic center to the southwest but dikes radiate to the east and north as well. The most conspicuous dikes to the southwest of the center (pl.) merge upward into a series of 30-Ma trachytic flows (Tt) at the top of Punta de la Sierra (Bohannon, 2011). The source of the 30-Ma flows is unknown, but their spatial proximity and compositional similarity to the dike swarm suggests that Dominguez Mountain should be considered as a possibility.

Major Laccoliths and Sills

Many of the larger intrusive bodies in BBNP were emplaced at about the same time as the Pine Canyon caldera (about 32 Ma). The laccoliths at the Rosillos Mountains, McKinney Hills, and Grapevine Hills (fig. 2) were emplaced between 33 and 32 Ma (appendix; Miggins and others, 2007), and may be related based on similar geochemical and petrologic characteristics (Maxwell and others, 1967). Although the timing of emplacement for these intrusions is similar to the Pine Canyon caldera, it is unlikely that they are directly related. However, it is clear there was a significant influx of magma rising into the park at the time of caldera eruption.

Integrated detailed geologic mapping and analysis of high-resolution aeromagnetic data indicate the major laccoliths and sill complexes in BBNP show a variety of geometries ranging from single to stacked, mostly concordant intrusive bodies (Scott and others, 2004a and b; Anderson, 2007). The surficial exposure of these intrusive bodies ranges from nearly completely exposed (Rosillos Mountains), to partly exposed (McKinney Hills, Grapevine Hills, Dagger Flat, and Bone Spring) (fig. 13).

The laccolith at Rosillos Mountains (Scott and others, 2004b; Anderson, 2007) is one of the largest in BBNP, and is semicircular in shape (10.5 km by 7.5 km) with its long axis striking north-northwest (fig. 13). Geophysical modeling shows the laccolith at Rosillos Mountains is one intrusive body greater than 600 m thick at the northern end, and less than 200 m thick at the southern end. The laccolith at McKinney Hills is a more complex feature consisting of several stacked, quasi-concordant intrusive bodies (cross section *B–B′*). The upper body is exposed in the eastern part where it overlies the Pen Formation, and the lower body is in the western part where it is mostly concealed, and underlies the Pen Formation (cross section *B–B′*). These relations led Maxwell and others (1967) to interpret "pine tree" geometry for the laccolith, with different bodies extending laterally at different stratigraphic levels. Aeromagnetic data indicate that the laccolith at Dagger Flat is adjacent to the laccolith at McKinney Hills, and although it has limited surface expression, its subsurface distribution is larger than the laccolith at McKinney Hills (fig. 13) (Scott and others, 2004a; Morgan and Shanks, 2008). A positive magnetic anomaly extends about 5 km east of the laccoliths at McKinney Hills and Dagger Flat (fig 13; intrusive 1); modeling of the anomaly indicates an intrusive body about 300 to 500 m thick with its top about 300 to 1,000 m depth (east end of cross section *B–B′*). It is unknown whether this is a separate body from the two laccoliths or an extension of one of the two. The laccolith at Grapevine Hills consists of a single intrusive body about 3.5 km wide and about 200 m thick. The laccolith at Bone Spring is about 50 to 100 m thick (cross section *A–A′*), and about 6 km by 3 km wide, with the long axis trending north-northeast (fig. 13). Aeromagnetic data show a laccolith similar in size to the laccolith at Bone Spring on the downthrown side of the Chalk Draw fault (intrusive 2), north of the Rosillos Mountains (fig. 13); the laccolith has limited surface expression, and is characterized by several small, scattered outcrops.

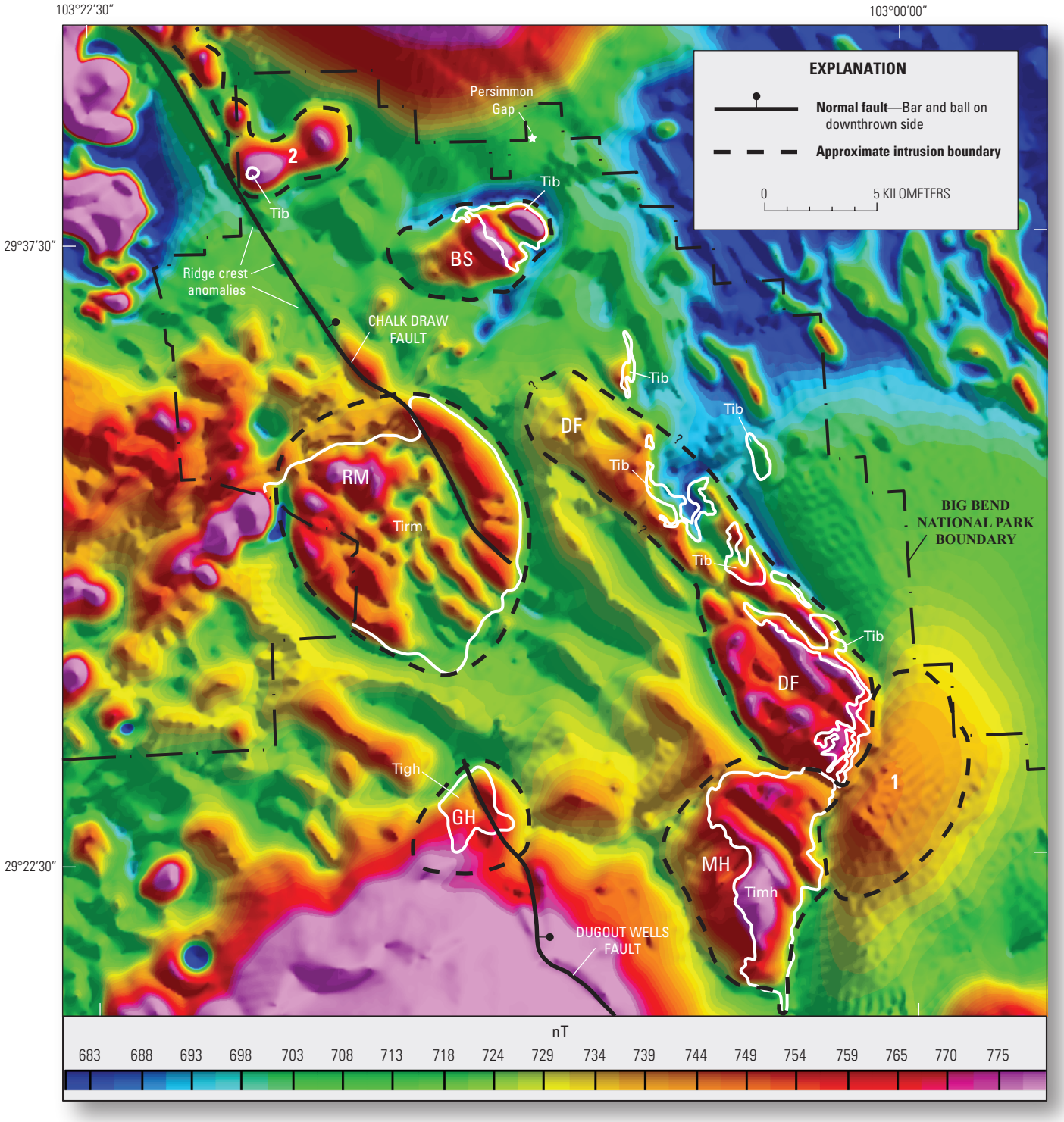

Figure 13. Reduced-to-pole magnetic anomaly map of northern BBNP. Map shows approximate intrusion boundaries (thick black-dashed lines) compared to intrusion surface exposure (solid white lines labeled by map unit). Map also shows linear magnetic anomalies correlated with Chalk Draw fault and northern end of the Dugout Wells fault. Laccoliths at Bone Spring, BS; Dagger Flat, DF; Grapevine Hills, GH; McKinney Hills, MH; Rosillos Mountains, RM; unnamed intrusion 1, 1; unnamed intrusion 2, 2; basaltic and other mafic composition intrusive rocks, Tib; fayalite syenite of McKinney Hills, Timh; syenite of Rosillos Mountains, Tirm; and fayalite syenite of Grapevine Hills, Tigh.

Tectonic Setting for BBNP Magmatism

Magmatic activity in the Big Bend region occurred from about 47 Ma to at least 17 Ma, extending from shortly after the Laramide orogeny to well after the onset of basin-and-range rifting; the opposing stress regimes induced by the two tectonic events influenced magma source, generation, and compostion. The Laramide orogeny corresponds to shallow subduction of the Farallon plate beneath the western margin of the North American plate (fig. 12) that resulted in an eastward-migrating continental arc in a compressional stress regime. A compressional regime during the Laramide orogeny was succeeded by an extensional regime associated with basin-and-range rifting after 31 Ma, but no later than 28 Ma (Henry and others, 1991). Basalts with a distinct rift-related composition common to basin-and-range rifting were first erupted around 24 Ma, and persisted until 17 Ma (Henry and others, 1986), and possibly longer, but none of these basalts have been identified in BBNP.

Barker (1977) proposed all Trans-Pecos magmatism resulted from rifting based on the abundance of alkalic rocks and the assumption that extension-related faulting and magmatism were contemporaneous. However, later studies have shown a compressional regime persisted until about 31 Ma, with an extensional regime starting no earlier than 31 Ma, and rift-related normal faulting began about 25 Ma (Stevens and Stevens, 1985; Henry and Price, 1986; Stevens, 1988; Henry and others, 1991). Price and others (1987) and James and Henry (1991) identified a compositional shift in mafic rocks throughout Trans-Pecos Texas corresponding to the stress regime change around 31 Ma.

White and others (2006) speculated that rifting began at around 36 Ma, based on the assumption that generation of peralkaline magma associated with the Pine Canyon caldera, required extension. They applied the early continental rift model of Lawton and McMillan (1999), developed for the Rio Grande rift in New Mexico, that suggested foundering of the subducting slab caused uplift, rifting, and peralkaline and bimodal volcanism. Parker and McMillan (2007) suggested that peak magmatism in Trans-Pecos Texas between 38–35 Ma was an indication of early rifting based on the assumption that peralkaline magma generation is restricted to extensional environments. However, structural data supporting the onset of rifting prior to 31 Ma are lacking (Henry and others, 1991).

Late Tertiary Basin-and-Range Faulting

The last major tectonic episode in BBNP was basin-and-range faulting which occurred in the park region from about 25 to 2 Ma (Henry, 1998). Basin-and-range faulting resulted from rifting across the Basin-and-Range Province of western North America. The rifting caused stretching or pulling apart of the western North American continental crust to form uplifted ranges and intervening down-dropped basins. Big Bend National Park is part of the Rio Grande rift, an eastern subprovince of the Basin-and-Range, which extends northward from Texas, through New Mexico, and into southern Colorado. Most basin-and-range faults in the BBNP area are north-northwest-striking, high-angle normal faults (fig. 2), which formed perpendicular to east-northeast directed extension in the region (Henry, 1998; Henry and Price, 1986).

Some of the basin-and-range faults formed local depositional basins, such as the Delaho bolson, which extends beyond the boundaries of BBNP, and Estufa bolson on the eastern flank of the Chisos Mountains (Stevens and Stevens, 1989). The Delaho bolson is characterized by numerous northwest-striking faults, and the Estufa bolson is bound on the west side by the Dugout Wells fault (fig. 2). The bolsons contain thick accumulations of Miocene to Pleistocene sediments (Ta and QTa, pl.). Smaller depositional basins in BBNP include the Solis basin (Maxwell and other, 1967), east of Mariscal Mountain (fig. 2), and several local basins in the Sierra del Carmen (pl.). Most of these basins also contain units as old as Pliocene to early Pleistocene age (QTa).

Southwest of the Chisos Mountains, northwest-striking faults in the Delaho bolson are steep (greater than 70° dips) and mostly down to the southwest (fig. 2; pl.). These faults repeat sections of the Chisos Formation and overlying Tertiary basin-fill sediments (Ta) from Goat and Kit Mountains, southward to Sierra de Chino (pl.; cross section *B–B′*). The fault with the greatest amount of offset juxtaposes Eocene and Oligocene sedimentary units of the Chisos Formation in the footwall against Miocene alluvium in the hanging wall, with about 500 m of throw. Dickerson and Muehlberger (1994) interpreted the Delaho bolson as a deep, rift basin based on the presence of syn-rift basaltic dikes with mantle-derived xenoliths in the northwestern part of the bolson near Terlingua (fig. 1).

Stevens (1969) and Muehlberger (1989) interpreted the northeast margin of the Delaho bolson to be defined by the Burro Mesa fault, and the southwest margin by the Terlingua fault (fig. 2), indicating the bolson extends over a distance of about 25 km in western BBNP. The Burro Mesa fault is a down-to-the-west normal fault exposed on the east flank of Burro Mesa. The northern segment of the fault is reported to have about 900 m of offset (Maxwell and others, 1967), and it downdrops rocks of the Chisos Formation against the Aguja and Pen Formations. The southern segment of the fault downdrops rocks of the Burro Mesa Formation and units as young Pliocene–Pleistocene basin-fill sediments (QTa), against units of the Chisos Formation, including the Bee Mountain Basalt Member (pl.). The southernmost part of the fault dies out in the undifferentiated units of the younger part of the Chisos Formation, west of Sierra Quemada (Maxwell and others, 1967).

The Terlingua fault (fig. 2) forms steep limestone cliffs on the northeast side of Mesa de Anguila near the mouth of Santa Elena Canyon, and kinematic data indicate mostly normal displacement (DeCamp, 1981). At the mouth of Santa Elena Canyon (fig. 1), the fault has about 850 to 900 m of displacement (Maxwell and others, 1967; DeCamp, 1981; Dickerson and Muehlberger, 1994; Lehman and Busbey, 2007), and juxtaposes the Aguja Formation in the hanging wall against Glen Rose Limestone in the foot wall. The fault zone extends 30 km southward into Mexico where throw increases to more than 1,300 m, and it defines the northeast edge of Sierra Ponce, the southeastern extension of Mesa de Anguila (DeCamp, 1981). Throw on the fault decreases northwest of Santa Elena Canyon.

Southwest view of Santa Elena Canyon showing the approximate trace of the Terlingua fault (thick dashed line; bar and ball on downthrown side), which forms the steep escarpment on the northeast side of Mesa de Anguila (Texas) and Sierra Ponce (Mexico). At the mouth of the canyon on the U.S. side, the fault juxtaposes Lower Cretaceous strata (Glen Rose Limestone) in the foot wall, against Upper Cretaceous strata (Aguja Formation) in the hanging wall. *(Photograph by Daniel P. Miggins)*

Calcite-lined fracture in Pliocene–Pleistocene alluvial-fan gravels (QTa) in the Dugout Wells fault zone near Estufa Spring; steepened dip of gravels caused by faulting. *(Photograph by Van S. Williams)*

The Estufa bolson (Stevens and Stevens, 1989) is about 25 km long and 10 km wide, and is bound on the west by the Dugout Wells fault (fig. 2; pl.; cross section *B*–*B′*). The Dugout Wells fault is covered along most of its projected trace, but extends northward to the Grapevine Hills area (figs. 2, 13). Southward, the fault loses throw and likely dies out about 1 to 2 km south of its intersection with cross section *C*–*C′*. The fault was interpreted to be active, based on offset caliche horizons and unlithified sediments, and disrupted stream drainages (Stevens and Stevens, 1989), but new mapping of surficial deposits in BBNP indicated no clear evidence for active faulting. The fault offsets rocks as young as Pliocene–Pleistocene basin-fill sediments (QTa) in the Estufa Spring area, and near its southern end.

Numerous northwest-striking basin-and-range faults in Sierra del Carmen (fig. 2; and pl.) originated from east-northeast-directed extension across the BBNP region (Henry, 1998). The major faults in the Sierra del Carmen are down to the east (cross sections *B*–*B′* and *C*–*C′*), and they formed a series of uplifted blocks and intervening grabens that characterize the range. The most prominent uplifted blocks in the Sierra del Carmen form steep limestone escarpments of Sierra del Caballo Muerto and Cuesta Carlota (pl.). Maxwell and others (1967) referred to the Sierra del Caballo Muerto as the backbone ridge of Sierra del Carmen, and it contains Sue Peaks, one of the highest points (1,784 m) in the entire range (east end of cross section *B*–*B′*; pl.). Normal faults bounding Sierra del Caballo Muerto have estimated offsets of about 500 m (Maxwell and others, 1967). The most prominent graben in Sierra del Carmen is Ernst basin (Ernst Valley of Maxwell and others, 1967), on the east side of Cuesta de Carlota (pl.).

East view toward Dugout Wells fault near Estufa Spring. Approximate location of fault is shown by dashed line, bar and ball on downthrown side. Low hills on downthrown side are Pliocene-Pleistocene basin-fill sediments (QTa) of Estufa bolson. Rocks on the upthrown side are gray and red units of the Canoe Formation. *(Photograph by Van S. Williams)*

The Rosillos Mountains, Chalk Draw basin, and Bone Spring areas of northern BBNP contain numerous northwest-striking basin-and-range faults, and a majority of these faults are down to the northeast (pl.; cross section *A–A′*). The most prominent is the Chalk Draw fault, which forms the escarpment on the west side of Chalk Draw basin (pl.; fig. 2). The fault strikes northwest, and juxtaposes rocks as old as the Santa Elena Limestone in the footwall, against mainly rocks of the Aguja Formation in the hanging wall, and offset is estimated to be about 700 m (pl.; cross section *A–A′*). The fault forms a linear anomaly in the reduced-to-pole magnetic data (fig. 13) (Anderson, 2004); the lineation in the magnetic data is defined by a series of aligned ridge-crest anomalies (fig. 13), which reflect offset of shallow, magnetic intrusive rocks in the subsurface. In the Chalk Draw fault area, these rocks are probably Tertiary mafic sills like those that have intruded parts of the Boquillas Formation on the mesa to the west (pl.). The fault extends southward across the northeastern edge of the Rosillos Mountains (pl.) where offset decreases from about 600 m along the northwestern part of the range, to about 200 m along the southeastern part. Numerous other northwest-striking faults offset the laccolith at Rosillos Mountains; geologic and geophysical models of the laccolith indicate these faults do not have significant vertical offset or any horizontal displacement (Anderson, 2007; Finn and Anderson, 2008).

New mapping revealed a series of northwest-striking faults that offset the laccolith at Bone Spring and Cretaceous sedimentary rocks of the Aguja Formation (cross section *A–A′*; pl.). These faults are steep (dips of greater than 70°), and kinematic data indicate mostly dip-slip movement (W.R. Page, R.B. Scott, and L. Snee, unpub. mapping). A down-to-the-northeast fault at the southwestern edge of the laccolith was originally interpreted by Page and others (2004) as an active fault, based on apparent offset of Quaternary terraces. Upon further investigation, however, the Quaternary terraces were observed not to be offset, and were mapped as terraces of different age, indicating the fault is likely a Tertiary basin-and-range fault-line scarp.

Basin-and-range faults predated integration of late Tertiary basins with the Rio Grande, which began about 2 Ma, and they were the last structures to shape BBNP's present-day landscape. The Quaternary Period (2.6 Ma to present) in BBNP was characterized by extensive erosion, downcutting, and some aggradation related to integration of BBNP basins with the Rio Grande.

Quaternary Landslides

The BBNP area contains several large landslide complexes (Qls) in the Chilicotal and Talley Mountains area (Collins and others, 2007, 2008), on the northwest flank of the Chisos Mountains (R.B. Scott, unpub. mapping; Bohannon, 2011), and on the northeast flank of the Rosillos Mountains (R.B. Scott and W.R. Page, unpub. mapping). The age of the landslides in BBNP is Quaternary (Collins and others, 2007; Berry and Williams, 2008); some Tertiary basin-and-range faults are concealed by the slide masses, and younger surficial units are shown to overlap parts of the landslides. The landslides are recognized by their hummocky, irregular upper surfaces, disrupted strata, and they characteristically occur adjacent to areas of high relief, where more competent rock units overlie, or are adjacent to, less competent Cretaceous mudstone, claystone, shale, and sandstone units.

The landslides at Chilicotal and Talley Mountain areas (pl.) were mapped and described by Collins and others (2007, 2008), and consist of a mixture of Tertiary syenite sill material which slid over incompetent mudstone and sandstone units of the Cretaceous–Tertiary Javelina and Black Peaks Formations. Detailed mapping indicates these are composite landslides resulting from multiple events since middle Pleistocene time when the climate was wetter in the region. Numerous pressure ridges were noted over the fan-shaped landslide surfaces, and younger surficial deposits overlap parts of the landslides in places.

One of the largest landslides in BBNP is on the northwest flank of the Chisos Mountains, north of Vernon Bailey and Pulliam Peaks (pl.) (R.B. Scott, unpub. mapping; Bohannon, 2011). The landslide is complex, having formed during several different events. The rocks within it are variably fractured, but in the higher parts of the slide, large bodies of rock are still intact, and the original stratigraphy is somewhat preserved. Near the toe of the slide, the rocks are nearly pulverized and different rock types are mixed together. Most of the rocks involved in this slide are the Chisos Formation, including the Ash Spring Basalt. All these units slid northwestward over Cretaceous–Tertiary mudstone.

The landslides on the north flank of the Rosillos Mountains (pl.) contain mostly Cretaceous sedimentary rocks of the Pen and Aguja Formations, and form rubbly zones downslope of the higher relief intrusive rocks. The landslides conceal Tertiary basin-and-range faults and are confined to zones where uplifted Cretaceous units flank the steep rim of the laccolith.

Cobb (1980) mapped landslide deposits in the Santiago Mountains, on the west side of Persimmon Gap. The landsides cover an area of a few square kilometers, and consist mostly of rocks of the Glen Rose Limestone that slid over incompetent mudstone and sandstone of the Pen and Aguja Formations. Cobb (1980) reported the age of the slides to be Tertiary, and he interpreted them to have formed during basin-and-range faulting, but characteristics of the slides indicate they are likely Quaternary, similar to the age of other major landslides in BBNP.

View to the southeast of the large landslide on the north flank of the Chisos Mountains. The image is derived from Google Earth™ (see *http://earth.google.com/*).

Ground view of the landslide in middle of photo (above yellowish-brown terrace), showing hummocky, irregular slide surface with disrupted strata. *(Photograph by Van S. Williams)*

Summary

The purpose of this map is to provide the National Park Service (NPS) and the public with an updated digital geologic map of BBNP. The geologic map of Maxwell and others (1967) is a comprehensive source of detailed geologic information for BBNP, and will remain an important data source for decades. However, the map is outdated and lacks a topographic base. Our objectives were to provide a new digital geologic map that can be utilized for standard GIS applications by NPS and the public, and to incorporate updated geologic information collected since the 1967 map was published, including the results of new studies carried out for this report.

New studies carried out for this project resulted in collaboration between the USGS, university professors and students, the Texas Bureau of Economic Geology, and the NPS. The map incorporates new detailed geologic mapping of surficial deposits over the entire BBNP, and provides data critical in carrying out GIS-based natural resource and ecosystem management activities. Surficial mapping also forms the foundation for understanding Quaternary and modern active processes in the park as they relate to the geologic history of the Rio Grande. New geologic mapping of Cretaceous–Eocene sedimentary units in the entire BBNP contributed to a highly refined understanding of the stratigraphy and structure of the park. The map presents new geologic mapping in the high Chisos Mountains, sheds light on features such as Sierra Quemada and Dominguez Mountain, and presents new findings on the Chisos Formation. New detailed mapping of the recently acquired Harte Ranch section presents new findings on the geometry and structure of the laccoliths at Rosillos Mountains and Bone Spring. An extremely important contribution in terms of mapping the volcanic and intrusive units in BBNP includes new isotopic age determinations and trace element geochemical analyses, which has helped to better define and constrain the age and composition of these rocks in BBNP. The map also identifies the distribution of major Quaternary landslides not shown in Maxwell and others (1967).

The oldest rocks in the park are Paleozoic units, which include the Ordovician Maravillas Formation, Silurian-Mississippian Caballos Novaculite, and the Mississippian-Pennsylvanian Tesnus Formation. Conodont samples from the Maravillas Formation collected for this project indicate the part of the formation exposed in the park is Late Ordovician in age. The Maravillas Formation and Caballos Novaculite were deposited in deep-water, basinal environments, and the Tesnus Formation is synorogenic flysch deposited in front of the advancing Marathon orogenic belt. The oldest recorded tectonic episode in BBNP is mountain building associated with the Marathon orogeny from Mississippian to Permian time (about 330–285 Ma). During this tectonism, deep ocean basin rocks originally deposited south of BBNP were thrust northwestward onto the North American continent by convergence between the North and South American plates. Only remnants of the Marathon orogeny can be seen in the present-day BBNP landscape; these remnants include small outcrop belts in the Persimmon Gap area containing Paleozoic rocks and northwest-directed thrust faults.

The absence of Triassic and Jurassic rocks in BBNP reflects a major period of erosion, which is locally characterized by an unconformity separating the Lower Cretaceous Glen Rose Limestone above, from rocks of the Mississippian–Pennsylvanian Tesnus Formation below. From the Late Triassic to the Late Cretaceous (about 200–85 Ma), the BBNP area experienced subtle effects of rifting, or seafloor spreading, between North and South America; this rifting controlled the opening of the Gulf of Mexico. During rifting, BBNP was part of the Diablo platform, where sediments of Lower and Upper Cretaceous limestone and shale units were deposited. Lower Cretaceous rocks in BBNP, including the Glen Rose Limestone, Del Carmen Limestone, and Santa Elena Limestone, consist of limestone and marl deposited in shallow, carbonate shelf environments of the Diablo platform. Lower Cretaceous rocks, including the Maxon Sandstone, Telephone Canyon Formation, and Sue Peaks Formation, are mixed clastic and carbonate rocks, which repeatedly interrupted carbonate deposition on the Diablo platform, and represented cyclic influx of terriginous material from tectonic uplift in source areas in the Marathon region, north of BBNP.

Upper Cretaceous sedimentary rocks in BBNP represented continued marine deposition, but there was a shift to mainly continental deposition reflected by the Javelina Formation, which was deposited mostly in fluvial, flood-plain environments. Continental deposition continued through the early Tertiary, and units of the Black Peaks, Hannold Hill, and Canoe Formations contain a variety of unique vertebrate fossils including dinosaurs, mammals, turtles, and crocodiles. The Late Cretaceous to early Tertiary Laramide orogeny (about 70–50 Ma) was a period of contractional deformation which produced uplifts, basins, and faults and folds broadly related to convergence of the North American continent and the Farallon oceanic plate at the western edge of the continent. Major Laramide structures in BBNP include the Mesa de Anguila monocline on the southwest margin of the park, the Sierra del Carmen-Santiago Mountains monocline, a thrust-faulted monocline bounding eastern BBNP, the Tornillo basin which developed between the uplifted monoclines, and the Mariscal Mountain and Cow Heaven anticlines.

BBNP is known for its volcanic landscape, and major volcanism in the park began about 47 Ma, with deposition of the Chisos Formation, and ended about 29 Ma, with eruption of the Burro Mesa Formation. Principal features formed during this period include volcanic flows extruded from a complex of vents and lava domes in western BBNP and Mexico, and the 32-Ma Pine Canyon caldera complex in the high Chisos Mountains, perhaps the most prominent geographic feature in the entire BBNP. It was during this time that major laccolithic complexes developed and intruded Cretaceous and Tertiary sedimentary rocks to form the Rosillos Mountains, McKinney Hills, and Grapevine Hills.

The last major tectonic episode to affect BBNP was basin-and-range faulting from about 25 to 2 Ma. Features of this time period include high-angle normal and oblique-slip faults that formed during periods of continental extension and rifting. Movement on some of the major faults formed local fault-controlled, depositional basins which flank the high Chisos Mountains, and include the Delaho and Estufa bolsons. Basin-and-range faults were the last structures to significantly modify the BBNP landscape into its present-day configuration.

The Quaternary Period (2.6 Ma to present) in BBNP was characterized by extensive erosion, down-cutting, and some aggradation related to integration of BBNP basins with the Rio Grande. The Quaternary geologic and climatic history in BBNP is recorded in multiple levels of pediment-capping gravel, alluvium, and alluvial fan deposits that cover much of the park. Based on relative-age indicators, the oldest deposits are middle (or early?) Pleistocene, and the youngest deposits are Holocene. The extensive erosion of the BBNP landscape during the Quaternary contributed to destabilization of bedrock slopes, which resulted in development of large, multi-event landslides in BBNP, including those at Chilicotal and Talley Mountains, and on the northwest flanks of the Chisos and Rosillos Mountains.

Acknowledgments

We are greatly appreciative to the **National Park Service** and **USGS National Cooperative Geologic Mapping Program** for funding the Big Bend geologic map project, and we especially thank **Bruce Heise** (NPS, Denver) for supporting the project by serving as NPS liaison with the USGS in developing and carrying out the project. We thank **NPS BBNP staff** for their support and collaboration on the project, including **Don Corrick**, geologist, **Jeff Bennett**, hydrologist, and **Bill Wellman**, Big Bend National Park Superintendent. Big Bend National Park staff kindly facilitated our studies by arranging permits, housing, and other important logistical activities required to do the work. We also appreciate the helpfulness, gratitude, and information-filled discussion with staff members including **Betty and Tom Alex**, **Vidal Davila**, and many others. We thank the many professors and students from numerous universities, and the Texas Bureau of Economic Geology, who contributed to the project by communicating results of their past and present studies, and by presenting talks at professional meetings and Big Bend symposia. Those contributors include: **William R. Muelhberger**, Emeritus, University of Texas (Austin); **Patricia W. Dickerson**, Visiting Research Fellow, American Geological Institute and University of Texas Jackson School of Geoscience (Austin); **Eddie Collins**, Bureau of Economic Geology (Austin); **Dan Barker**, University of Texas (Austin); **Jim and Margaret Stevens**, formerly of Lamar University and currently residing in Terlingua, Tex.; **Fred McDowell**, University of Texas (Austin); **Dee Ann Cooper**, Research Fellow, Texas Natural Science Center, University of Texas (Austin); **John White** and **Christian Benker**, Eastern Kentucky University; **Art Busbey and students**, Texas Christian University; **Richard Hanson and students**, Texas Christian University; **Timothy Duex and students**, University of Louisiana (Lafayette); **Don Parker and students**, Baylor University; **Joseph Satterfield and students**, San Angelo State University; **Kevin Urbanzcyk and students**, Sul Ross University; and **Minghua Ren**, University of Texas (El Paso). **Anita G. Harris** (USGS) processed, analyzed, and identified conodont faunas from the Maravillas Formation. **William Cobban** (USGS) identified some Late Cretaceous fossils from BBNP. Discussions with USGS scientists **Carol Finn**, **John Gray**, **Larry Snee**, **Lisa Morgan**, and **Pat Shanks**, on their studies at BBNP also helped improve the report. USGS geologists **Ren Thompson** and **Chris Fridrich** also provided valuable input to improve the report. The New Mexico Bureau of Mines and Geology geochronology research labs (under the direction of **William C. McIntosch**) analyzed a subset of our samples for argon geochronology. SGS Canada analyzed samples for major element geochemical analyses in 2007. We appreciate the comprehensive review of the report by **Christopher D. Henry** of the Nevada Bureau of Mines and Geology, and **Jeremiah B. Workman** of the USGS; their comments vastly improved the report.

References Cited

Adams, D.T., 2004, Field relations and geochemistry of peralkalic rhyolitic lava domes and flows and associated mafic lava in the southwest portion of the Cerro Castellan 7.5′ quadrangle, Big Bend National Park, west Texas: Waco, Baylor University, M.S. thesis, 121 p.

Albritton, D.D., Jr., and Smith, J.F., Jr., 1957, The Texas lineament: Proceedings of the 20th International Geological Congress, Mexico City, Mexico, p. 508–518.

Anderson, E.D., 2004, Mapping and visualizing faults using aeromagnetic data and GIS in northern Big Bend National Park, Texas [abs.]: Geological Society of America Abstracts with Programs, v. 36, no. 4, p. 127.

Anderson, E.D., 2007, Integrating 2D geologic data with geophysics to generate 3D geologic map of Rosillos Mountains in Big Bend National Park, Texas [abs.]: Geological Society of America Abstracts with Programs, v. 39, no. 6, p. 634.

Anderson, J.E., Brown, J.B., Jr., Gries, J.C., Lovejoy, E.M.P., McKalips, D., and Barnes, V.E., 1982, Geologic atlas of Texas Fort Stockton sheet: The University of Texas at Austin, Bureau of Economic Geology, scale 1:250,000.

Barker, D.S., 1977, Northern Trans-Pecos magmatic province: introduction and comparison with the Kenya rift: Geological Society of America Bulletin, vol. 88, p. 1424–1427.

Barker, D.S., Henry, C.D., and McDowell, F.W., 1986, Pine Canyon caldera, Big Bend National Park—A mildly peralkaline magmatic system, *in* Price, J.G., Henry, C.D., Parker, D.F., and Barker, D.S., eds., Igneous geology of Trans-Pecos Texas—Field trip guide and research articles: University of Texas at Austin, Bureau of Economic Geology Guidebook 23, p. 266–285.

Barnes, V.E., 1979, Geologic atlas of Texas Emory Peak-Presidio sheet: The University of Texas at Austin, Bureau of Economic Geology, scale 1:250,000.

Beatty, H.L., 1992, Fluvial sedimentology and sandstone petrography of the Hannold Hill Formation (Eocene), Big Bend National Park, Texas: Lubbock, Texas Tech. University, M.S. thesis, 113 p.

Becker, S.W., 1976, Field relations and petrology of the Burro Mesa Riebeckite Rhyolite, Big Bend National Park, Texas: Santa Cruz, University of California, M.S. thesis, 116 p.

Befus, K.S., Hanson, R.E., Lehman, T.M., and Griffin, W.R., 2008, Cretaceous basaltic phreatomagmatic volcanism in west Texas: maar complex at Pena Mountain, Big Bend National Park: Journal of Volcanology and Geothermal Research, v. 173, p. 245–264.

Benker, S.C., 2005, The petrology of the South Rim Formation, Big Bend National Park, Texas: Richmond, Eastern Kentucky University, M.S. thesis, 94 p.

Berry, M.E., and Williams, V.S., 2004, New 1:100,000-scale mapping of surficial geology in Big Bend National Park, Texas [abs.]: Geological Society of America Abstracts with Programs, v. 36, no. 5, p. 128.

Berry, M.E., and Williams, V.S., 2007, Quaternary geology of Big Bend National Park, Texas [abs.]: Geological Society of America Abstracts with Programs, v. 39, no. 6, p. 635.

Berry, M.E., and Williams, V.S., 2008, Surficial deposits of Big Bend National Park, *in* Gray, J.E., and Page, W.R., eds., Geological, geochemical, and geophysical studies by the U.S. Geological Survey in Big Bend National Park, Texas: U.S. Geological Survey Circular 1327, p. 15–27.

Birkeland, P.W., 1999, Soils and geomorphology (3rd ed.): New York, Oxford University Press, 430 p.

Bohannon, R.G., 2011, Geologic map of the Chisos Mountains, Big Bend National Park, Texas: U.S. Geological Survey Scientific Investigations Map 3140, scale 1:50,000.

Breyer, J.A., Busbey, A.B., Hanson, R.E., Befus, K.E., Griffin, W.R., Hargrove, U.S., and Bergman, S.C., 2007, Evidence for Late Cretaceous volcanism in Trans-Pecos, Texas: Journal of Geology, v. 115, p. 243–251.

Bumgardner, J.E., 1976, Geology of the gabbro sill surrounding Mariscal Mountain, Big Bend National Park, Texas: Austin, University of Texas, M.S. thesis, 101 p.

Busbey, A.B., III, and Lehman, T.L., 1989, Vertebrate paleontology, biostratigraphy, and depositional environments, Latest Cretaceous and Tertiary, Big Bend area, Texas: Society of Vertebrate Paleontology Guidebook, 49th Annual Meeting of Society of Vertebrate Paleontology, Austin, Texas, 76 p.

Carmen, M.F., Cameron, B., Gunn, K.L., Cameron, L., and Butler, J.C., 1975, Petrology of Rattlesnake Mountain sill, Big Bend National Park: Geological Society of America Bulletin, v. 86, p. 177–193.

Carmen, M.F., Stewart, R.M., and Casey, J.F., 2003, Characterization of the Alamo Creek Basalt, Big Bend National Park, Texas: Texas Journal of Science, v. 55, no. 2, p. 99–128.

Chapin, C.E., and Cather, S.M., 1983, Eocene tectonics and sedimentation in the Colorado Plateau, Rocky Mountain area, *in* Lowell, J.D., and Gries, R., Rocky Mountain Foreland Basins and Uplifts, Rocky Mountain Association of Geologists, p. 33–56.

Chuchla, R.J., 1981, Reconnassaince geology of the Sierra Rica area, Chihuahua, Mexico: Austin, University of Texas, M.A. thesis, 199 p.

Cobb, R.C., 1980, Structural geology of the Santiago Mountains between Pine Mountains and Persimmon Gap, Trans-Pecos, Texas: Austin, University of Texas, M.A. thesis, 69 p.

Cobb, R.C., and Poth, S., 1980, Superposed deformation in the Santiago and northern Del Carmen Mountains, *in* Dickerson, P.W., Hoffer, J.M., and Callender, X.X., eds., Trans-Pecos region, southeastern New Mexico and west Texas, New Mexico Geological Society Fall Field Conference Guidebook 31, p. 71–75.

Cobban, W.A., Hook, S.C., and McKinney, K.C., 2008, Upper Cretaceous molluscan record along a transect from Virden, New Mexico, to Del Rio, Texas: New Mexico Geology, v. 30, no. 3, p. 75–92.

Collins, E.W., Muehlberger, W.R., and Dickerson, P.W., 2007, Landslides in Chilicotal Mountain, Glenn Spring Quadrangle, Texas, Big Bend National Park [abs.]: Geological Society of America Abstracts with Programs, v. 39, no. 6, p. 634.

Collins, E.W., Muehlberger, W.R., and Dickerson, P.W., 2008, Geologic map of the Glenn Spring quadrangle, Big Bend National Park, Texas: University of Texas at Austin, Bureau of Economic Geology Miscellaneous Map no. 46, scale 1:24,000.

Connell, S.D., Hawley, J.W., and Love, D.W., 2005, Late Cenozoic drainage development in the southwestern basin and range of New Mexico, southeasternmost Arizona, and western Texas, *in* Lucas, S.G., Morgan, G.S., and Zeigler, K.E., eds., New Mexico's Ice Ages: New Mexico Museum of Natural History and Science Bulletin, v. 28, p. 125–150.

Cooper, D.A.R., 2000, The *Allocrioceras hazzardi* Zone (Turonian/Coniacian boundary) in the Boquillas Formation of the Big Bend region, Trans-Pecos, Texas: Lafayette, University of Louisiana, M.S. thesis, 65 p.

Cooper, D.A.R., Stevens, J.B., Stevens, M.S., and Cooper, R.W., 2004, A geochemical analysis of thin beds of kaolinite in the mid- to upper Coniacian, San Vicente member, Boquillas Formation, Big Bend region, Trans-Pecos Texas [abs.]: Geological Society of America Abstracts with Programs, v. 36, no. 5, p. 129.

Cooper, R.W., Cooper, D.A.R., Stevens, J.B., and Stevens, M.S., 2007, Mapping of the Upper Cretaceous Boquillas Formation in Big Bend National Park, Texas [abs.]: Geological Society of America Abstracts with Programs, v. 39, no. 6, p. 635.

Cooper, R.W., Cooper, D.A.R., and Stevens, J.B., 2008, Geology of the Hot Springs Trail area, Ernst and San Vicente Members of the Boquillas Formation, *in* Cooper, D.A.R., ed., The southern extension of the Western Interior Seaway: Geology of Big Bend National Park and Trans-Pecos Texas: Geological Society of America and the Houston Geological Society, p. 24–33.

Cooper, R.W., Stevens, J.B., Cooper, D.A.R., and Stevens, M.S., 2005, Proposed: Revise the contact between Ernst and San Vicente Members, Boquillas Formation, Big Bend National Park, Trans-Pecos, Texas [abs.]: Geological Society of America Meeting, South Central Section Meeting, San Antonio, Tex.

Dean, D.J., and Schmidt, J.C., 2008, From channel to floodplain—geomorphic transformation of the Rio Grande in the Big Bend Region of Texas, Chihuahua, and Coahuila: EOS Transactions, American Geophysical Union, v. 89, no. 53, Fall Meeting Supplement, Abstract H31H-06.

DeCamp, D.W., 1981, Structural geology of Mesa de Anguila, Big Bend National Park, Trans-Pecos Texas: Austin, University of Texas, M.A. thesis, 185 p.

DeCamp, D.W., 1985, Structural geology of Mesa de Anguila, Big Bend National Park, *in* Dickerson, P.W., and Muelhberger, W.R., eds., Structure and tectonics of Trans-Pecos Texas: West Texas Geological Society Publication 85-81, p. 127–135.

Dethier, D.P., 2001, Pleistocene incision rates in the western United States calibrated using Lava Creek B tephra: Geology, v. 29, no. 9, p. 783–786.

Dickerson, P.W., 1980, Structural zones transecting the southern Rio Grande rift, *in* Dickerson, P.W., Hoffer, J.M., and Callender, eds., Trans-Pecos region, southeastern New Mexico and west Texas, New Mexico Geological Society Fall Field Conference Guidebook 31, Trans-Pecos region, p. 63–70.

Dickerson, P.W., and Muehlberger, W.R., 1994, Basins in the Big Bend segment of the Rio Grande rift, Trans-Pecos Texas, *in* Keller, G.R., and Cather, S.M., eds., Basins of the Rio Grande Rift: Structure, stratigraphy, and tectonic setting: Geological Society of America Special Paper 291, p. 283–297.

Dickinson, W.R., Klute, M.A., Hayes, M.J., Janeke, S.U., Lundin, E.R., McKittrick, M.A., and Olivares, M.D., 1988, Paleogeographic and paleotectonic setting of Laramide sedimentary basins in the central Rocky Mountain region: Geological Society of America Bulletin, v. 100, p. 1023–1039.

Drenth, B.J., and Finn, C.A., 2007, Aeromagnetic mapping of the structure of Pine Canyon caldera and Chisos Mountains intrusion, Big Bend National Park, Texas: Geological Society of America Bulletin, v. 119, p. 1521–1534.

Duex, T.W., 2007, Evidence of caldera activity in Sierra Quemada, Big Bend National Park, Texas [abs.]: Geological Society of America Abstracts with Programs, v. 39, no. 6, p. 511.

Duex, T.W., Kinsland, G.L., and Tucker, D.R., 1994, The Sierra Quemada caldera: a major event in the geologic history of Big Bend National Park, Texas, *in* Laroche, T.M., and Viveiros, J.J., eds., Structure and tectonics of Big Bend and southern Permian basin, Texas: West Texas Geological Society Guidebook, v. 94-95, p. 213–219.

Duex, T.W., and Tucker, D.R., 1989, Geologic history of the Sierra Quemada caldera, Big Bend Park Texas [abs.]: Geological Society of America Abstracts with Programs, v. 21, no. 1, p. 9.

Ellison, S.P., Jr., and Powell, J.D., 1989, Tesnus (Mississippian) conodonts, Brewster County, Texas, *in* Zeigler, W., ed., Papers on Ordovician to Triassic conodonts: 1st International Senckenberg Conference and 5th European Conodont Symposium (ECOS V), Contribution lll, Courier Forschungsinstitut Senckenberg, v. 117, p. 359–373.

Erdlac, R.J., Jr., 1990, A Laramide-age push-up block—The structure and formation of the Terlingua-Solitario structural block, Big Bend region, Texas: Geological Society of America Bulletin, v. 102, p. 1065–1076.

Ewing, T.E., 1991, The tectonic framework of Texas: Bureau of Economic Geology, The University of Texas at Austin, map plate 1:750,000-scale, 36 p. pamphlet.

Finn, C., and Anderson, E., 2008, Aeromagnetic and radioelement analyses identify igneous rocks in Big Bend National Park region, *in* Gray, J.E., and Page, W.R., eds., Geological, geochemical, and geophysical studies by the U.S. Geological Survey in Big Bend National Park, Texas: U.S. Geological Survey Circular 1327, p. 85–91.

Gile, L.H., Hawley, J.W., and Grossman, R.B., 1981, Soils and geomorphology in the Basin and Range area of Southern New Mexico—Guidebook to the Desert Project: New Mexico Bureau of Mines and Mineral Resources, Memoir 39, 222 p.

Gile, L.H., Peterson, F.F., and Grossman, R.B., 1966, Morphological and genetic sequences of carbonate accumulation in desert soils: Soil Science, v. 101, no. 5, p. 347–360.

Goldhammer, R.K., 1999, Mesozoic sequence stratigraphy and paleogeographic evolution of northeast Mexico, *in* Bartolini, C., Wilson, J.L., and Lawton, T.F., eds., Mesozoic sedimentary and tectonic history of north-central Mexico: Geological Society of America Special Paper 340, p. 1–58.

Gray, J.E., and Page, W.R., eds., 2008, Geological, geochemical, and geophysical studies by the U.S. Geological Survey in Big Bend National Park, Texas: U.S. Geological Survey Circular 1327, 93 p.

Gray, J.E., Theodorakos, P.M., and Krabbenhoft, D.P., 2008, Evaluation of mercury contamination at inactive mercury mines in and around Big Bend National Park, *in* Gray, J.E., and Page, W.R., eds., Geological, geochemical, and geophysical studies by the U.S. Geological Survey in Big Bend National Park, Texas: U.S. Geological Survey Circular 1327, p. 57–64.

Gregory, J.L., 1981, Volcanic stratigraphy and K-Ar ages of the Manuel Benavides area, Northern Chihuahua, Mexico, and correlations with Trans Pecos Texas volcanic province: Austin, University of Texas, M.S. thesis, 135 p.

Gunderson, R., Cameron, K., and Cameron, M., 1986, Mid-Cenozoic high-K calc-alkalic and alkali volcanisim in eastern Chihuahua, Mexico: Geology and geochemistry of the Benavides-Pozos area: Geological Society of America Bulletin, v. 97, p. 737–753.

Gustavson, T.C., 1991, Arid basin depositional systems and paleosols—Fort Hancock and Camp Rice Formations (Pliocene-Pleistocene), Hueco Bolson, west Texas and adjacent Mexico: Bureau of Economic Geology, University of Texas at Austin, 49 p.

Harlan, S.S., Geissman, J.W., Henry, C.D., and Onstott, T.C., 1995, Paleomagnetism and $^{40}Ar/^{39}Ar$ geochronology of Gabbro Sills at Mariscal Mountain anticline, southern Big Bend Park, Texas: Implications for the timing of Laramide folding and vertical axis rotations in the southern Cordilleran orogenic belt: Tectonics, v. 14, no. 2, p. 307–321.

Hartnell, J.A., 1980, The vertebrate paleontology, depositional environment, and sandstone provenance of Early Eocene rocks on Tornillo Flat, Big Bend National Park, Brewster County, Texas: Baton Rouge, Louisiana State University, M.S. thesis, 174 p.

Head, M.J., Gibbard, P., and Salvador, A. 2008, The Quaternary—it's character and definition: Episodes, v. 31, no. 2, p. 234–238.

Henry, C.D., and Davis, L.L., 1996, Tertiary volcanic, volcaniclastic, and intrusive rocks adjacent to the Solatario, *in* Henry, C.D., and Muehlberger, W.R., eds., Geology of Solatario Dome, Trans-Pecos Texas: University of Texas at Austin, Bureau of Economic Geology Report of Investigations no. 240, p. 81–105.

Henry, C.D., Davis, L.L., Kunk, M.J., and McIntosh, W.C., 1998, Tertiary volcanism of the Bofecillos Mountains and Big Bend State Ranch Park, Texas; revised stratigraphy and $^{40}Ar/^{39}Ar$ geochronology: Bureau of Economic Geology Report of Investigations no. 253, 74 p.

Henry, C.D., and McDowell, F.W., 1986, Geochronology of magmatism in the Tertiary volcanic field, Trans-Pecos Texas, *in* Price, J.G., Henry, C.D., Parker, D.F., and Barker, D.S., eds., Igneous geology of Trans Pecos Texas—Field Trip Guide and research articles: University of Texas at Austin, Bureau of Economic Geology Guidebook 23, p. 99–122.

Henry, C.D., McDowell, F.W., Price, J.G., and Smyth, R.C., 1986, Compilation of potassium-argon ages of Tertiary igneous rocks, Trans-Pecos Texas: Bureau of Economic Geology Geological Circular 86-2, 34 p.

Henry, C.D., 1998, Geology of Big Bend Ranch State Park, Texas: Bureau of Economic Geology, Guidebook 27, 72 p.

Henry, C.D., and Price, J.G., 1984, Variations in caldera development in the Tertiary volcanic field of Trans-Pecos Texas: Journal of Geophysical Research, v. 89, no. B10, p. 8765–8786.

Henry, C.D., and Price, J.G., 1986, Early basin and range development in Trans-Pecos Texas and adjacent Chihuahua: magmatism, and orientation, timing, and style of extension: Journal of Geophysical Research, v. 91, no. B6, p. 6213–6224.

Henry, C.D., Price, J.G., and James, E.W., 1991, Mid Cenozoic stress evolution and magmatism in the southern Cordillera, Texas and Mexico: transition from continental arc to intraplate extension: Journal of Geophysical Research, v. 96, p. 13545–13560.

Henry, C.D., Price, J.G., Parker, D.F., and Wolff, J.A., 1989, Mid-Tertiary silicic alkali magmatism of Trans-Pecos Texas: rheomorphic tuffs and extensive silicic lavas, *in* Chapin, C.E., and Zidek, J., eds., Field excursions to volcanic terranes in the western United States, Volume 1, Southern Rocky Mountain Region: New Mexico Bureau of Mines and Mineral Resources Memoir, v. 46, p. 231–274.

Holt, G.S., 1998, Trace element partioning of alkali feldspar in Burro Mesa rhyolite and other units of the Trans-Pecos magmatic province: Waco, Baylor University, M.S. thesis, 119 p.

James, E.W., and Henry, C.D., 1991, Compressional changes in Trans-Pecos Texas magmatism coincident with Cenozoic stress realignment: Journal of Geophysical Research, v. 96, p. 13561–13575.

Lawton, T.F., and McMillan, N.J, 1999, Arc abandonment as a cause for passive rifting: comparison of Jurassic Mexican borderland rift and the Cenozoic Rio Grande Rift: Geology, v. 27, p. 779–782.

Le Maitre, R.W., Bateman, P., Dudek, A., Keller, J., Lameyre, M., Le Bas, M.J., Sabine, P.A., Schmid, R., Sorensen, H., Streckeisen, A., Woolley, A.R., and Zanettin, B., 1989, A classification of igneous rocks and a glossary of terms: Oxford, Blackwell Scientific Publications, 193 p.

Lehman, T.M., 1985, Stratigraphy, sedimentology, and paleontology of Late Cretaceous (Campanian-Maastrichtian) sedimentary rocks in Trans-Pecos Texas: Austin, University of Texas, Ph.D. dissertation, 310 p.

Lehman, T.M., 1991, Sedimentation and tectonism in the Laramide Tornillo Basin of West Texas: Sedimentary Geology, v. 75, p. 9–28.

Lehman, T.M., 2002, Revisions to the Tornillo Group (Upper Cretaceous-Eocene), Big Bend National Park, Texas [abs]: Geological Society of America Abstracts with Programs, v. 34, no. 3, p. A-10.

Lehman, T.M., 2004, Mapping of Upper Cretaceous and Paleogene strata in Big Bend National Park, Texas [abs.]: Geological Society of America Abstracts with Programs, v. 36, no. 5, p. 129.

Lehman, T.M., 2007, Upper Cretaceous and Paleogene strata south of the Chisos Mountains, Big Bend National Park, Texas [abs.]: Geological Society of America Abstracts with Programs, v. 39, p. 510.

Lehman, T.M. and Busbey, A.B., 2007, Society of Vertebrate Paleontology Fall 2007 Big Bend Field Trip Field Guide: Society of Vertebrate Paleontology, Austin, Texas, 61 p.

Lehman, T.M., McDowell, F., and Connelly, J., 2006, First isotopic (U-Pb) age for Late Cretaceous *Alamosaurus* vertebrate fauna of West Texas, and its significance as a link between two faunal provinces: Journal of Vertebrate Paleontology, v. 26, no. 4, p. 922–928.

Lonsdale, J.T., Maxwell, R.A., Wilson, J.A., and Hazzard, R.T., 1955, Big Bend National Park, Texas, March 18–19, 1955, Field Trip Guidebook: West Texas Geological Society, 142 p.

Machette, M.N., 1985, Calcic soils of the southwestern United States, *in* Weide, D.L., ed., Soils and Quaternary geology of the southwestern United States: Geological Society of America Special Paper 203, p. 1–21.

Mack, G.H., Seager, W.R., Leeder, M.R., Perez-Arlucea, M., and Salyards, S.L., 2006, Pliocene and Quaternary history of the Rio Grande, the axial river of the southern Rio Grande rift, New Mexico, USA: Earth-Science Reviews, v. 79, p. 141–162.

Maler, M.O., 1987, Structural history of Dead Horse and Tramway grabens, Big Bend National Park, Texas: Austin, University of Texas, M.A. thesis, 196 p.

Maler, M.O., 1990, Dead Horse graben: a west Texas accommodation zone: Tectonics, v. 9, no. 6, p. 1357–1368.

Mandel, R.D., 2002, Stop 11, Rio Grande Holocene valley fill, *in* White, J.C., ed., The geology of Big Bend National Park—what have we learned since Maxwell and others (1967)?: Field Trip Guide, Geological Society of America South-Central Meeting (2002, Alpine, Texas), p. 51–54.

Maxwell, R.A., 1968, The Big Bend of the Rio Grande, A guide to the rocks, landscape, geologic history, and settlers of the area of Big Bend National Park: Bureau of Economic Geology, The University of Texas at Austin, Guidebook 7, 138 p.

Maxwell, R.A., and Dietrich, J.W., 1965, Geology of the Big Bend area: West Texas Geological Society Field Trip Guidebook 65-51, 196 p.

Maxwell, R.A., and Dietrich, J.W., 1970, Correlation of Tertiary rock units, west Texas: Texas Bureau of Economic Geology Report of Investigations, no. 70, 34 p.

Maxwell, R.A., Lonsdale, J.T., Hazzard, R.T., and Wilson, J.A., 1967, Geology of Big Bend National Park, Brewster County, Texas: The University of Texas at Austin, Bureau of Economic Geology Publication 6711, 320 p.

McBride, E.F., 1989, Stratigraphy and sedimentary history of the Pre-Permian rocks of the Marathon uplift, *in* Hatcher, R.D., Jr., Thomas, W.A., and Viele, G.W., eds., The Appalachian-Ouachita orogen in the United States: Boulder Colorado, Geological Society of America, The Geology of North America, v. F-2, chap. 20, p. 603–620.

McKnight, J.P., 1970, Geology of the Bofecillos Mountains area, Trans-Pecos Texas: Bureau of Economic Geologic Quadrangle Map 37, scale 1:24,000.

Miggins, D., Anthony, E., Ren, M., and Budahn, J., 2007, New $^{40}Ar/^{39}Ar$ ages, geochemistry, and stratigraphy for mafic and rhyolitic volcanic units from Big Bend National Park, Texas [abs]: Geological Society of America Abstracts with Programs, v. 39, no. 6, p. 635.

Miggins, D., Ren, M., and Anthony, E., 2008, Volcanic geology of several prominent outcrops in the western part of Big Bend National Park, *in* Gray, J.E., and Page, W.R., eds., Geological, geochemical, and geophysical studies by the U.S. Geological Survey in Big Bend National Park, Texas, U.S. Geological Survey Circular 1327, p. 29–42.

Miggins, D., Scott, R.B., and Snee, L.S., 2004, New $^{40}Ar/^{39}Ar$ ages from Big Bend National Park [abs.]: Geological Society of America Abstracts with Programs, v. 36, no. 5, p. 128.

Monti, J., 1984, Seismic mapping of alluvial fans and sub-fan bedrock in Big Bend National Park, Texas: College Station, Texas A & M University, M.S. thesis, 49 p.

Morgan, L.A., and Shanks, W.C., 2008, Where magma meets limestone; an example of skarn deposits in Big Bend National Park, *in* Gray, J.E., and Page, W.R., Geological, geochemical, and geophysical studies by the U.S. Geological Survey in Big Bend National Park, Texas: U.S. Geological Survey Circular 1327, p. 43–55.

Moustafa, A.R., 1988, Structural Geology of Sierra del Carmen, Trans-Pecos Texas: Bureau of Economic Geology Geologic Quadrangle Map no. 54, scale 1:33,000.

Muehlberger, W.R., 1980, Texas Lineament revisited, *in* Dickerson, P.W., Hoffer, J.M., and Callender, eds., Trans-Pecos region, southeastern New Mexico and west Texas, New Mexico Geological Society Fall Field Conference Guidebook 31, Trans-Pecos region, p. 113–121.

Muehlberger, W.R., 1989, Summary of the structural geology of Big Bend National Park and vicinity, *in* Muehlberger, W.R., and Dickerson, P.W., leaders, 28th International Geological Congress Field Trip Guidebook T317: American Geophysical Union, p. 179–197.

Muehlberger, W.R., and Dickerson, P.W., 1989, A tectonic history of Trans-Pecos Texas, *in* Muehlberger, W.R., and Dickerson, P.W., Leaders, 28th International Geological Congress fieldtrip guidebook T317: American Geophysical Union, p. 35–54.

Noble, P.J., 1994, Silurian radiolarian zonation for the Caballos Novaculite, Marathon uplift, west Texas: Bulletin of American Paleontology, v. 106, no. 345, 55 p.

Ogley, D.S., 1978, Eruptive history of the Pine Canyon caldera, Big Bend National Park, Texas: Austin, University of Texas, M.S. thesis, 68 p.

Page, W.R., and Harris, A.G., 2007, Late Ordovician conodonts from the Maravillas Formation near Persimmon Gap, Big Bend National Park, Texas [abs.]: Geological Society of American Abstracts with Programs, v. 39, no. 6, p. 635.

Page, W.R., Turner, K.J., and Bohannon, R.G., 2008, Tectonic History of Big Bend National Park, *in* Gray, J.E., and Page, W.R., eds., Geological, geochemical, and geophysical studies by the U.S. Geological Survey in Big Bend National Park, Texas, U.S. Geological Survey Circular 1327, p. 3–13.

Page, W.R., Williams, V.S., and Berry, M.E., 2004, Quaternary faults in northwestern Big Bend National Park, Texas [abs.]: Geological Society of America Abstracts with Programs, v. 36, no. 5, p. 128.

Parker, D.F., 2002, Horseshoe Canyon volcanic dome, *in* White, J.C., ed., The Geology of Big Bend National Park; what we have learned from Maxwell and others (1967)?: Field Trip Guide, Geological Society of America South Central Meeting, Alpine Texas, p. 24–32.

Parker, D.F., and McMillan, N.J., 2007, Early onset of Rio Grande rift magmatism in west Texas [abs.]: Geological Society of America Abstracts with Programs, v. 39, no. 6, p. 511.

Pazzaglia, F.J., and Hawley, J.W., 2004, Neogene (rift flank) and Quaternary geology and geomorphology, *in* Mack, G.H., and Giles, K.A., eds., The geology of New Mexico, a geologic history: New Mexico Geological Society Special Publication 11, p. 407–437.

Poole, F.G., Perry, W.J., Jr., Madrid, R.J., and Amaya-Martinez, R., 2005, Tectonic synthesis of the Ouachita-Marathon-Sonora orogenic margin of southern Laurentia: stratigraphic and structural implications for timing of deformational events and plate tectonic model, *in* Anderson, T.H., Nourse, J.A., McKee, J.W., and Steiner, M.B., eds., The Mojave-Sonora Megashear hypothesis: development, assessment, and alternatives: Geological Society of America Special Paper 393, p. 543–596.

Poth, S., 1979, Structural transition between the Santiago and Sierra del Carmen Mountains in northern Big Bend National Park, Texas: Austin, University of Texas, M.A. thesis, 55 p.

Price, J.G., Henry, C.D., Barker, D.S., and Parker, D.F., 1987, Alkalic rocks of contrasting tectonic settings in Trans-Pecos Texas: Geological Society of America Special Paper 215, p. 335–346.

Purchase, C., 2002, Stop 10, Geomorphic changes in the Rio Grande/Rio Bravo channel and floodplain, *in* White, J.C., ed., The geology of Big Bend National Park—what have we learned since Maxwell and others (1967)?: Field Trip Guide, Geological Society of America South-Central Meeting 2002, Alpine, Texas, p. 50–51.

Renne, P.R., Swisher, C.C., Deino, A.L., Karner, D.B., Owens, T.L., and DePaolo, D.J., 1998, Intercalibration of standards, absolute ages and uncertainties in $^{40}Ar/^{39}Ar$ dating: Chemical Geology, v. 145, p. 117–152.

Ritter, S.P., and Cepeda, J.C., 1991, The Hechiceros caldera: a recently identified mid-Tertiary caldera in eastern Chihuahua, Mexico: Journal of Geophysical Research, v. 96, p. 16241–16250.

Runkel, A.C., 1988, Stratigraphy, sedimentation, and vertebrate paleontology of Eocene rocks in the Big Bend region of southwest Texas: Austin, University of Texas, Ph.D. dissertation, 283 p.

Runkel, A.C., 1990, Lateral and temporal changes in volcanogenic sedimentation: analysis of two Eocene sedimentary aprons, Big Bend region, Texas: Journal of Sedimentary Geology, v. 60, no. 5, p. 747–760.

Schiebout, J.A., 1974, Vertebrate paleontology and paleoecology of Paleocene Black Peaks Formation, Big Bend National Park, Texas: Texas Memorial Museum Bulletin, 88 p.

Schiebout, J.A., Rigsby, C.A., Rapp, S.D., Hartnell, J.A., and Standhardt, B.R., 1987, Stratigraphy of Cretaceous-Tertiary and Paleocene-Eocene transition rocks of Big Bend National Park, Texas: Journal of Geology, v. 95, p. 359–375.

Schucker, D.E., and Nelson, D.O., 1988, New potassium argon dates of mafic rocks within Big Bend National Park, Texas: Texas Journal of Science, v. 40, p. 71–78.

Scott, R.B., Snee, L.W., Drenth, B., and Anderson, E.D., 2004a, Sloppy pancake stacks: Oligocene laccoliths of northern Big Bend National Park [abs.]: Geological Society of America Abstracts with Programs, v. 36, no. 5, p. 127.

Scott, R.B., Snee, L.S., Finn, C.A., Drenth, B., and Anderson, E., 2004b, Oligocene Rosillos Mountains laccolith, Big Bend National Park, Texas [abs]: Geological Society of America Abstracts with Programs, v. 36, no. 5., p. 128.

Scott, R.B., Turner, K.J., Budhan, J, and Miggins, D.P., 2007, Sierra Quemada—a failed caldera, Big Bend National Park [abs.]: Geological Society of America Abstracts with Programs, v. 39, no. 6, p. 512.

Shanks, W.C., Jr., Hellgren, E.C., Stricker, C., Gemery-Hill, P.A., and Onorato, D.P., 2008a, Stable isotope and trace element studies of black bear hair, Big Bend ecosystem, Texas and Mexico, *in* Gray, J.E., and Page, W.R., eds., Geological, geochemical, and geophysical studies by the U.S. Geological Survey in Big Bend National Park, Texas: U.S. Geological Survey Circular 1327, p. 77–84.

Shanks, W.C., Jr., Morgan, L.A., Gray, J.E., Manning, A.H., and Gemery-Hill, P.A., 2008b, The waters of Big Bend: geochemical variations, ages and sources, *in* Gray, J.E., and Page, W.R., eds., Geological, geochemical, and geophysical studies by the U.S. Geological Survey in Big Bend National Park, Texas: U.S. Geological Survey Circular 1327, p. 65–76.

Smith, C.I., 1981, Geologic setting, stratigraphy, and facies distribution of Lower Cretaceous rocks in northern Mexico: West Texas Geological Society Field Trip Guidebook, Publication 81-74, p. 1–27.

Stevens, J.B., 1969, Geology of the Castolon area, Big Bend National Park, Brewster County, Texas: Austin, University of Texas, Ph.D. dissertation, 129 p.

Stevens, J.B., 1988, Mid-Tertiary and Pleistocene sections, Sotol Vista to Cerro Castellan, Big Bend National Park, southwestern Brewster County, Trans-Pecos Texas, *in* Hayward, O.T., ed., South-central section of the Geological Society of America, Centennial Field Guide, v. 4: Geological Society of America, p. 429–434.

Stevens, J.B., and Stevens, M.S., 1985, Basin and range deformation and depositional timing, Trans-Pecos Texas, *in* Dickerson, P.W., and Muehlberger, W.R., eds., Structure and tectonics of Trans-Pecos Texas: West Texas Geological Society, Publication 85-81, p. 157–164.

Stevens, M.S., 1977, Further study of Castolon local fauna (early Miocene), Big Bend National Park, Texas: Texas Memorial Museum, Pearce-Sellards Series, no. 28, 69 p.

Stevens, M.S., 1991, Osteology, systematics, and relationships of earliest Miocene *Mesocyon venator* (Carnivora: Canidae): Journal of Vertebrate Paleontology, v. 11, no. 1, p. 45–66.

Stevens, M.S., and Stevens, J.B., 1989, Neogene-Quaternary deposits and vertebrate faunas, Trans-Pecos Texas, *in* Busby, A.B., III, Lehman, T.M., and Wilson, J.A., eds., Vertebrate paleontology, biostratigraphy, and depositional environments, latest Cretaceous and Tertiary, Big Bend area, Texas [guidebook for the Big Bend field trip]: Society of Vertebrate Paleontology [annual meeting, Austin, Tex., 1989], p. 67–90.

Stevens, M.S., and Stevens, J.B., 2003, Carnivora (Mammalian, Felidae, Canidae, and Mustelidae) from the earliest Hemphillian Screw Bean local fauna, Big Bend National Park, Brewster County, Texas: Bulletin of the American Museum of Natural History, v. 13, no. 279, p. 177–211.

Stevens M.S., Stevens, J.B., and Dawson, M.R., 1969, New early Miocene Formation and vertebrate local fauna, Big Bend National Park, Brewster County, Texas: Texas Memorial Museum, Pearce-Sellards Series, no. 15, 53 p.

Stewart, R.M., 1984, Stratigraphy and petrology of the Alamo Creek basalt, Big Bend National Park, Texas: Houston, University of Texas, M.S. thesis, 186 p.

Thomas, W.A. 1991, The Appalachian-Ouachita rifted margin of southeastern North America: Geological Society of America Bulletin, v. 103, no. 3, p. 415–431.

Thurwachter, J.E., 1984, Sedimentology of Neogene basin-fill deposits, lower Tornillo Creek area, Big Bend National Park, Texas: Austin, University of Texas, M.S. thesis, 86 p.

Turner, K.J., Budahn, J.R., and Miggins, D.P., 2008, A reinterpretation of some correlations of Chisos Group mafic lavas with new geochemistry and geochronology, Big Bend National Park, Texas [abs.]: Geological Society of America Abstracts with Programs, v. 40, no. 6, p. 134.

Udden, J.A., 1907, A sketch of the geology of the Chisos country, Brewster County, Texas: University Of Texas Bulletin 93, 101 P.

Urbanczyk, K.M., And White, J.C., 2000, Pine Canyon Caldera, Big Bend National Park, Texas: A New Interpretation [Abs.]: Geological Society Of America Abstracts With Programs, V. 32, No. 3, P. 43.

Walker, J.D., And Geissman, J.W., 2009, 2009 GSA Geologic Time Scale: GSA Today, April/May 2009, P. 60–61.

White, J.C., Benker, S.C., Ren, M., Urbanczyk, K.M., and Corrick, D.W., 2006, Petrogenesis and tectonic setting of peralkaline Pine Canyon Caldera, Trans-Pecos Texas, Usa: Lithos, V. 91, P. 74–94.

Wilson, J.A., and Runkel, A.C., 1989, Field guide to the Paleocene stratigraphy and vertebrate paleontology of the Big Bend region, *in* Busbey, A.B., and Lehman, T.M., eds., Vertebrate Paleontology, Biostratigraphy, and Depositional Environments of the latest Cretaceous to Tertiary, Big Bend area, Texas: 49th Annual Meeting of the Society of Vertebrate Paleontology, Austin, Texas, p. 47–59.

Wilson, J.L., 1954, Ordovician stratigraphy in Marathon folded belt: American Association of Petroleum Geologists Bulletin, v. 38, p. 2455–2475.

Appendix

Cerro Castellan, a distinctive geologic landform near Castolon. Shown in lower part of photograph are white and red undifferentiated tuffaceous sediments and dark gray basaltic lava (Bee Mountain Basalt Member) of the Chisos Formation, overlain by light-gray and reddish-brown rocks of the Burro Mesa Formation. New isotopic age determinations in the appendix were critical in refining the stratigraphy and the age of the Chisos and South Rim Formations, and in defining and constraining the age of the Burro Mesa Formation. *(Photograph by William R. Page)*

Appendix. Summary of $^{40}Ar/^{39}Ar$ and U-Pb zircon ages for Big Bend National Park.

Map sample number	Field sample number[1]	Map unit name	Map unit symbol	UTM Easting	UTM Northing	Age (Ma)	Material analyzed[2]	Technique	Comment[1]
					Basaltic flow				
1	12DM-4-30-03	Basaltic flow	Tfb	656339	3235035	29.10±0.05	G.C.	$^{40}Ar/^{39}Ar^{A}$	Plateau age (steps 4–5) comprising 56.0% of gas; lava, near Burro Mesa pouroff
						29.53±0.33	Biotite	$^{40}Ar/^{39}Ar^{A}$	Plateau age (steps 6-10) comprising 67.0% of gas
					Burro Mesa Formation				
2	13DM-4-30-03	Rhyolite member	Tbr	657049	3234726	29.25±0.07	Sanidine	$^{40}Ar/^{39}Ar$ laser[B]	Weighted mean age of 10 sanidine crystals; porphyritic lava, east of Burro Mesa pouroff
3	60DM-3-20-04	Rhyolite member	Tbr	652719	3227747	29.33±0.07	Sanidine	$^{40}Ar/^{39}Ar$ laser[B]	Weighted mean age of 10 sanidine crystals; lava, Trap Mountain
4	10DM-4-30-03	Rhyolite member	Tbr	655175	3235400	29.35±0.10	Sanidine	$^{40}Ar/^{39}Ar$ laser[B]	Weighted mean age of 10 sanidine crystals; lava, Burro Mesa pouroff
5	22DM-5-2-03	Rhyolite member	Tbr	654659	3230725	29.35±0.09	Sanidine	$^{40}Ar/^{39}Ar$ laser[B]	Weighted mean age of 7 sanidine crystals; lava, north face of Goat Mountain
6	7DM-4-30-03	Rhyolite member	Tbr	646319	3224846	29.45±0.08	Sanidine	$^{40}Ar/^{39}Ar$ laser[B]	Weighted mean age of 9 sanidine crystals; lava, Cerro Castellan
7	3aBS26.2.03	Wasp Spring member	Tbw	646054	3224792	29.27±0.07	Sanidine	$^{40}Ar/^{39}Ar$ laser[B]	Weighted mean age of 9 sanidine crystals; basal tuff, Cerro Castellan
8	165aDM-3-22-05	Wasp Spring member	Tbw	645362	3229090	29.37±0.05	Sanidine	$^{40}Ar/^{39}Ar$ laser[B]	Weighted mean age of 10 sanidine crystals; ash-flow tuff, west of Bee Mountain
9	81DM-3-22-04	Wasp Spring member	Tbw	648044	3224841	29.39±0.12	Sanidine	$^{40}Ar/^{39}Ar$ laser[B]	Weighted mean age of 10 sanidine crystals; pumice in nonwelded tuff, east of Tuff Canyon
10	10BS26.2.03	Wasp Spring member	Tbw	655195	3235320	29.48±0.16	Sanidine	$^{40}Ar/^{39}Ar$ laser[B]	Weighted mean age of 4 sanidine crystals; ash-flow tuff, Burro Mesa pouroff
11	48DM-3-17-04	Intrusive rocks, undivided	Tbi	653283	3235005	29.03±0.12	Sanidine	$^{40}Ar/^{39}Ar$ laser[B]	Weighted mean age of 10 sanidine crystals; intrusion, west of Burro Mesa pouroff
12	14DM-4-30-03	Intrusive rocks, undivided	Tbi	657734	3234322	29.09±0.07	Sanidine	$^{40}Ar/^{39}Ar$ laser[B]	Weighted mean age of multiple sanidine crystals; dike, east of Burro Mesa Pouroff and northwest of Blue Creek Ranch
					Trachytic lava				
13	23DM-5-2-03	Trachytic lava, undivided	Tt	658961	3233003	30.23±0.11	Plagioclase	$^{40}Ar/^{39}Ar^{A}$	Plateau age (steps 2–7) comprising 86.4% of gas; trachyte lava, north of Blue Creek Ranch
14	8BS26.2.03	Trachytic lava, undivided	Tt	654249	3230460	30.29±0.05	G.C.	$^{40}Ar/^{39}Ar^{A}$	Plateau age (steps 4–6) comprising 66.1% of gas; trachyte lava, west face of Goat Mountain
						30.33±0.13	Plagioclase	$^{40}Ar/^{39}Ar^{A}$	Plateau age (steps 5–6) comprising 55.9% of gas
15	1aDM-4-29-03	Trachytic lava, undivided	Tt	647190	3225460	30.42±0.06	G.C.	$^{40}Ar/^{39}Ar^{A}$	Plateau age (steps 4–5) comprising 69.4% of gas; basaltic trachyandesite lava, Tuff Canyon
					Tuffs of unknown origin				
16	336KT3.4.05	not mapped separately		663301	3226539	28.1±1.0	Sanidine	$^{40}Ar/^{39}Ar$ laser[B]	Weighted mean age of 5 sanidine crystals; ash-flow tuff, south of Sierra Quemada
17	212DM-12-2-06	not mapped separately		660614	3221885	30.34±0.11	Sanidine	$^{40}Ar/^{39}Ar$ laser[B]	Weighted mean age of 15 sanidine crystals; ash-flow tuff, south face Punta de la Sierra, block originating from horizon below base of trachytic lava
18	11:48KT2-3-08	not mapped separately		653367	3219450	30.40±0.07	Sanidine	$^{40}Ar/^{39}Ar$ laser[B]	Weighted mean age of 15 sanidine crystals; tuff, Triangulation Station Mountain

Appendix. Summary of $^{40}Ar/^{39}Ar$ and U-Pb zircon ages for Big Bend National Park.—Continued

Map sample number	Field sample number[1]	Map unit name	Map unit symbol	UTM Easting	UTM Northing	Age (Ma)	Material analyzed[2]	Technique	Comment[1]
				Sierra Quemada related rocks					
19	5BS4.3.05	Intrusive rocks, undivided	Tqi	662294	3228308	29.06±0.91	Zircon	U-Pb[D]	Weighted mean age of 18 spots; syenite intrusion, southeast Sierra Quemada
20	7BS6.3.05	Intrusive rocks, undivided	Tqi	661298	3230542	29.45±0.48	Zircon	U-Pb[D]	Weighted mean age of 36 spots; rhyolite intrusion, northwest Sierra Quemada
21	6BS17.1.05	Ring dike	Tqd	661067	3228522	29.93±0.40	Zircon	U-Pb[D]	Weighted mean age of 32 spots; ring dike, southwest Sierra Quemada
22	5BS3.3.05	Intrusive rocks, undivided	Tqi	661161	3229029	30.42±0.44	Zircon	U-Pb[D]	Weighted mean age of 30 spots; rhyolite intrusion, southwest Sierra Quemada
23	9BS6.3.05	Intrusive rocks, undivided	Tqi	661397	3231037	31.09 ± 0.48	Zircon	U-Pb [D]	Weighted mean age of 32 spots; rhyolite dike, northwest Sierra Quemada
				South Rim Formation					
24	TCP-407[a]	Emory Peak rhyolite mbr.	Tse	664723	3235774	31.93 ± 0.13	Sanidine	$^{40}Ar/^{39}Ar$ [A]	Plateau age (steps 3–9) comprising 79.4% of gas; vitrophyre, Emory Peak
25	144DM-3-12-05	Emory Peak rhyolite mbr.	Tse	658904	3233673	32.1 ± 0.3	Sanidine	$^{40}Ar/^{39}Ar$ laser [B]	Weighted mean age of 10 sanidine crystals; tuff, north of Blue Creek Ranch
26	16DM-5-1-03	Emory Peak rhyolite mbr.	Tse	664764	3236232	32.25 ± 0.05	Sanidine	$^{40}Ar/^{39}Ar$ laser [B]	Weighted mean age of 10 sanidine crystals; ash-flow? tuff, Emory Peak
27	19DM-5-1-03	Emory Peak rhyolite mbr.	Tse	665275	3236438	32.25 ± 0.07	Sanidine	$^{40}Ar/^{39}Ar$ laser [B]	Weighted mean age of 10 sanidine crystals; rhyolite, east side Emory Peak
28	TPC-325[a]	Boot Rock mbr.	Tsb	665209	3235781	32.17 ± 0.09	Sanidine	$^{40}Ar/^{39}Ar$ [A]	Plateau age (steps 2–4) comprising 69.4% of gas; ash-flow tuff, Pinnacle Pass in The Basin
29	BB089KW[b]	Boot Rock mbr.	Tsb	656140	3241284	32.33 ± 0.07	Sanidine	$^{40}Ar/^{39}Ar$ laser [B]	Weighted mean age of 9 sanidine crystals; ash-flow tuff, east Burro Mesa
30	BJD-PCR	Pine Canyon rhyolite mbr.	Tsp	669400	3238130	32.11 ± 0.23	Sanidine	$^{40}Ar/^{39}Ar$ [A]	Plateau age (steps 2–10) comprising 94.1% of gas; vitrophyre, Pine Canyon pouroff
31	131DM-2-11-05	Pine Canyon rhyolite mbr.	Tsp	668896	3239465	32.33 ± 0.07	Sanidine	$^{40}Ar/^{39}Ar$ laser [B]	Weighted mean age of 10 sanidine crystals; tuff, west side Lost Mine Peak
32	33DM-5-4-03	Ring dike	Tsd	675590	3237184	32.6 ± 0.3	Zircon	U-Pb [C]	Weighted mean age of 10 spots; dike, Hayes Ridge, mouth of Pine Canyon
						31.99 ± 0.32	K-Feldspar	$^{40}Ar/^{39}Ar$ [A]	Weighted mean age (steps 5–11) comprising 47.5% of gas
33	128DM-2-10-05	Intrusive rocks, undivided	Tsi	676919	3237517	31.5 ± 0.3	Zircon	U-Pb [C]	Weighted mean age of 5 spots; sill, Nugent Mountain
34	TPC-329[a]	Intrusive rocks, undivided	Tsi	666303	3238568	32.03±0.25	Sanidine	$^{40}Ar/^{39}Ar$[A]	Plateau age (steps 3–9) comprising 74.4% of gas; feeder dike of Casa Grande dome
35	132DM-2-11-05	Intrusive rocks, undivided	Tsi	668944	3239435	32.21±0.05	Sanidine	$^{40}Ar/^{39}Ar$ laser[B]	Weighted mean age of 10 sanidine crystals; dike, east side Lost Mine Peak
36	94DM-3-25-04	Intrusive rocks, undivided	Tsi	676957	3243033	32.4±0.3	Zircon	U-Pb[C]	Weighted mean age of 8 spots; sill, near K-bar park housing
						31.69±0.19	K-Feldspar	$^{40}Ar/^{39}Ar$[A]	Weighted mean age (steps 2–7) comprising 84.8% of gas
						32.32±0.22	Amphibole	$^{40}Ar/^{39}Ar$[A]	Plateau age (steps 3–4) comprising 72.7% of gas
37	139DM-2-12-05	Intrusive rocks, undivided	Tsi	662378	3240130	32.4±0.4	Zircon	U-Pb[C]	Weighted mean age of 10 spots; rhyolite intrusion, Windows Trail south of Vernon Bailey Peak
				Chisos Formation, younger part					
38	198DM-11-28-06	Younger part, undivided	Tcy	647467	3222486	32.96±0.06	Sanidine	$^{40}Ar/^{39}Ar$ laser[B]	Weighted mean age of 15 sanidine crystals; possibly reworked pumaceous tuff, southeast of Cerro Castellan
39	168KT-2-7-07	Tule Mountain Trachyandesite Mbr.	Tctm	633209	3232371	33.18±0.10	G.C.	$^{40}Ar/^{39}Ar$[B]	Plateau age (steps 3–9) comprising 90.6% of gas; lava flow Sierra Aguja

Appendix. Summary of $^{40}Ar/^{39}Ar$ and U-Pb zircon ages for Big Bend National Park.—Continued

Map sample number	Field sample number[1]	Map unit name	Map unit symbol	UTM Easting	UTM Northing	Age (Ma)	Material analyzed[2]	Technique	Comment[1]
				Chisos Formation, younger part—Continued					
40	45DM-3-16-04	Tule Mountain Trachyandesite Mbr.	Tctm	648354	3237603	33.84±0.05	G.C.	$^{40}Ar/^{39}Ar^{A}$	Average age (steps 5–7) comprising 43.7% of gas; lava flow, top of Tule Mountain
						32.71±0.24	Plagioclase	$^{40}Ar/^{39}Ar^{A}$	Average age (steps 3–7) comprising 71.9% of gas
						33.88±0.54	G.C.	$^{40}Ar/^{39}Ar^{B}$	Isochron age (steps 1–8)
41	11:40KT2-3-08	Bee Mountain Basalt Mbr.	Tcbm	653332	3219378	33.07±0.15	G.C.	$^{40}Ar/^{39}Ar^{A}$	Plateau age (steps 3–10) comprising 89.6% of gas; lava flow above Mule Ear Spring Tuff, Triangulation Station Mountain
42	167bDM-3-24-05	Bee Mountain Basalt Mbr.	Tcbm	647307	3222725	33.68±0.09	G.C.	$^{40}Ar/^{39}Ar^{A}$	Weighted mean age (steps 3–5) comprising 65.0% of gas; lava flow above Mule Ear Spring Tuff, southeast of Cerro Castellan
43	83DM-3-22-04	Mule Ear Spring Tuff Mbr.	Tcme	652928	3229535	33.64±0.08	Sanidine	$^{40}Ar/^{39}Ar$ laser^{B}	Weighted mean age of 10 sanidine crystals; ash-flow tuff, southeast side Kit Mountain
44	53DM-3-18-04	Mule Ear Spring Tuff Mbr.	Tcme	654142	3230075	33.64±0.09	Sanidine	$^{40}Ar/^{39}Ar$ laser^{B}	Weighted mean age of 10 sanidine crystals; ash-flow tuff, west side Goat Mountain
45	118DM-2-6-05	Mule Ear Spring Tuff Mbr.	Tcme	654779	3226838	33.65±0.06	Sanidine	$^{40}Ar/^{39}Ar$ laser^{B}	Weighted mean age of 10 sanidine crystals; ash-flow tuff, Mule Ear Spring
46	124DM-2-9-05	Mule Ear Spring Tuff Mbr.	Tcme	646239	3227255	33.67±0.06	Sanidine	$^{40}Ar/^{39}Ar$ laser^{B}	Weighted mean age of 9 sanidine crystals; ash-flow tuff, northwest of Tuff Canyon
47	8DM-4-30-03	Mule Ear Spring Tuff Mbr.	Tcme	646430	3224157	33.67±0.09	Sanidine	$^{40}Ar/^{39}Ar$ laser^{B}	Weighted mean age of 9 sanidine crystals; ash-flow tuff, southeast of Cerro Castellan
48	68DM-3-21-04	Younger part, undivided	Tcy	654102	3224373	33.84±0.06	Sanidine	$^{40}Ar/^{39}Ar$ laser^{B}	Weighted mean age of 10 sanidine crystals; tuff, above Bee Mountain Basalt flows at Round Mountain
49	2BS26.2.03	Bee Mountain Basalt Mbr.	Tcbm	645906	3224908	33.37±0.48	G.C.	$^{40}Ar/^{39}Ar^{A}$	Isochron age (steps 3–8); lava flow at Cerro Castellan
50	BJD-BEM	Bee Mountain Basalt Mbr.	Tcbm	669612	3242290	33.70±0.05	G.C.	$^{40}Ar/^{39}Ar^{A}$	Average age (steps 3–4) comprising 29.1% of gas; lava flow, along road into The Basin
51	153DM-3-18-05	Bee Mountain Basalt Mbr.	Tcbm	659130	3231741	33.76±0.12	G.C.	$^{40}Ar/^{39}Ar^{A}$	Preferred age (steps 5–7) comprising 52.8% of gas; lowest lava flow, off Dodson Trail just south of Blue Creek
52	163DM-3-22-05	Bee Mountain Basalt Mbr.	Tcbm	647497	3229499	34.03±0.17	G.C.	$^{40}Ar/^{39}Ar^{A}$	Weighted mean age (steps 4-8) comprising 75.2% of gas; lava flow, Bee Mountain
53	5DM-4-29-03	Undifferentiated lava flow	Tcl	658262	3236538	38.87±0.09	G.C.	$^{40}Ar/^{39}Ar^{A}$	Total gas age (steps 1-8) comprising 100.0% of gas; lava flow, north of Blue Creek Ranch, along Ross Maxwell Scenic Drive
54	71DM-3-21-04	Younger part, undivided	Tcy	653343	3223772	39.72±0.19	Sanidine	$^{40}Ar/^{39}Ar$ laser^{B}	Weighted mean age of 7 sanidine crystals; tuff, west of Round Mountain
55	72DM-3-21-04	Younger part, undivided	Tcy	653206	3223428	39.86±0.06	Sanidine	$^{40}Ar/^{39}Ar$ laser^{B}	Weighted mean age of 17 sanidine crystals; tuff, west of Round Mountain
56	5BS26.2.03	Younger part, undivided	Tcy	645572	3225308	40.55±0.18	Sanidine	$^{40}Ar/^{39}Ar$ laser^{B}	Weighted mean age of 8 sanidine crystals; tuff, base of Cerro Castellan
57	73DM-3-21-04	Younger part, undivided	Tcy	652922	3223079	40.83±0.07	Sanidine	$^{40}Ar/^{39}Ar$ laser^{B}	Weighted mean age of 20 sanidine crystals; tuff, west of Round Mountain
58	2BS27.2.03	Ash Spring Basalt Mbr.	Tcas	658187	3236904	40.92±0.07	G.C.	$^{40}Ar/^{39}Ar^{A}$	Total gas age (steps 1–8) comprising 100.0% of gas; lava flow, north of Blue Creek Ranch, along Ross Maxwell Scenic Drive
						40.38±0.35	G.C.	$^{40}Ar/^{39}Ar^{B}$	Integrated age (steps 1–10) comprising 100% of gas
						43.39±0.19	Plagioclase	$^{40}Ar/^{39}Ar^{A}$	Weighted mean age (steps 4–7) comprising 69.5% of gas

Appendix. Summary of $^{40}Ar/^{39}Ar$ and U-Pb zircon ages for Big Bend National Park.—Continued

Map sample number	Field sample number[1]	Map unit name	Map unit symbol	UTM Easting	UTM Northing	Age (Ma)	Material analyzed[2]	Technique	Comment[1]
				Chisos Formation, younger part—Continued					
59	BB012KW[b]	Younger part, undivided	Tcy	656700	3242021	41.41±0.07	Sanidine	$^{40}Ar/^{39}Ar$ laser[B]	Weighted mean age of 8 sanidine crystals; ash-flow tuff, east side Burro Mesa
60	88DM-3-25-04	Younger part, undivided	Tcy	646644	3237469	41.75±0.11	Sanidine	$^{40}Ar/^{39}Ar$ laser[B]	Weighted mean of 10 sanidine crystals; ash-flow tuff, northwest side Tule Mountain, possibly related to Christmas Mountains caldera complex
61	BB078KW[b]	Younger part, undivided	Tcy	654825	3244105	42.06±0.07	Sanidine	$^{40}Ar/^{39}Ar$ laser[B]	Weighted mean age of 10 sanidine crystals; ash-flow tuff, northeast side Burro Mesa, possibly related to Christmas Mountains caldera complex
62	51DM-3-17-04	Younger part, undivided	Tcy	652884	3234415	42.6±0.4	Zircon	U-Pb[C]	Weighted mean age of 8 spots; tuff, west of Burro Mesa pouroff
						42.31±0.10	Sanidine	$^{40}Ar/^{39}Ar$ laser[B]	Weighted mean age of 8 sanidine crystals
63	75DM-3-21-04	Younger part, undivided	Tcy	652154	3222503	45.3 ± 0.7	Zircon	U-Pb[C]	Weighted mean age of 5 spots; tuff, west of Round Mountain
64	135DM-2-11-05	Alamo Creek Basalt Mbr.	Tcac	643279	3237789	44.41±0.22	G.C.	$^{40}Ar/^{39}Ar$[B]	Integrated age (steps 1–10) comprising 100% of gas; lava flow, Alamo Creek
65	213DM-12-2-06	Alamo Creek Basalt Mbr.	Tcac	660269	3221192	45.54±0.52	G.C.	$^{40}Ar/^{39}Ar$[B]	Integrated age (steps 1–10) comprising 100% of gas; lava flow, northwest of Punta de la Sierra
66	1BS26.2.03	Alamo Creek Basalt Mbr.	Tcac	645234	3224700	46.11±0.21	G.C.	$^{40}Ar/^{39}Ar$[B]	Plateau age (steps 2–10) comprising 99.9% of gas; lava flow, northeast of Castolon
67	76DM-3-21-04	Alamo Creek Basalt Mbr.	Tcac	651743	3223673	46.42±0.07	G.C.	$^{40}Ar/^{39}Ar$[A]	Plateau age (steps 3–5) comprising 61.8% of gas; lava flow, southwest of Round Mountain
68	150DM-3-16-05	Alamo Creek Basalt Mbr.	Tcac	651196	3226913	46.61±0.10	G.C.	$^{40}Ar/^{39}Ar$[A]	Plateau age (steps 3–5) comprising 71.0% of gas; lava flow, southwest of Trap Mountain
69	145DM-3-12-05	Alamo Creek Basalt Mbr.	Tcac	636582	3231113	47.04±0.17	G.C.	$^{40}Ar/^{39}Ar$ [A]	Plateau age (steps 4–5) comprising 61.5% of gas; lava flow, southeast of Sierra Aguja
70	106DM-2-3-05	Alamo Creek Basalt Mbr.	Tcac	647443	3232280	47.04±0.25	G.C.	$^{40}Ar/^{39}Ar$[A]	Plateau age (steps 4–6) comprising 57.0% of gas; lava flow, Black Mesa
71	163KT2.7.07	Alamo Creek Basalt Mbr.	Tcac	633879	3232404	47.09±0.33	G.C.	$^{40}Ar/^{39}Ar$[B]	Plateau age (steps 5–10) comprising 85.4% of gas; lowest lava flow, Sierra Aguja
				Miscellaneous intrusions					
72	04LS08[c]	Rhyolitic and felsic intrusive rocks, undivided	Tir	667903	3229922	28.1±0.3	Zircon	U-Pb[C]	Weighted mean age of 4 spots; central rhyolite plug, Tortuga Mountain
73	04LS09[c]	Basaltic and mafic intrusive rocks, undivided	Tib	668255	3229480	28.63±0.15	G.C.	$^{40}Ar/^{39}Ar$[A]	Total gas age (steps 1–8) comprising 100% of gas; basalt sill surrounding Tortuga Mountain
74	148DM-3-13-05	Intrusive rocks, undivided	Ti	642190	3232087	28.7±0.4	Zircon	U-Pb[C]	Weighted mean age of 7 spots; Pena Mountain
75	147DM-3-13-05	Intrusive rocks, undivided	Ti	642190	3232087	28.77±0.08	Sanidine	$^{40}Ar/^{39}Ar$ laser[B]	Weighted mean age of 10 sanidine crystals; Pena Mountain
76	H86-35[d]	Basaltic and mafic intrusive rocks, undivided	Tib	656251	3252499	29.03±0.08	G.C.	$^{40}Ar/^{39}Ar$[A]	Plateau age (steps 3–6) comprising 67.9% of gas; basalt sill, north of Slickrock Mountain
77	G-11[e]	Rhyolitic and felsic intrusive rocks, undivided	Tir	678363	3229779	30.22±0.09	K-Feldspar	$^{40}Ar/^{39}Ar$[A]	Weighted mean age (steps 8–12) comprising 44.0% of gas; laccolith at Glenn Spring
78	04LS010[c]	Basaltic and mafic intrusive rocks, undivided	Tib	669150	3229283	30.68±0.27	G.C.	$^{40}Ar/^{39}Ar$[A]	Total gas age (steps 1–8) comprising 100% of gas; basalt sill, east of Tortuga Mountain

Appendix. Summary of $^{40}Ar/^{39}Ar$ and U-Pb zircon ages for Big Bend National Park.—Continued

Map sample number	Field sample number[1]	Map unit name	Map unit symbol	UTM Easting	UTM Northing	Age (Ma)	Material analyzed[2]	Technique	Comment[1]
Miscellaneous intrusions—Continued									
79	127DM-2-10-05	Andesitic and intermediate intrusive rocks, undivided	Tia	674618	3237746	31.45±0.18	G.C.	$^{40}Ar/^{39}Ar^{A}$	Total gas age (steps 1–8) comprising 100.0% of gas; sill, near mouth of Pine Canyon
80	38DM-3-14-04	Rhyolitic and felsic intrusive rocks, undivided	Tir	657588	3249797	31.7±0.6	Zircon	U-Pb[C]	Weighted mean age of 5 spots; rhyolite laccolith, Slickrock Mountain
81	27DM-5-2-03	Fayalite Syenite of Grapevine Hills	Tigh	674236	3254439	31.9±0.2	Zircon	U-Pb[C]	Weighted mean age of 10 spots
						31.62±0.30	K-Feldspar	$^{40}Ar/^{39}Ar^{A}$	Plateau age (steps 4–9) comprising 59.1% of gas
82	04LS14[c]	Syenite of Rosillos Mountain	Tirm	668367	3268309	32.1±0.2	Zircon	U-Pb[C]	Weighted mean age of 12 spots
83	04LS323-1[c]	Fayalite Syenite of McKinney Hills	Timh	688581	3249524	32.2±0.3	Zircon	U-Pb[C]	Weighted mean age of 8 spots
84	6323[f]	Rhyolitic and felsic intrusive rocks, undivided	Tir	668411	3246888	33.0±0.2	Zircon	U-Pb[C]	Weighted mean age of 8 spots; fayalite syenite of Government Spring
85	175DM-11-21-06	Rhyolitic and felsic intrusive rocks, undivided	Tir	645203	3243462	41.6±0.4	Zircon	U-Pb[C]	Weighted mean age of 9 spots; rhyolite sill, Maverick Mountain
86	34bDM-5-4-03	Basaltic and mafic intrusive rocks, undivided	Tib	677182	3221686	46.5±0.3	Zircon	U-Pb[C]	Weighted mean age of 5 spots; basalt sill, Mariscal Mountain
						36.11±0.19	K-Feldspar	$^{40}Ar/^{39}Ar^{A}$	Average age (steps 9–11) comprising 55.9% of gas

[1]Additional geochronological information on the sample will be published in a later report.

[2]G.C. Groundmass Concentrate.

[a]Sample submitted by Fred McDowell, Bureau of Economic Geology, University of Texas at Austin, Austin, Tex.

[b]Sample submitted by Kay Wache, Martin-Luther-Universitaet Halle-Wittenberg, Department of Geological Science, Halle, Germany.

[c]Sample submitted by Larry Snee, U.S. Geological Survey, Denver, Colo.

[d]Sample submitted by Christopher Henry, Nevada Bureau of Mines and Geology, Reno, Nev.

[e]Sample submitted by Patricia Dickerson and Bill Muehlberger, University of Texas at Austin, Austin, Tex.

[f]Sample submitted by Minghua Ren, University of Texas at El Paso, El Paso, Tex.

[A]Analysis obtained using furnace heating method at Denver Argon Laboratory, U.S. Geological Survey, Denver, Colo.

[B]Analysis obtained by laser fusion (indicated) and/or furnace heating methods at New Mexico Geochronology Research Laboratory, Socorro, N. Mex.

[C]Analysis obtained using SHRIMP-RG at Stanford USGS MicroAnalysis Center (SUMAC), Stanford University, Stanford, Calif.

[D]Analysis obtained by LA-ICPMS at Arizona Laserchron Center, University of Arizona, Tucson, Ariz.

Prepared by the ***Denver Publishing Service Center***, Denver, Colorado
Manuscript approved for publication November 30, 2010
Edited by ***Gayle M. Dumonceaux***
Layout and graphic design by ***Carol A. Quesenberry***

Back Cover Photographs (left to right):
Yellow rock nettle *(Daniel P. Miggins)*
Texas Banded gecko *(Daniel P. Miggins)*